SWELLING AND MECHANICAL PROPERTIES OF POLYMER NETWORK SYSTEMS(Dissertation_全文)

AUTHOR(S):

Urayama, Kenji

SWELLING AND MECHANICAL PROPERTIES OF POLYMER NETWORK SYSTEMS

KENJI URAYAMA

1996

SWELLING AND MECHANICAL PROPERTIES OF POLYMER NETWORK SYSTEMS

KENJI URAYAMA

1996

CONTENTS

Chapter 1
General Introduction

Polymer networks (including polymer gels which are polymer networks containing solvent), prepared by crosslinking polymer chains, have been focused in both the academic and the industrial fields as attractive materials having some unique features which are not seen in uncrosslinked polymers.[1,2] For instance, polymer networks reveal rubber elasticity (after large deformation is imposed, the original shape is recovered immediately when the external strain or stress is released). In solvents, polymer networks do not dissolve nor precipitate, but do swell or deswell accompanied by a large volume change, depending on solubility of the constituent polymer in a solvent. These features originate from the 3-dimensional polymer network structure having infinite molecular weight, and the flexibility of constituent polymeric chains. Due to these unique features, polymer networks have been attempted to apply to various kinds of industrial devices. The basic aspect of physical properties for polymer network systems has also attracted attention of many physicists as well as chemists.

Polymer networks are often classified into two groups according to the type of crosslink.[3] One is prepared by crosslinking polymer chains by means of a crosslinker which has the reactive sites to the functional groups in the polymer chains. In this case, the polymer chains are crosslinked by covalent bonds, and the resulting polymer networks are called *chemical gels*. Especially, a system in which a prepolymer has functional groups at both chain ends is called an *end-linking* system. The end-linking system is often used as a model network system for the basic studies on rubber elasticity, because the molecular weight of the prepolymer can be regarded as the

molecular weight between chemical crosslinks under the complete progress of end-linking reaction.[4]

On the other hand, polymer network systems crosslinked in different ways from covalent bonds are called *physical gels*. For instance, poly(vinyl alcohol) (PVA) or gelatin forms a gel by cooling its solution. The crosslinking sites in PVA and gelatin gels are believed to be microcrystalline domains[5,6] and helical domains,[7] respectively. Thermoplastic elastomer (TPE), which has received considerable attention as a new type of polymer network systems,[8] also belongs to this category. Generally, TPEs are multiblock copolymers, or graft copolymers, which form microphase separated structure (at room temperature) comprising the soft segment domains revealing entropic elasticity and the hard segment domains acting as crosslinking sites. Polystyrene-polybutadiene-polystyrene (SBS) triblock copolymers and segmented polyurethaneureas (SPUs) are known as the typical TPEs. The physical properties of TPEs are strongly influenced by the microphase separated structure. As described above, there are various types of the structure of crosslinks in physical gels. One commom feature of physical gels is that the sol-gel transition is thermo-reversible.

Table 1-1 summarizes the categories of polymer networks depending on the type of crosslinking, together with the structure of crosslinking sites and examples.[9] A *network by entanglements* is also added to the third row in Table 1-1. Polymer melts and concentrated solutions where polymer chains are well entangled are known to behave like crosslinked rubbers within a certain time scale, although they do not have any permanent crosslinks.[10] This behavior is represented by the plateau region of storage modulus in a time scale.[11] Topological constraints, *i.e.*, entanglements, originating from the uncrossablility of polymer chains, are believed to act as temporary

Table 1-1. Types of polymer networks

Type	Crosslink	Structure of Junctions	Examples
Chemical gels	Covalent bond (Localized)	Points	Crosslinked rubber Thermosetting resins
Physical gels	Hydrogen bond Ionic bond Helix formation, *etc.* (Localized)	Domains	Biological gels Thermoplastic elastomers
Networks by entanglements	(Delocalized)	Topological constraints	Polymer melts Concentrated polymer solutions

crosslinks,[12] which have a finite life time, called "reptation time".[3] On the other hand, entanglements trapped in a crosslinked network (so-called *trapped entanglements*) are not disentangled due to the existence of crosslinks. The roles of trapped entanglements in the elasticity of polymer networks have been one of the most fundamental problems in the physics of rubber elasticity, as will be described below.

The elasticity of chemically-crosslinked networks has attracted a lot of theoretical and experimental physicists, and they have tried to relate it quantitatively with the structural parameters such as number of network chains and junctions. Phantom[13,14]and affine[15,16] network models were proposed in 1940's, and they are now classified in classical network models. Considerable progress has been made in theoretical as well as experimental studies on the elasticity of polymer networks, but there is still a dispute about the effect of trapped entanglements on elastic modulus. Some researchers[17-21] have argued that trapped entanglements suppress the thermal fluctuations of chemical crosslinks, but do not contribute to elastic modulus. They have expressed the shear modulus (G) of a polymer network as

$$G = G_c \qquad (1.1)$$

where G_c is the modulus contributed from chemical crosslinks. Equation (1.1) is common to phantom and affine models. The detailed expression is given by $G=(\nu_e-\mu_e)RT$ for phantom network model, and $G=\nu_e RT$ for affine network model. Here, ν_e, μ_e, R, and T are the number of moles of network chains and junctions per unit volume, the gas constant, and the absolute temperature. The constrained junction theory by Flory and Erman[17] predicts G lies between the predictions by phantom and affine network models. Others[22-28] have insisted that trapped entanglements contribute similarly as chemical crosslinks to elastic modulus, and shown the following form of G.

$$G = G_c + G_N^{\circ} T_e \qquad (1.2)$$

Here, G_N° is the plateau modulus of an uncrosslinked polymer melt with high molecular weight, and T_e is the trapping factor representing the proportion of the entanglements that contribute to elastic modulus. Equation (1.2) was phenomenologically derived by Langley[22] and Dossin and Graessley.[23] It should be noted that Eq. (1.2) predicts a larger value of G than Eq. (1.1).

In order to elucidate the effect of trapped entanglements on elastic modulus, the elastic moduli of model networks, which are prepared in the bulk state by end-linking prepolymers having a definite molecular weight, have been measured as a function of the molecular weight of prepolymer by many researchers.[18,19,25-28] However, in spite of a considerable accumulation of such data, the dispute has not yet been settled. Another experimental approach is necesarry to conclude clearly this dispute. An alternative experiment for this problem is to measure the elastic moduli of model polymer networks, which are crosslinked *in solution* by end-linking prepolymers with high molecular weight, as a function of polymer concentration at crosslinking (*i.e.*, at preparation). If elastic modulus is determined only by the number of chemical crosslinks, G is simply proportional to the number of polymer chains in solution. Then, G increases linearly with the polymer volume fraction at preparation (ϕ_o) as

$$G \propto \phi_o^{1} \qquad (1.3)$$

On the other hand, if trapped entanglements contribute to elastic modulus similarly to chemical crosslinks, G should be scaled as

$$G \propto \phi_o^{\alpha} \quad (\alpha \approx 2) \qquad (1.4)$$

Equation (1.4) is based on the analogy of the concentration dependence of plateau modulus for polymer solutions.[12] Since the difference in the exponents for the power laws in Eqs. (1.3) and (1.4) is significantly large, the

experiment for ϕ_o dependence of G will clearly conclude the above problem. However, the quantitative experiments concerning ϕ_o dependence of G for polymer networks have never been performed.

One of the ultimate goals in the physics of rubber elasticity is to determine the strain energy density function (W) for elastomers in an explicit form. The function W is a fundamental physical quantity governing the stress-strain behavior of elastomers. Generally, W is written as $W=W(I_1,I_2,I_3)$ using the invariants of deformation tensor, where $I_1=\lambda_1^2+\lambda_2^2+\lambda_3^2$, $I_2=\lambda_1^2\lambda_2^2+\lambda_2^2\lambda_3^2+\lambda_3^2\lambda_1^2$, and $I_3=\lambda_1^2\lambda_2^2\lambda_3^2$, λ_i being the principal ratio in i-direction. The classical theory for rubber elasticity predicts the form of W as[13-15,29,30]

$$W = \frac{G}{2}(I_1 - 3) \qquad (1.5)$$

The classical theory assumed that the conformation of network chains is Gaussian, and the polymer network is composed of the hypothetical *phantom* chains which can move freely across the other chains. Rivlin and Saunders[31] showed that W is a function of I_1 and I_2, which is not in accord with the prediction by the classical theory, from their experimental results for the biaxial extension of natural rubber vulcanizates. They also indicated that the experimental results are well described by the following Mooney equation[32]:

$$W = C_1(I_1 - 3) + C_2(I_2 - 3) \qquad (1.6)$$

where C_1 and C_2 are constants independent of I_1 and I_2. The constant C_2 is often attributed to the interaction between network chains, *i.e.*, entanglements. However, the later precise experiments[33,34] for the biaxial extension of rubbery materials indicated that the observed results were not correctly described by Eq. (1.6); C_2 is not constant but a complicated function of I_1 and I_2. Quite a number of molecular theories[13-17,35-41] and phenomenological equations[32,42-46] have been proposed for the explicit form of W. Most of

these molecular theories have concentrated on how to treat entanglements. However, Gottlieb and Gayload[47] have showed that none of these molecular theories[13-17,36-39] described the experimental data[33] satisfactorily for the biaxial extension of isoprene rubber, and especially, the disagreement in small deformation region was pronounced. As I_1 decreased (the strains became smaller), the experimental values of $\partial W/\partial I_1$ increased rapidly, and those of $\partial W/\partial I_2$ decreased abruptly, in comparison with the theoretical predictions. Here, it should be noted that all of the past experimental and theoretical studies assume the incompressibility of elastomers (*i.e.*, Poisson's ratio (μ) is equal to 1/2 and I_3=1), resulting in the form of $W=W(I_1,I_2)$. The reported values of μ for elastomers are close to 1/2, but not exactly equal to 1/2.[33,48,49] Under this circumstance, elastomers should be treated as compressible materials, and W should be expressed as $W=W(I_1,I_2,I_3)$ for detailed discussion. The characteristic behavior of $\partial W/\partial I_1$ and $\partial W/\partial I_2$ in small deformation region observed in the experiments may originate from the non-zero compressibility of real elastomers ($\mu \neq 1/2$ and $I_3 \neq 1$). From this viewpoint, it is very interesting to eliminate the assumption of incompressibility, and to analyze the stress-strain behavior using experimental values of μ.

Poisson's ratio μ is one of the elastic constants governing the elastic behavior of materials together with Young's modulus and shear modulus.[50] However, there are several studies[33,48,49] on μ of polymer networks, while Young's modulus and shear modulus have been investigated by many researchers.[18-28,51-58] The values of μ for polymeric materials reflect the flexibility of polymer chains. For instance, the values of μ for rubbery materials were reported[33,48,49] to be very close to 1/2 which means incompressible, while that for glassy polystyrene[59] was evaluated to be 0.33

which is fairly smaller than 1/2. The flexibility of network chains in polymer gels depends strongly on the solubility of constituent polymer in solvent. In the case of physical gels whose crosslinks are microcrystallites, the degree of crystallinity is also an important factor controlling the flexibility of network chains. It was reported in a few studies[56,57] that the stress-strain behavior and Young's modulus of PVA gels are greatly affected by the solvents as well as the degree of crystallinity. These factors are expected to influence the value of μ, but the details have not been studied yet.

In addition to rubber elasticity, swelling phenomenon is one of the most characteristic properties of polymer networks. Thermodynamics for swelling of polymer networks has been studied by many researchers.[3,28,51-54,60-70] Floly and Rehner[60] first treated it theoretically, assuming that the free energy of polymer network systems consists of the elastic term (F_{el}) related to the deformation of network chains on swelling and the osmotic term (F_{osm}) with respect to the mixing entropy for the network and the solvent. They represented F_{el} by using Gaussian chain statistics, and F_{osm} by employing mean field theory. The expressions of F_{el} and F_{osm} for polymer networks crosslinked in solution with the polymer volume fraction ϕ_o are given by

$$\frac{F_{el}}{k_B T} = N_A \nu_1(\mu_e \phi - \nu_e \phi_o^{2/3}\phi^{1/3}) \tag{1.7}$$

$$\frac{F_{osm}}{k_B T} = N_A (\ln(1-\phi) + \phi + \chi \phi^2) \tag{1.8}$$

Here, F_{el} and F_{osm} is respectively the elastic and osmotic free energies per site occupied by a monomer, and N_A, k_B, ν_1, ϕ and χ are the Avogadro's number, the Boltzmann constant, the molar volume of solvent, the polymer volume fraction in swollen network, and the polymer-solvent interaction parameter, respectively. The dependence of the polymer volume fraction in equilibrium swollen networks (ϕ_e) on ϕ_o is given by the minimization of total free energy with respect to ϕ as follows.[67]

$$\phi_e \propto N^{-3/5} \phi_o^{1/4} \quad (1.9)$$

Here, N is the polymerization index of network chain, and ϕ is assumed to $\phi \ll 1$. De Gennes[3] argued that Gaussian statistics and mean field theory are not applicable to semidilute concentration regime in which excluded volume effect and concentration fluctuation are considerable. The c^* theorem, proposed by de Gennes,[3] assumes that ϕ_e is identified with the overlapping concentration for network chains (ϕ^*) as

$$\phi_e \approx \phi^* \propto N^{-4/5} \quad (1.10)$$

The c^* theorem postulates the complete disinterpenetration of network chains (*i.e.*, no overlapping of network chains) in equilibrium swollen state, and regards ϕ^* as the reference state irrespective of ϕ_o. The following familiar scaling relation between ϕ_e and the elastic modulus of equilibrium swollen networks (E_s) was first derived from the c^* theorem.

$$E_s \propto \phi_e^{9/4} \quad (1.11)$$

Equation (1.11) has been experimentally confirmed for various kinds of polymer network system.[51-54] The validity of the c^* theorem has often been believed on the basis of the confirmation of Eq. (1.11). However, it should be emphasized that Eq. (1.11) can be derived without assuming the complete disinterpenetration of network chains on swelling.[65] In other words, the confirmation of Eq. (1.11) does not necessarily support the validity of c^* theorem. Accordingly, in order to elucidate the interspersion state of network chains in equilibrium swollen state, another experiments which do not rely on Eq. (1.11) are necessary (for instance, the experiments for ϕ_o dependence of E_s and ϕ_e), and another theoretical approach may be needed.

The studies on the kinetics of swelling of polymer networks have much progressed since Tanaka *et al.*[71,72] proposed the equation of motion for polymer networks, which is written as

$$\zeta \frac{\partial \boldsymbol{v}}{\partial t} = \text{div } \boldsymbol{s} \qquad (1.12)$$

Here, ζ, $\boldsymbol{v}$ and $\boldsymbol{s}$ are the friction coefficient between the network and solvent, the displacement vector and the stress tensor for small volume elements in polymer networks, respectively. Swelling processes of tgels with various shapes have been both theoretically[72-74] and experimentally[72-77] investigated on the basis of Eq. (1.12).

The studies on the swelling of gels have mainly been made under no external stress field. Recently, an interesting phenomenon for the swelling of gels under a constant uniaxial strain has been reported[78]. When a constant uniaxial strain is imposed on an equilibrated swollen gel in solvent, the gel swells further, and the sustaining stress is simultaneously reduced to a certain level. Tthe times characteristic of the induced swelling and of the resultant stress relaxation agree with each other. These results mean that the further swelling is induced by an external strain or stress, and causes the mechanical relaxation. The magnitude and the kinetics of further swelling and mechanical relaxation is expected to strongly depend on deformation modes: for example, equibiaxial, and strip-biaxial deformations *etc.*. However, the effects of deformation modes on further swelling and mechanical relaxation behavior have not yet been clarified.

The strain-induced swelling suggests that for a polymer gel deformed *in solvent* μ is essentially a time-dependent quantitiy. Poisson's ratio is generally defined under a uniaxial deformation by the ratio of the strains parallel and perpendicular to stretching direction ($\varepsilon_{\parallel}$ and $\varepsilon_{\perp}$, respectively):

$$\mu = -\frac{\varepsilon_{\perp}}{\varepsilon_{\parallel}} \qquad (1.13)$$

The strain-induced swelling makes $\varepsilon_{\perp}$ time-dependent, which means that μ is time-dependent. The swelling causes the increase in the width of deformed gels, resulting in the decrease of μ. If elongation is made fast so that the

strain-induced swelling would be negligible, we will get μ close to 1/2, reflecting the incompressibility of gel itself. On the other hand, when the time scale of extension is much longer than the characteristic time for swelling (*i.e.*, the strain-induced swelling is equilibrated), μ is dominantly determined by the strain-induced swelling. Hereafter, we call the former and latter μ the *initial Poisson's ratio* (μ_0) and the *equilibrium Poisson's ratio* (μ_∞), respectively. The value of μ_∞ was theoretically evaluated to be 1/6,[78] which was found to agree well with the experimental results.[79] In the time scale between the two extreme cases, μ is time-dependent, and has an intermediate value between μ_0 and μ_∞. The time-dependent Poisson's ratio is one of the unique properties of polymer gels, but there have been no quantitative studies on the time dependence of μ of polymer gels.

The elastic properties of polymer network systems have mainly been studied in either preparation or equilibrium swollen state. On the other hand, there are several studies[53,80-82] on the elasticity of deswollen polymer networks. The "deswollen polymer networks" mentioned here are dry networks prepared by removing solvent from networks crosslinked in solution. We here treat a deswollen network whose constituent polymer has a glass transition temperature much lower than the room temperature. This deswollen (dry) networks reveal rubber elasticity. The structure and the elasticity of deswollen networks are still an unsettled subject in the physics of rubber elasticity.[3,10,41] The deswelling process is accompanied by the reduction of the dimension of network chains due to the volume decrease of material. The contraction of network chains on deswelling has often been called *supercoiling*. Supercoiled chains are assumed to have a contracted conformation in comparison with Gaussian chains. Hence, the structure and the mechanical properties of deswollen networks are expected to be much

different from those of the networks crosslinked in the bulk state, although both of them are dry networks. However, the details on the conformation of supercoiled chains and the effects of supercoiling on the mechanical properties of deswollen networks are unclear at present. In the earlier studies[80-82], no attention to the effects of supercoiling on the elasticity of networks was paid, and the deswollen networks were treated similarly to the networks crosslinked in the bulk state. Another topic for deswelling is that a deswollen network, which are prepared at a low concentration, can exhibit a remarkable extensibility relative to conventional elastomers.[70] This expectation is based on the two reasons: The amount of trapped entanglement which is one of the origins limiting extensibility, is considerably reduced by crosslinking at a low concentration. The end-to-end distance of network chains in undeformed state is decreased by deswelling. However, noticeable extensibility of deswollen polymer networks has not yet been reported.

The main aims in this study are summarized as follows:

1) To estabish how to measure Poisson's ratio of polymer gels, and to elucidate the time dependece of Poisson's ratio originating from strain-induced swelling
2) To clarify the origin of the characteristic behavior of the stress-strain relations at small deformations for real elastomers
3) To establish the theoretical description for the elasticity and thermodynamics of the swelling for polymer networks
4) To clarify the effect of supercoiling on the elasticity of deswollen polymer networks

In this chapter, the motive of this thesis has been mentioned. Some current problems about the swelling and elastic properties of polymer

network systems have been described together with the historical background of this research field. The contents of this thesis are as follows:

In Chapter 2, the values of initial Poisson's ratio μ_0 of poly(vinyl alcohol) gels are measured. The dependence of μ_0 on the swelling solvents and the degree of crystallinity is investigated.

In Chapter 3, the dependence of Poisson's ratio of gels, when elongated in solvent, on the experimental time scale is theoretically and numerically investigated. The degree of swelling and mechanical relaxation induced by an external stress or strain under various deformation modes are calculated from the thermodynamics for the swelling of gels under constraints. The processes of swelling and mechanical relaxation are simulated on the basis of the kinetics of swelling for constrained gels.

In Chapter 4, the stress-strain behavior of segmented polyurethaneureas (SPUs) under pure shear deformation is analyzed using the value of μ_0 obtained experimentally. The data of stress-strain relations for various rubber vulcanizates, which were reported in earlier studies,[33,34] are re-analyzed using the experimental values of μ_0. The theoretical values of $\partial W/\partial I_i$ (i=1,2,3) at zero strain limit are derived from the infinitesimal elasticity theory taking the compressibility into account, and the theoretical predictions are compared with the experimental results for the SPUs and the four types of rubber vulcanizates.

In Chapters 5 and 6, degree of equilibrium swelling and elastic modulus of polysiloxane networks crosslinked in solution are investigated as a function of polymer concentration at crosslinking. Two types of polysiloxane networks are employed in order to elucidate the effect of trapped entanglement on elasticity. One is prepared by end-linking poly(dimethylsiloxane) with high molecular weight which is entangled in the

uncrosslinked state (Chapter 5). The other is made by end-linking oligo(dimethylsiloxane) with low molecular weight which is not entangled in the uncrosslinked state (Chapter 6). The experimental results obtained in Chapters 5 and 6 are compared with the predictions by the c^* theorem and the affine model regarding preparation concentration as the reference state.

In Chapter 7, initial Young's modulus and stress-strain relations of deswollen polydimethylsiloxane networks are investigated as a function of polymer concentration at crosslinking. The details of supercoiled structure are estimated from the mechanical properties of deswollen networks. The remarkable extensibility of the deswollen polydimethylsiloxane network, which is prepared at a low concentration, is both experimentally and theoretically demonstrated.

References

1. "*Adv. Polym. Sci., Vol. 44*", Dusek, K., Ed., Springer-Verlag, Berlin and Heidelberg, 1982.
2. "*Synthesis, Characterization, and Theory of Polymeric Networks and Gels*", Aharoni, S. M., Ed., Prenum Press, New York, 1992.
3. de Gennes, P.-G., "*Scaling Concepts in Polymer Physics*", Cornell University Press, Ithaca and London, 1979.
4. See, for example: Mark, J. E. and Erman, B., "*Rubber Elasticity - A Molecular Primer*", Wiley, New York, 1988.
5. Keller, A. in "*Structure-Property Relationships of Polymeric Solids*", Ed. by Hiltner, A. Prenum, New York, 1983.
6. Kanaya, T., Ohkura, M., Kaji, K., Furusawa, M. and Misawa, M., *Macromolecules*, **27**, 5609 (1994).
7. Moris, E. R. and Rees, D. A., *J. Mol. Biol.*, **138**, 363 (1980).
8. "*Thermoplasic Elastomers*", Ed. by Legge, N. R., Holden, G., and Schroeder, H. E., Hanser Publishers, Munich, Vienna, New York, 1987.
9. Kohjiya, S., *Macromol. Symp.*, **93**, 27 (1995).
10. Graessley, W. W., *Adv. Polym. Sci.*, **16**, 3 (1974).
11. Onogi, S., Masuda, T. and Kitagawa, K., *Macromolecules*, **3**, 109 (1970).
12. Ferry, J. D., "*Viscoelastic Properties of Polymers*", 3rd Ed., Wiley, New York, 1980.
13. James, H. M., *J. Chem. Phys.*, **15**, 651 (1947).
14. James, H. M. and Guth, E., *J. Chem. Phys.*, **15**, 669 (1947).
15. Flory, P. J., "*Principles of Polymer Chemistry*", Cornell University Press, Ithaca, 1953.
16. Wall, F. T., *J. Chem. Phys.*, **11**, 527 (1943).

17. Flory, P. J. and Erman, B., *Macromolecules*, **15**, 800 (1982).
18. Mark, J. E., *Adv. Polym. Sci.*, **44**, 1 (1982).
19. Queslel, J. P. and Mark, J. E., *J. Polym. Sci. Polym. Phys. Ed.*, **22**, 1201 (1984).
20. Soni, V. K. and Stein, R. S., *Macromolecules*, **23**, 5257 (1990).
21. Erman, B. and Mark, J. E., *Macromolecules*, **25**, 1917 (1992).
22. Langley, N. R., *Macromolecules*, **1**, 348 (1968).
23. Dossin, L. M. and Graessley, W. W., *Macromolecules*, **12**, 123 (1979).
24. Pearson, D. S. and Graessley, W. W., *Macromolecules*, **13**, 1001 (1980).
25. Gottlieb, M., Macosko, C. W., Benjamin, G. S., Meyers, K. O. and Merril, E. W., *Macromolecules*, **14**, 1039 (1981).
26. Valles, E. M., Rost, E. J., and Macosko, C. W., *Rubber Chem. Technol.*, **57**, 55 (1984).
27. Opperman, W. and Rennar, N., *Prog. Colloid. Polym. Sci.*, **75**, 49 (1987).
28. Patel, S. K., Molone, S., Cohen, C., Gillmor, J. R. and Colby, R. H., *Macromolecules*, **25**, 5241 (1992).
29. Treloar, L. R. G., "*The Physics of Rubber Elasticity*", 3rd Ed., Clarendon Press, Oxford (1975).
30. Flory, P. J., *Proc. Royal Soc. London*, **A351**, 35 (1976).
31. Rivlin, R. S. and Saunders, D. W., *Phil. Trans. Royal Soc. London, Ser. A*, **243**, 251 (1951).
32. Mooney, M. J., *J. Appl. Phys.*, **11**, 582 (1940).
33. Kawabata, S., Matsuda, M., Tei, K. and Kawai, H., *Macromolecules*, **14**, 154 (1981).
34. Fukahori, Y. and Seki, W., *Polymer*, **33**, 502 (1992).
35. Ronca, G. and Allegra, G., *J. Chem. Phys.*, **63**, 4990 (1975).

36. Edwards, S. F., *Br. Polym. J.*, **9**, 140 (1977).
37. Ball, R. C., Doi, M., Edwards, S. F. and Warner, M., *Polymer*, **22**, 1010 (1981).
38. Marrucci, G., *Macromolecules*, **14**, 434 (1981).
39. Gaylord, R. J., *Polym. Bull.*, **8**, 325 (1982); **9**, 181 (1983).
40. Edwards, S. F. and Vilgis, T. A., *Polymer*, **27**, 483 (1986); **28**, 375 (1987).
41. Heinrich, G., Straube, E. and Helmis, G., *Adv. Polym. Sci.*, **85**, 33 (1988).
42. Rivlin, R. S., *Phil. Trans. Royal Soc. London*, **A241**, 379 (1948); **A242**, 173 (1949).
43. Valanis, K. C. and Landel, R. F., *J. Appl. Phys.*, **38**, 2997 (1967).
44. Ogden, R. W., *Proc. Royal Soc. London*, **A326**, 565 (1972).
45. Kilian, H. G., *Polymer*, **22**, 209 (1982).
46. Tschoegl, N. W. and Gurer, C., *Macromolecules*, **18**, 680 (1985).
47. Gottlieb, M. and Gaylord, R. J., *Macromolecules*, **20**, 130 (1987).
48. Wood, L. A. and Martin, G. M., *Rubber Chem. Technol.*, **37**, 850 (1964).
49. Holownia, B. P., *Rubber Chem. Technol.*, **48**, 246 (1975).
50. Landau, L. D. and Lifshitz, E. M., "*Theory of Elasticity*", Nauka, Moscow, 1987.
51. Zrinyi, M. and Horkay, F., *Polym. Bull.*, **3**, 665 (1980).
52. Candau, S., Peter, A. and Herz, J., *Polymer*, **22**, 1504 (1981).
53. Vasiliev, V. G., Rogovina, L. Z. and Slonimsky, G. L., *Polymer*, **26**, 1667 (1985).
54. Zrinyi, M. and Horkay, F., *Macromolecules*, **17**, 2805 (1987).
55. Brereton, M. G. and Klein, P. G., *Polymer*, **29**, 970 (1988).

56. Takigawa, T., Kashihara, H. and Masuda, T., *Polym. Bull.*, **24**, 613 (1990).
57. Takigawa, T., Kashihara, H., Urayama, K. and Masuda, T., *Polymer*, **33**, 2334 (1992).
58. Matzen, D. and Straube, E., *Colloid & Polym. Sci.*, **270**, 1 (1992).
59. Badger, R. M. and Blaker, R. H., *J. Phys. Chem.*, **53**, 1056 (1949).
60. Flory, P. J. and Rehner, J., *J. Chem. Phys.*, **11**, 521 (1943).
61. Gee, G., *Rubber Chem. Tech.*, **18**, 716 (1945).
62. Flory, P. J., *Ind. Engng Chem.* **38**, 417 (1946).
63. Gee, G., Herbert, J. B. M. and Roberts, R. C., *Polymer*, **6**, 541 (1965).
64. Rempp, P., Herz, J., Hild, G. and Picot, C., *Pure Appl. Chem.*, **43**, 77 (1975).
65. Brochard, F., *J. Phys. (Paris)*, **40**, 1049 (1979).
66. Brotzmann, R. W. and Eichinger, B. E., *Macromolecules*, **14**, 1445 (1981); *Macromolecules*, **15**, 531 (1982).
67. Bastide, J., Picot, C. and Candau, S., *J. Macromol. Sci., Phys.*, **B19**, 13 (1981).
68. Gottlieb, M. and Gaylord, R. J., *Macromolecules*, **17**, 2024 (1984).
69. Oikawa, H. and Murakami, K., *Macromolecules*, **24**, 1117 (1991).
70. Obukhov, S. P., Rubinstein, M. and Colby, R. H., *Macromolecules*, **27**, 3191 (1994).
71. Tanaka, T., Hocker, L. O. and Beneddek, G. B., *J. Chem. Phys.*, **59**, 5151 (1973).
72. Tanaka, T. and Fillmore, D. J., *J. Chem. Phys.*, **70**, 1214 (1979).
73. Peters, A. and Candau, S. J., *Macromolecules*, **19**, 1952 (1986); **21**, 2278 (1988).
74. Li, Y. and Tanaka, T., *J. Chem. Phys.*, **90**, 5161 (1989).

75. Chiarelli, P. and Derossi, D., *Prog. Coll. Polym. Sci.*, **78**, 4 (1988).
76. Zrinyi, M., Rosta, J. and Horkay, F., *Macromolecules*, **26**, 3097 (1993).
77. Hakki, A. and Herz, J. E., *J. Chem. Phys.*, **101**, 9054 (1994).
78. Takigawa, T., Urayama, K., Morino, Y. and Masuda, T., *Polym. J.*, **25**, 929 (1993).
79. Takigawa, T., Doctoral Dissertation, Kyoto University, 1995.
80. Mark, J. E. and Johnson, R. M., *Macromolecules*, **5**, 41 (1972).
81. Price, C., Allen, G., de Candia, F., Kirkham, M. C. and Subramaniam, A., *Polymer*, **11**, 486 (1970).
82. Ong, C. S. and Stein, R. S., *J. Polym. Sci., Polym. Phys. Ed.*, **12**, 1599 (1974).

Chapter 2
Effects of Swelling Solvent and Degree of Crystallinity on Initial Poisson's Ratio of Poly(Vinyl Alcohol) Gels

2.1 Introduction

As mentioned in Chapter 1, Poisson's ratio (μ) of polymer gels deformed in solvent is essentially a time-dependent quantity due to the strain-induced swelling. Two kinds of limiting values of μ are defined as initial Poisson's ratio (μ_0) and equilibrium Poisson's ratio (μ_∞) according to the two limits of the short and long time scales. If a gels is elongated fast so that the strain-induced swelling would be negligible, we obtain μ_0. The values of μ_0 are equivalent to those obtained by experiments in air, even if the elongation is made in solvent. The values of μ_0 reflect mechanical properties of the gel itself. In this chapter, μ_0 is exclusively discussed. Most of conventional extensional experiments, which are made under a constant crosshead speed, correspond to this situation, because the process of strain-induced swelling is very slow. When the time scale of experiments is comparable to the characteristic time of strain-induced swelling, the effect of the strain-induced swelling is significant. We treat this case in Chapter 3.

Studies on the mechanical properties of polymer gels such as stress-strain relations and elastic moduli have been performed in air extensively.[1-4] However, the precise measuments on μ_0 of polymer gels have not been made yet, in spite of its importance. The values of μ_0 for polymeric materials reflect the flexibility of the constituent polymer chains. For example, rubber-like materials show μ_0 close to 0.5,[5-7] but μ_0 of glassy polymers is much lower than that of rubbers; μ_0 of glassy polystyrenes is reported to be 0.33.[8] The flexibility of network chains of polymer gels is greatly influenced by the

solubility of the constituent polymer in a swelling solvent. The flexibility of network chains in the poly(vinyl alcohol) (PVA) gels of which crosslinks are microcrystallines is strongly dependent on the degree of crystallinity as well as the swelling solvents. Actually, stress-strain relations and initial Young's moduli of PVA gels were affected by the solvents used for swelling and the annealing temperatures.[3,4] However, the effects of these factors on μ_0 have not been investigated yet.

Measurement of μ_0 is also important to examine the true stress-strain relations, because the evaluation for the cross-section of deformed samples in process of elongation needs the value of μ_0. All the past studies have *a priori* assumed the incompressibility of materials (μ_0=0.5) for the calculation of true stress.

In this chapter, we evaluate μ_0 from the measurement of dimensional changes of PVA gels during uniaxial elongation. We investigate μ_0 for the three types of gels: PVA gels swollen in a good solvent (a mixture of water and dimethylsulfoxide (DMSO)), PVA gels swollen in a poor solvent (ethanol), and PVA hydrogels swollen in water which are prepared by annealing the PVA gels. The dependence of μ_0 on the polymer content and initial strain rate is investigated for the PVA gels swollen in the mixed solvent. The annealing temperature dependence of μ_0 is discussed for PVA hydrogels. Finally, we show the true stress-strain relations of the gels using the experimental values of μ_0.

2.2 Theoretical Background

In order to describe the deformation of gel samples, we set 3-dimensional Cartesian coordinates as shown in Fig. 2-1. When a sample is extended in the x-direction, the sample dimension in the x-direction is

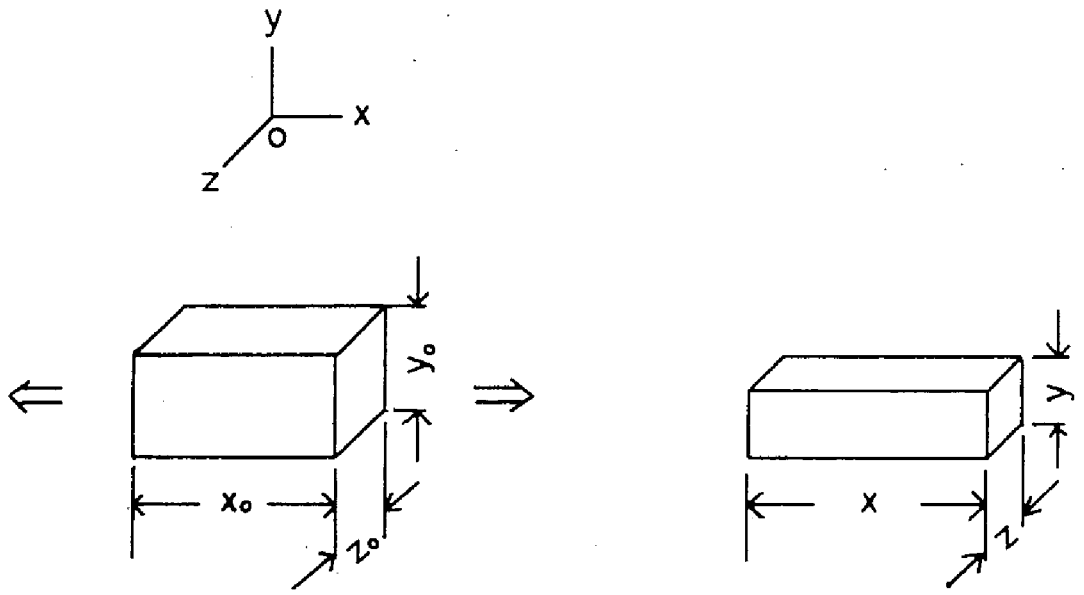

Figure 2-1. Schematic representation of the sample before and after deformation: (A) before; (B) after.

increased, and the dimensions in the y- and z-directions are reduced in most cases. In this deformation, the deformation gradient tensor has only the diagonal components. Each component (λ_1, λ_2, λ_3) of diagonal part can be written as follows.

$$\lambda_1 = \frac{x}{x_0}, \quad \lambda_2 = \frac{y}{y_0}, \quad \lambda_3 = \frac{z}{z_0} \tag{2.1}$$

Here, x_0, y_0 and z_0 are the initial dimensions, and x, y and z are those after extension in each direction. y and z can be time (t) dependent quantity. Hereafter, we deal with the limiting values of y and z at $t \rightarrow 0$. The Finger-type deformation gradient tensor ($\boldsymbol{F}^{-1}$) can be written as follows.[9] For isotropic materials, $\lambda_2 = \lambda_3$.

$$\boldsymbol{F}^{-1} = \begin{bmatrix} \lambda_1 & 0 & 0 \\ 0 & \lambda_2 & 0 \\ 0 & 0 & \lambda_2 \end{bmatrix} \tag{2.2}$$

A generalized definition for Poisson's ratio μ is given by[10]

$$\lambda_2 = \lambda_1^{-\mu} \tag{2.3}$$

When the deformation is applied to the sample, the increase of volume is expressed by

$$det(\boldsymbol{F}^{-1}) = \lambda_1^{-2\mu+1} \tag{2.4}$$

It can be easily shown from Eq. (2.4) that μ is equal to 0.5, when the material is incompressible ($det(\boldsymbol{F}^{-1}) = 1$). The cross-sectional area (S) perpendicular to the direction of extension is given by

$$S = S_0\lambda_1^{-2\mu} \tag{2.5}$$

Here, S_0 is the initial value which is y_0z_0. Under a uniaxial elongation, all the components except the xx one of stress tensor (σ) are equal to zero. The true stress (σ) is written by

$$\sigma \equiv \sigma_{xx} = (\sigma_{xx})_E\lambda_1^{2\mu} \tag{2.6}$$

Here, $(\sigma_{xx})_E$ is the xx component of the engineering stress tensor (σ_E). When the specimen is extended in x-direction with a constant speed of v, Hencky strain (ε) in x-direction is defined by [11]

$$\varepsilon = \ln \lambda_1 \tag{2.7}$$

The initial rate of strain ($\dot{\varepsilon}_0$) can be given by

$$\dot{\varepsilon}_0 = \frac{v}{x_0} \tag{2.8}$$

2.3 Experimental

2.3.1 Gel Samples

The PVA used in this study was supplied by Unitika Co., Japan. The degree of polymerization was 1700, and the degree of saponification was 99.5 mol%. The solvent used was a mixture (D/W) of DMSO and water (4:1 by weight). PVA was dissolved into the solvent at 105°C . The hot solution was casted into 6 × 6 × 20 mm metal mold. Three types of gels were prepared. (1) The gel sample-coded as PVA GEL (D/W) was prepared by cooling the solution to -20°C and then maintaining in a freezer for 24h. (2) The gel sample-coded as PVA GEL (EtOH) was obtained from PVA GEL (D/W) by exchanging the mixed solvent for ethanol. (3) In order to obtain PVA hydrogel samples which were coded as PVA HYDROGEL, PVA GEL(EtOH) were dried in a vacuum oven at 30°C, and then annealed in a oil bath for 1h. The annealing temperature was designated by T_a, which were 100, 105, 110 and 115°C, as shown in Table 2-1, in which all the experimental data obtained in this study are tabulated. PVA HYDROGEL was finally obtained by immersing the annealed gel in water until the equilibrium swelling was achieved.

Table 2-1. Polymer Concentration (c), Crosshead Speed (v), the Constant of Eq. (2-9) (k), Initial Poisson's Ratio (μ_0) and Initial Young's Modulus (E_0) for PVA GEL (D/W), PVA GEL (EtOH) and PVA HYDROGEL

	c (kg/m^3)	v (mm/min)	k	μ_0	E_0 (Pa)
		PVA GEL (D/W)			
	77.3	30	0.99	0.474±0.006	5.8×10^4
	111	0.5	1.18	0.455±0.003	1.3×10^5
	111	3	1.05	0.453±0.002	1.6×10^5
	111	30	1.07	0.472±0.004	1.2×10^5
	111	100	1.04	0.463±0.004	1.4×10^5
	111	300	1.10	0.456±0.005	1.1×10^5
	145	30	1.06	0.470±0.003	3.1×10^5
in air	111	30	0.99	0.485±0.005	1.1×10^5
		PVA GEL (EtOH)			
	413	30	1.10	0.338±0.003	4.0×10^7
		PVA HYDROGEL			
T_a=100°C	542	30	1.18	0.429±0.002	4.5×10^6
T_a=105°C	617	30	1.02	0.430±0.002	6.1×10^6
T_a=110°C	723	30	1.04	0.447±0.003	1.0×10^7
T_a=115°C	798	30	1.05	0.426±0.003	2.1×10^7

2.3.2 Measurements

Uniaxial elongation of PVA gels was performed in solvent by using a Orientec RTM-250 tensile tester with a specially designed solvent bath. The extension processes of the samples were recorded with video camera. The nominal extension rate (λ_a) was determined by the distance between the sample cramps. λ_l was determined by measuring the distance between the two marked points with relatively short distance (~3mm) in the central region of sample. The distance was measured on the monitor screen. By comparing λ_l with λ_a, we confirmed that (λ_l-1) is proportional to (λ_a-1) as shown by the following equation with using a constant $k\cong1$:

$$\lambda_l-1 = k(\lambda_a-1) \qquad (2.9)$$

Figure 2-2 shows the plots of λ_l *vs.* λ_a for PVA GEL(D/W) with c=111kg/m^3 and v=30mm/min. As can be seen from this figure, all data points fall on a straight line. The slope of the straight line corresponds to the value of k in Eq. (2.9). The value of k determined by least-square method was 1.07. For the other samples, λ_l and λ_a shows the linear relation similar to those for PVA GEL(D/W) with c=111kg/m^3 and v=30mm/min. The values of k for the other samples are also listed in Table 2-1. As is seen from Table 2-1, the experimental values of k are a little scattered, but they are slightly larger than unity except PVA GEL(D/W) with c=77.3kg/m^3 and that with c=111kg/m^3 measured in air. The larger value of k than unity suggests that the central region of the specimen is elongated to larger extent than the edges. This non-uniform elongation is due to the effect of cramps; the edge part of sample is collapsed at cramps. When deformation is applied to the system, the extent of elongation at the collapsed edges would be smaller than that at the central region. The value k=0.99 for the two samples is close to unity and indicates that the effect of cramps is small.

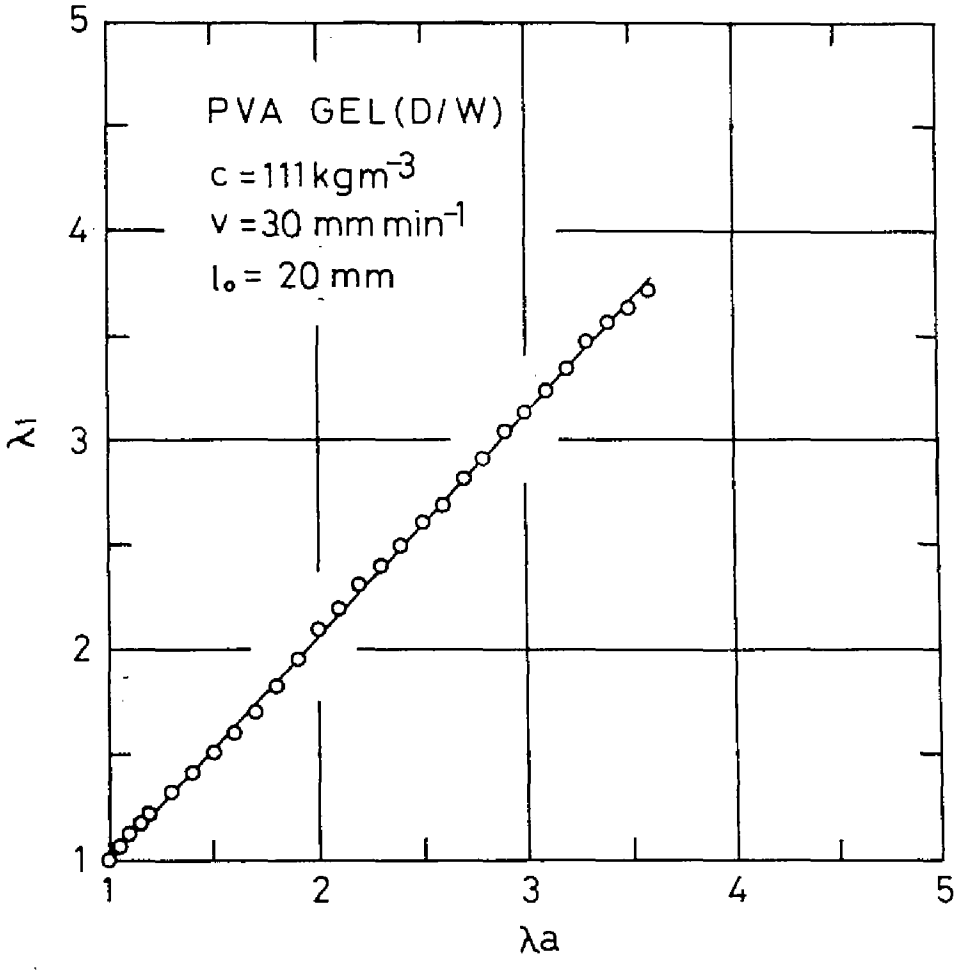

Figure 2-2. Plots of actual extension rate (λ_1) *versus* nominal extension rate(λ_a) for PVAGEL(D/W) at c=111kg/m^3, v=30mm/min.

λ_2 was determined by measuring the width at a guide line position on the monitor screen. The true stress (σ) - strain (ε) relations of the various PVA gels were obtained using the experimental values of μ_o.

It is well known that PVA gels display aging effects. To avoid the effects, all the experiments in this study were completed within 2 hours. This will be discussed later.

2.4 Results and Discussion

2.4.1 Effect of Elongation Speed on μ_o

Figure 2-3 shows the plots of $-\log \lambda_2$ *vs.* $\log \lambda_1$ for PVA GEL(D/W) with c=111kg/m^3 and v=30mm/min. The relation between $-\log \lambda_2$ and $\log \lambda_1$ is expressed by a straight line. The slope determined by least-square method was 0.472±0.004. The standard deviation, 0.004 in this case, stands for the scattering of data points in the figure. As is evident from Eq. (2.3), the slope of the line corresponds to μ_o of the sample. The value of μ_o for the samples studied are listed in Table 2-1. There was a linear relation between $-\log \lambda_2$ and $\log \lambda_1$ in all specimens examined in this study, suggesting that μ_o of each sample is constant over a wide range of strain examined here.

The value of μ_o measured at various v for PVA GEL(D/W) at c=111kg/m^3 in solvent and in air are tabulated in Table 2-1. We plotted μ_o against $\dot{\varepsilon}_o$ calculated using v. The plots are shown in Fig. 2-4. The values of μ_o for the samples stretched in solvent show almost the same value in $\dot{\varepsilon}_o$ range of 4.17×10^{-4} s^{-1} to 2.50×10^{-1} s^{-1}. This means that μ_o is almost constant in the time scales used for the experiments. The experimental time scale estimated by $1/\dot{\varepsilon}_o$, is ranging from 4.0×10^{0} s to 2.4×10^{3} s. As is seen from Fig. 2-4, the value of μ_o estimated by extension in air is a little larger than, but almost the same as that in solvent. This suggests that no solvent flow

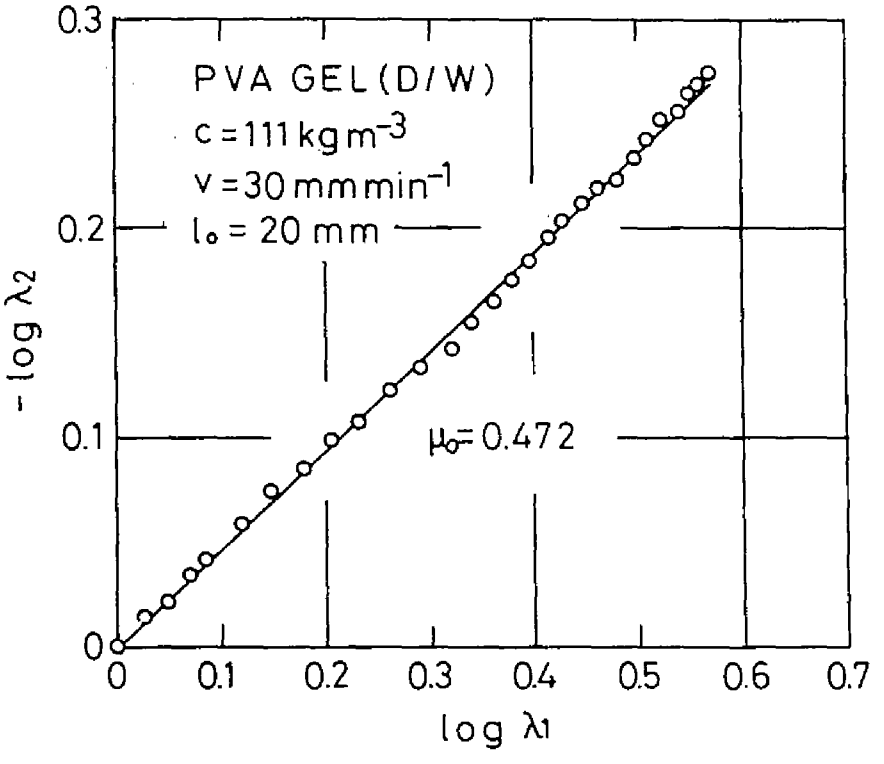

Figure 2-3. Double logarithmic plots of λ_2 *versus* λ_1 for PVAGEL(D/W) at c=111kg/m^3, v=30mm/min.

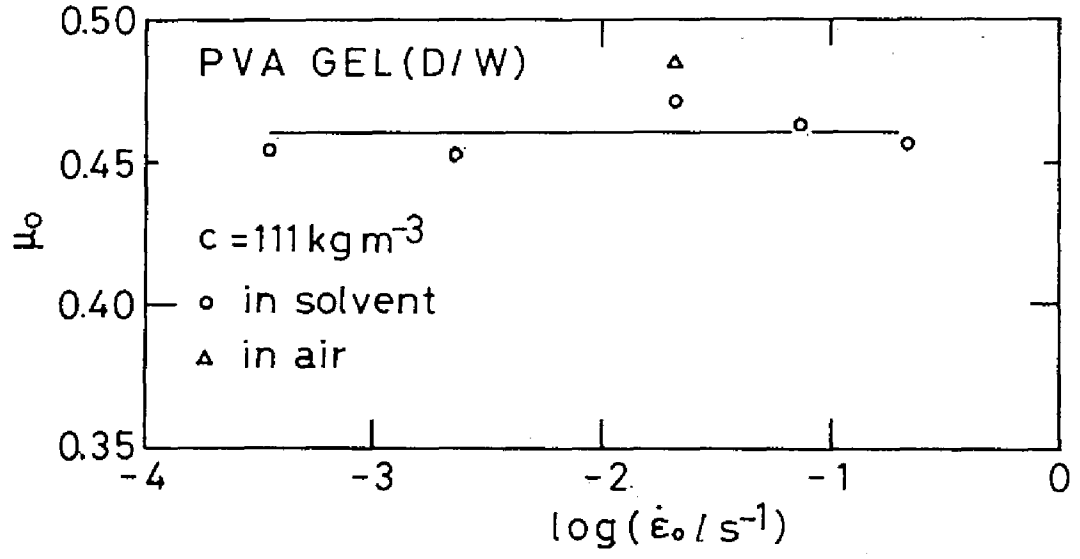

Figure 2-4. Poisson's ratio (μ_o) plotted against the logarithm of the initial rate of strain ($\dot{\varepsilon}_o$) for PVAGEL(D/W) at c=111kg/m^3. Symbols: (○) extension in solvent; (△) extension in air.

between inside and outside of gel occur in the time scale of the experiments in this study.

It was suggested[12,13] that a gel swells because of the increased osmotic pressure due to the stretching in the long time scale, *i.e.*, the strain-induced swelling. This condition is obtained only when $1/\dot{\varepsilon}_0$ is much larger than the characteristic time for the diffusion of network (τ_D), which is order of y^2/D where D is the diffusion constant for the network. The constant D for PVA GEL(D/W) is unknown at present, but D for polyacrylamide-water system was reported to be the order of 10^{-7}cm^2/s.[13,14] Using this value for PVA GEL(D/W), τ_D is roughly estimated as 10^6 s, which is much larger than the experimental time scale in this study. This estimation means that the strain-induced swelling is negligible in the elongational experiments in this study. In order to satisfy the osmotic equilibrium condition, the sample should be elongated at $\dot{\varepsilon}_0$ less than the order of 10^{-6} s^{-1}, where the equilibrium Poisson's ratio μ_∞ is obtained. However, such a slow extensional experiment is difficult to be performed for PVA GEL(D/W) because of aging of the samples. For example, we have observed a stress increase after about 3 hours in the stress relaxation experiment at the fixed strain of 0.05. The increase of stress is due to the aging effects and/or the crystallization caused by orientation. This fact implies that a very slow elongational experiment inevitably involves the structural change in PVA GEL(D/W). On the other hand, polyacrylamide gels in water under a constant uniaxial strain, in which no structural change in the gel occurs in the long time-scale experiments, was reported to show the increase in the width of sample at the long times.[13] As mentioned before, Poisson's ratio obtained under this condition is μ_∞, which differs from μ_0.

2.4.2 Effect of Polymer Concentration and Degree of Crystallinity on μ_o

The values of μ_o measured at v=30mm/min ($\dot{\varepsilon}_o$=2.50×10^{-1} s^{-1}) were plotted against the polymer concentration c in Fig. 2-5. The value of μ_o of PVA GEL (D/W) is independent of c in the range from 75kg/m^3 to 145kg/m^3. The log σ - log ε curves for PVA GEL(D/W) in the c range examined here do not show the shoulder, and the mechanical behavior resembles that of crosslinked rubbers as also reported before.[4] The crosslinking density increases with increasing c. The result shown in Fig. 2-5 indicates that the crosslinking density has little effect on μ_o of PVA GEL(D/W) within the c range examined here.

It was reported[3] that the swelling and mechanical properties of PVA hydrogels are controlled mainly by T_a in course of the hydrogel preparation process. PVA HYDROGEL shows a shoulder on the log σ - log ε curve, and the shoulder is closely related to a breakdown process of the microcrystalline domains which behave as crosslink points. The shoulder becomes pronounced as T_a increases, which originates from the increase in the degree of crystallinity. In this study, the same behavior was also observed: The stress-strain relation is linear at small strains and becomes nonlinear in large strain range. All the points in the plot of $-\log \lambda_2$ *vs.* $\log \lambda_1$ for all specimens of PVA HYDROGEL fall on a straight line over the entire ε range studied here. This clearly suggests that μ_o value for PVA HYDROGEL is kept constant through the whole extension process, regardless of the breakdown of microcrystalline domains. This experimental fact is a little surprising, because it implies that the structural change in the gel has no effect on μ_o.

As can be seen from Table 2-1 and Fig. 2-5, the values of μ_o for PVA HYDROGEL at different T_a are almost identical, suggesting that the crystallinity has little influence upon μ_o for PVA HYDROGEL within the T_a

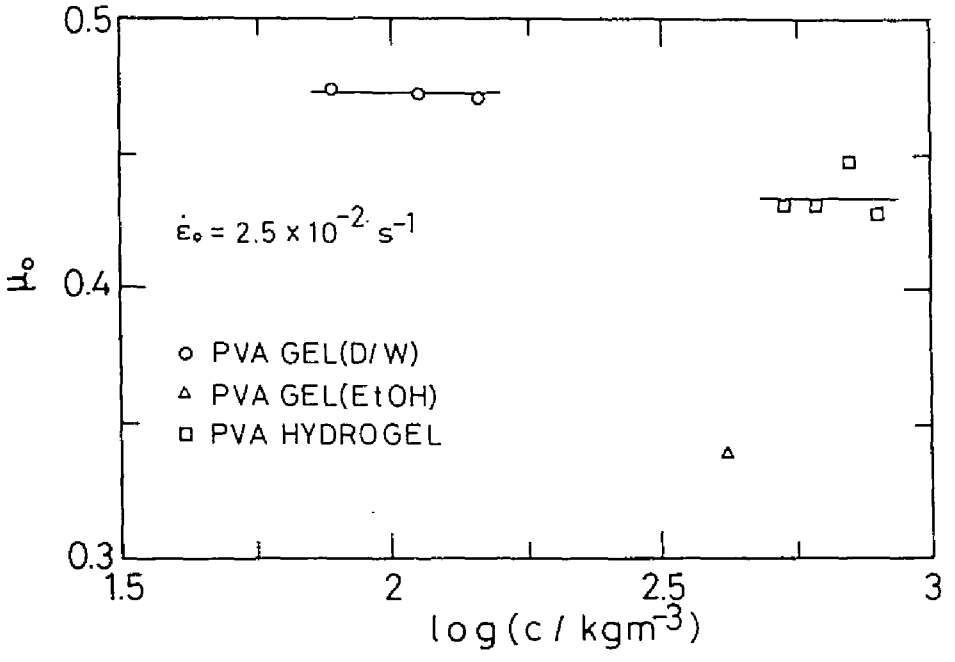

Figure 2-5. Poisson's ratio (μ_o) plotted against the logarithm of the polymer concentration (c) at $\dot{\varepsilon}_o$=2.50×10^{-1} s^{-1}. Symbols: (○) PVA GEL(D/W); (⊡) PVA HYDROGEL; (⏢) PVA GEL(EtOH).

range investigated here. The μ_o values for PVA HYDROGEL were slightly lower than those for PVA GEL(D/W). The difference might be due to the difference in the structure of gel network. Naito reported[14] that water as well as the mixed solvent is a good solvent for PVA. This means that the chains between the crosslinking domains in PVA HYDROGEL and PVA GEL(D/W) are also flexible. The microcrystalline domains in PVA GEL (D/W) which has never been annealed are relatively small.[4] On the other hand, PVA HYDROGEL has the microcrystalline domains with finite sizes formed by annealing.[3] The flexibility of amorphous chains for PVA HYDROGEL should be restricted to some extent near the crosslinking domains. The less flexibility of polymer chains leads to the creation of void in the network structure during elongational deformation. The difference in the degree of flexibility of PVA chains originating from the different size of the microcrystalline domains might explain why μ_o of PVA HYDROGEL is slightly lower than that of PVA GEL(D/W).

2.4.3 Effect of Swelling Solvents on μ_o

The μ_o value of PVA GEL(EtOH) was evaluated to be 0.338, which is much lower than those of PVA GEL(D/W) and PVA HYDROGEL as shown in Fig. 2-5. Ethanol is a poor solvent for PVA. PVA GEL(EtOH) is opaque resulting from a phase-separated structure, which consists of the PVA-rich phase and solvent-rich phase.[4] Most of PVA chains exist in PVA-rich phase. The glass transition temperature (T_g) of PVA has been reported[15] to be 85°C. The PVA chains in PVA GEL(EtOH) are expected to be in glassy state at the measuring temperature (25°C). The flexibility of PVA chains in PVA GEL(EtOH) is much lower than that in PVA GEL (D/W) and PVA

HYDROGEL. The low value μ_o=0.338 obtained for PVA GEL(EtOH) is analogous to the value μ_o=0.33 of a glassy polystyrene.[8]

2.4.4 True Stress-Strain Relations of PVA Gels

Figure 2-6 shows the double logarithmic plots of σ - ε relation for PVA GEL (D/W) with c=111kg/m^3 and v=30mm/min in which σ was calculated with μ_o=0.472 obtained experimentally. The σ - ε relation calculated with μ_o=0.5 is also shown in the figure. The values of σ calculated with μ_o=0.5 are always larger than those with μ_o<0.5, because the calculation with μ_o=0.5 under-estimates the cross-section of the elongated samples. The differences between the two curves are found to be small, though the difference becomes larger as the strain increases. The ratio of σ calculated with μ_o=0.472 to that with μ_o=0.5 is 1.08 at the breaking point (ε=1.41).

Figure 2-7 shows log σ - log ε curves for PVA GEL(D/W) with c=111kg/m^3 at various v. The true stress σ for each sample was calculated with μ_o obtained experimentally. The curves are shifted vertically by a indicated in the figure in order to prevent from overlaps. The values of E_0 for PVA GEL(D/W) at different v are summarized in Table 2-1. The shape of all the curves are identical, and no shoulder is observed. E_0 is independent of v as shown in Table 2-1. This suggests that all curves can be superposed by vertical shifts. The stress relaxation during extension was not observed for PVA GEL(D/W) in $\dot{\varepsilon}_o$ range from 4.17×10^{-4}s^{-1} to 2.50×10^{-1} s^{-1}. On the other hand, the shape of log σ - log ε curve for PVA HYDROGEL was changed depending on $\dot{\varepsilon}_o$ ranging from 1.67×10^{-3} s^{-1} to 5.00×10^{-1} s^{-1},[3] which was closely related with the stress relaxation in course of extension. No indication of stress relaxation during the elongation of PVA GEL (D/W)

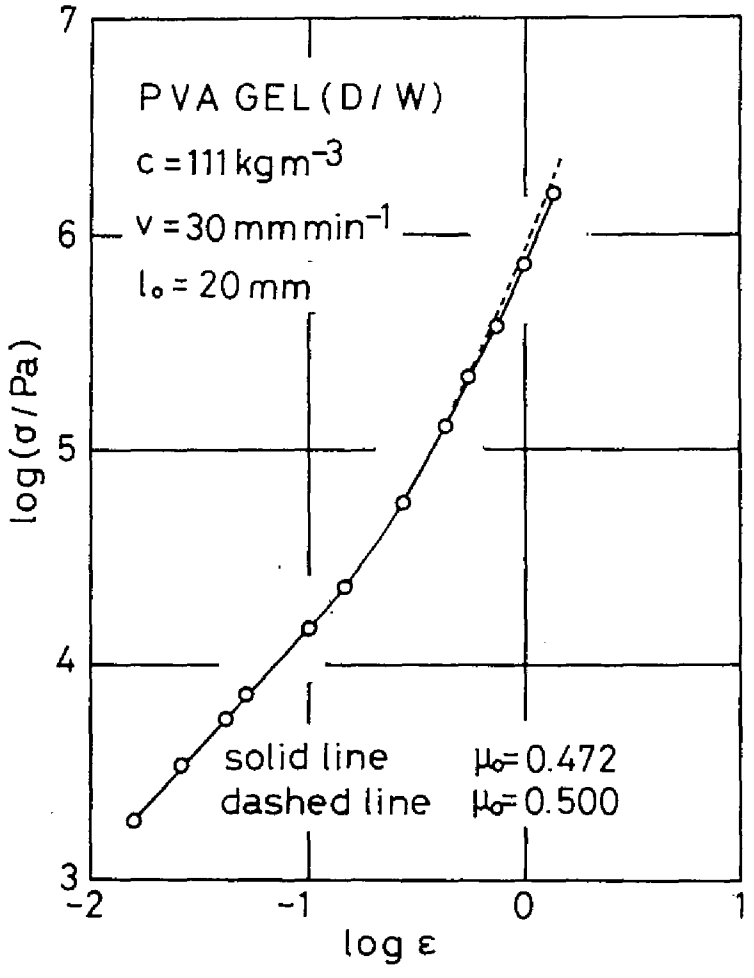

Figure 2-6. Double logarithmic plots of stress (σ) *versus* strain (ε) for PVA GEL(D/W) at c=111kg/m^3. The solid line is for μ_o=0.472; dashed line for μ_o=0.5.

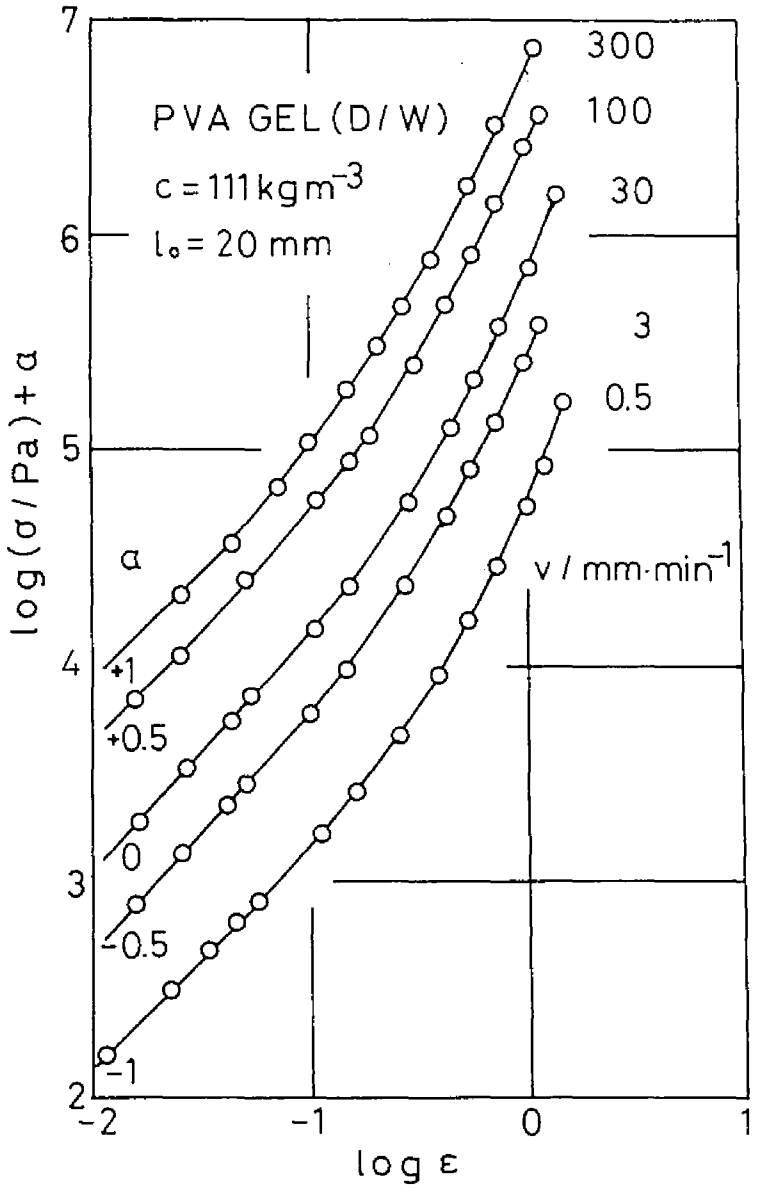

Figure 2-7. Double logarithmic plots of stress (σ) *versus* strain (ε) for PVA GEL(D/W) at c=111kg/m^3. Numerals in the figure indicate the crosshead speed (v).

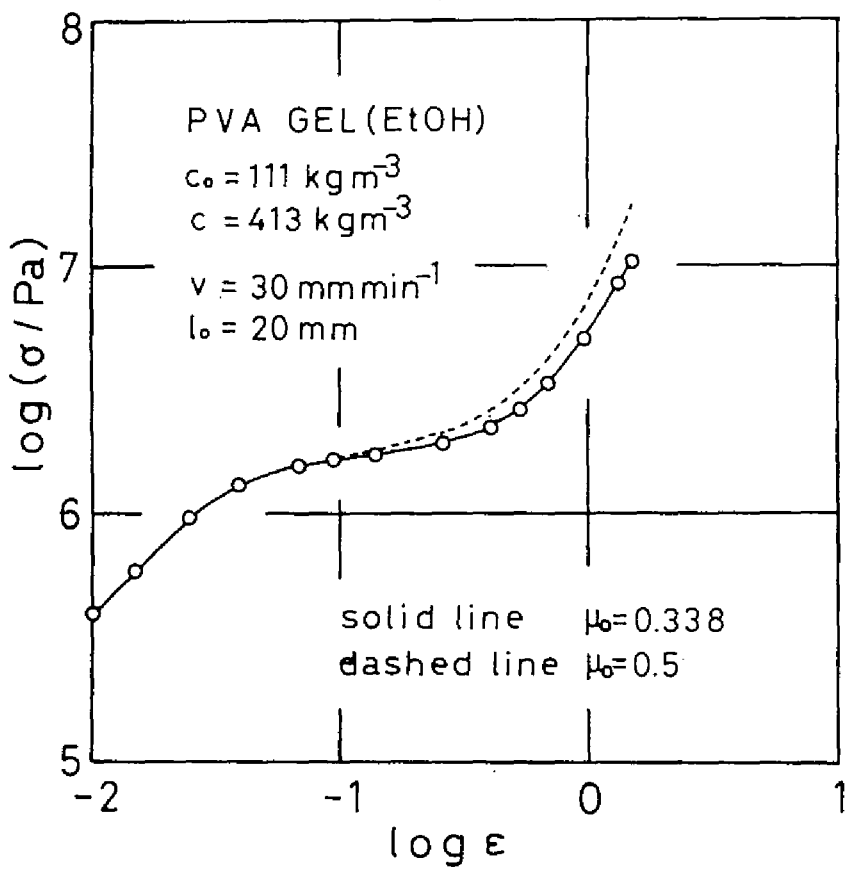

Figure 2-8. Double logarithmic plots of stress (σ) *versus* strain (ε) for PVA GEL(EtOH) at c=413kg/m^3, v=30mm/min. The solid line is for μ_0=0.338; dashed line for μ_0=0.5.

suggest that the size of microcrystalline domains is small, which prevents the stress concentration on the crosslinking domains.

In Fig. 2-8, plots of log σ *vs.* log ε for PVA GEL(EtOH) at c=413kg/m^3 and v=30mm/min are shown. The concentration c was determined by measuring the weight of a equilibrium deswollen gel in ethanol. The concentration c_o is the polymer concentration at which PVA was initially dissolved in the mixed solvent. The true stress σ is calculated by using μ_o=0.338 obtained in this study. For a comparison, the curve obtained by assuming μ_o=0.5 is also shown by a dashed line. The value of E_0 of PVA GEL(EtOH) is listed in Table 2-1. True σ values calculated with μ_o=0.338 is lower than that with μ_o=0.5 in the high ε region. At the breaking point(ε=1.59), the ratio of σ for μ_o=0.338 to that for μ_o=0.5 is 1.67. The curve calculated with μ_o=0.338 shows steeper upturn in high ε region, compared with that with μ_o=0.5. The shoulder in the logσ-logε curve is attributed to the breakdown process of the PVA-rich phase in the two-phase structure.[4]

2.5 Conclusions

The values of Poisson's ratio μ_o for the three types of PVA gels were obtained by uniaxial elongation experiments. The values for PVA gels swollen in a mixed solvent of DMSO and water, which are good solvents for PVA, were close to 0.5, independently of polymer concentration. The annealed PVA gels swollen in water, which have the crosslinking domains in finite size, showed the slightly lower value of μ_o than the unannealed ones. On the other hand, μ_o of PVA gels in ethanol, which is a poor solvent, was much lower than those of PVA gels swollen in good solvents. The difference in μ_o value between those gel samples was explained by the degree of

flexibility of PVA chains. There was a linear relation between $-\log \lambda_1$ and $\log \lambda_2$ over a wide range of ε for each sample, indicating that μ_o is kept constant throughout the whole extension process. It was found that μ_o is time-independent in the relatively short time region, in which no flow of solvent occurs. The true stress-strain curve for each gel was obtained using the experimental value of μ_o.

References

1. Nishinari, K., Watase, M., Ogino, K. and Nambu, M., *Polym. Commun.*, **24**, 345 (1983).
2. Cha, W.-I., Hyon, S.-H. and Ikada, Y., *Macromol. Chem.*, **193**, 1913 (1992).
3. Takigawa, T., Kashihara, H. and Masuda, T., *Polym. Bull.*, **24**, 613 (1990).
4. Takigawa, T., Kashihara, H., Urayama, K. and Masuda, T., *Polymer*, **33** 2335 (1992).
5. Wood, L. A. and Martin, G. M., *Rubber Chem. Technol.*, **37**, 850 (1964).
6. Holownia, B. P. *Rubber Chem. Technol.*, **48**, 246 (1975).
7. Kawabata, S., Matsuda, M., Tei, K. and Kawai, H., *Macromolecules*, **14**, 154 (1981).
8. Badger, R. M. and Blanker, R. H., *J. Phys. Chem.*, **53**, 1056 (1949).
9. Bird, R. B., Armstrong, R. C. and Hassager, O., "*Dynamics of Polymeric Liquids*", Vol.1, John Wiley & Sons, New York, 1977.
10. Yamamoto, M., "*Buttai no henkeigaku (Deformation Theory of Bodies)*", Seibundoshinkosha, Tokyo, 1972.
11. Kamei, E. and Onogi, S. *Appl. Polym. Symp.*, **27**, 19 (1975).
12. Alexander, S. and Rabin, Y., *J. Phys.: Condens. Matter*, **2**, 49 (1990).
13. Takigawa, T., Urayama, K., Morino Y. and Masuda, T., *Polym. J.*, **25**, 929 (1993).
14. Tanaka, T. and Fillmore, D. J., *J. Chem. Phys.*, **70**, 1214 (1979).
15. Naito, R., *Kobunshikagaku*, **15**, 597 (1958).

Chapter 3
Theoretical Studies on Time-Depedent Poisson's Ratio and Mechanical Relaxation of Swollen Networks

3.1 Introduction

Studies on the mechanical properties of polymer gels have been extensively performed by many researchers. Most of them have been concerned with the mechanical properties of the gel itself. In other words, the mechanical tests have been performed in air.[1-4] It was recently reported[5] that an applied constant strain induces a further swelling of equilibrium swollen gels in solvent, and the stress relaxation is caused by the strain-induced swelling. The strain-induced swelling originates from the change of the equilibrium state due to the application of external strain (stress), and the degree of the strain-induced swelling is controlled by the thermodynamics of gel systems. Then, the mechanical behavior of gels in solvent is much more complicated than that in air, because the results obtained by experiments in solvent will be dependent on the thermodynamic properties as well as the mechanical properties of the gel system. The mechanical behavior in solvent is strongly affected by a characteristic time for swelling governed by the diffusional motion. When the experimental time scale is much shorter than the characteristic time for swelling, the results obtained are equivalent to those in the experiments in air, *i.e.*, the thermodynamic effect (the strain-induced swelling) is negligible. Actually, most of the past studies on the mechanical properties of gels have treated this situation. The results shown in Chapter 2 are also obtained in this situation. On the other hand, if the experimental time scale is much longer than the characteristic time for swelling, the results will reflect the thermodynamic properties of the gel

system comprising of the polymer network and the surrounding solvent. In the time scale between the two extreme cases, gels will show the complicated mechanical behavior which is the combination of both the mechanical properties of gel itself and the thermodynamic ones of gel system. One of the physical quantities, which embody this complicated situation, is the time (t) -dependent Poisson's ratio (μ). As described in Chapter 2, the initial Poisson's ratio μ_0 of gels in good solvents was close to 1/2 meaning incompressible. On the other hand, the value of μ at thermodynamic equilibrium, *i.e.*, the equilibrium Poisson's ratio (μ_∞), was reported to be *ca.* 1/6 for polyacrylamide gels in water (good solvent).[5] When the time scale of extension is comparable to that of swelling, the value of μ has an intermediate between μ_0 and μ_∞. In this chapter, the t-dependence of μ for gels in solvent during and after elongation is theoretically and numerically investigated.

The stress relaxation caused by the strain-induced swelling was both theoretically and experimentally investigated for uniaxially stretched gels.[5,6] The degree and process of the stress relaxation in the experiments were well described by a theory based on the thermodynamics and the kinetics for the swelling of constrained gels. The degree and process of the strain-induced swelling and the mechanical relaxation are expected to depend strongly on deformation modes, but the details are unknown at present. In this chapter, we investigate theoretically the strain-induced swelling and the resulting mechanical relaxation (stress relaxation and creep) of gels in solvent under a constant strain or stress applied by the three types of deformation modes; equibiaxial, strip-biaxial(pure shear) and uniaxial streching. The magnitude of the further swelling and mechanical relaxation are derived from the Flory-type free energy for constrained gels. The kinetics of swelling and mechanical relaxation is considered on the basis of the equation of motion for

polymer network and the constitutive equation of gels. We consider here a thin disk-shaped gel in the case of biaxial deformation, and a long rod-shaped gel for uniaxial deformation. The time dependence of the stress relaxation and creep is calculated using the two methods different in the treatment of the process of strain-induced swelling. One assumes the isotropic swelling process (*zero-th order approximation*).[5] The other considers the anisotropic swelling process caused by the difference in the dimensionality of diffusion (*first order approximation*).[6] Which of two methods describes the experimental results more precisely is not clear at present due to the lack of experimental data. Therefore, we employ here these two methods.

In the next section, the basic equations on the theromodynamics and kinetics for the swelling of constrained gels are described. From the basic equations in Section 3-2, the t dependence of μ for a uniaxially stretched gel in solvent during and after elongation is derived (Section 3-3). The dependence of the equilibrium properties for constrained gels on deformation modes is investigated, and the process of mechanical relaxation under each deformation mode is also shown (Section 3-4 and 3-5).

3.2 Basic Equations of Gel Systems

3.2.1 Thermodynamics of Swelling of Gels under Various Constraints

In a Cartesian coordinates, we consider the uniaxial (in x-direction) and biaxial deformation (in x- and y- direction) of an isotropic rectangular gel in solvent, which swells at equilibrium in non-deformed state. The non-deformed state is refered to as the reference state in this study. In Fig. 3-1 we show schematically the 3-dimensional Cartesian coordinates and the kinds of deformations employed in this study. Using a free energy expression

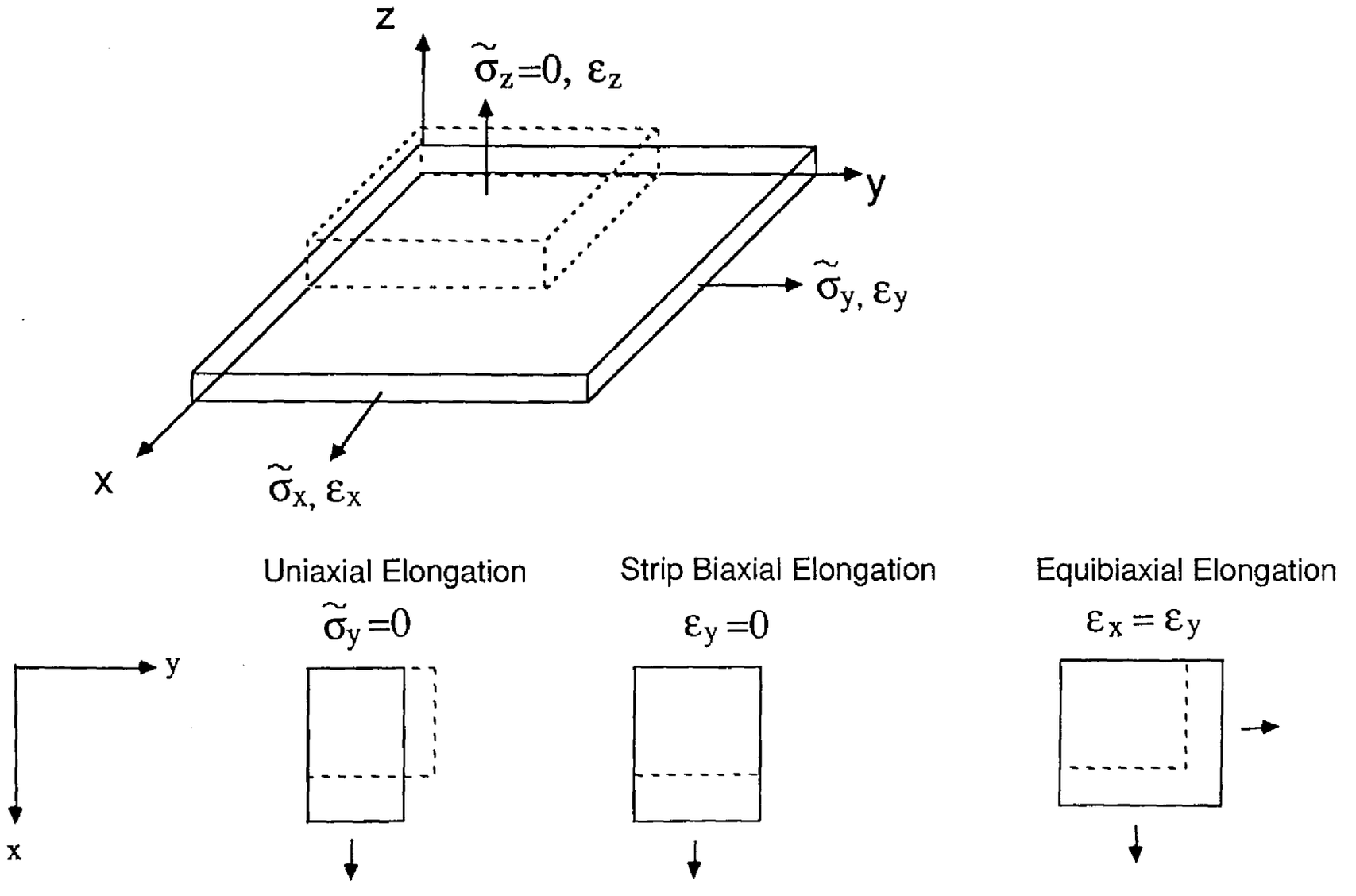

Figure 3-1. Schematic representation for the 3-dimensional coordinates and the types of the deformations employed in this study.

similar to that of a uniaxially stretched gel proposed by Hirotsu *et al.*,[7] we can write the free energy (F) for a biaxially stretched gel as follows.

$$F = F_o + N_s k_B T\{ln(1 - \phi) + \chi\phi\} + \frac{1}{2} N_s k_B T \left\{ \sum_{i=x,y,z} \alpha_i^2 - 3 - ln\left(\frac{V}{V_o}\right) \right\} - \sum_{i=x,y} f_i l_{io} (\alpha_i - 1) \quad (3.1)$$

where F_o is the free energy of pure polymer and solvent, k_B the Boltzmann constant, T the absolute temperature, N_S the number of a solvent molecule, ϕ the polymer volume fraction, χ the polymer-solvent interaction parameter, N_c the number of active chains in the reference state, and f_i the external forces in the i-direction. The quantity, α_i, is a principal ratio in the i-direction, and $\alpha_x\alpha_y\alpha_z=V/V_o=\phi_o/\phi$, where V and V_o are respectively the volumes in deformed and reference state, and ϕ_o is the value of ϕ in the reference state. The shear modulus G_o in the reference state is given by $G_o=N_c k_B T$. We obtain the expression for the uniaxially stretched gels, if $f_y=0$ and $\alpha_y=\alpha_z$ are used in Eq. (3.1). The osmotic stress (π_i, i=x, y and z) acting normally (inward) on the gel surface perpendicular to i-axis is defined as

$$\pi_i = - \frac{1}{\alpha_j \alpha_k} \left(\frac{\partial F}{\partial \alpha_i} \right) \quad (3.2)$$

Hereafter, we deal with the gels with ϕ_o «1, and also ϕ «1. At equilibrium, π_i =0 is satisfied, *i.e.*,

$$-\pi_x = \frac{k_B T}{v_s} (\chi - \frac{1}{2}) \frac{V}{\phi_o^2} + \frac{N_c k_B T}{2\alpha_y \alpha_z} (2\alpha_x - \frac{1}{\alpha_x}) - \frac{f_x}{\alpha_y \alpha_z} = 0 \quad (3.3a)$$

$$-\pi_y = \frac{k_B T}{v_s} (\chi - \frac{1}{2}) \frac{V}{\phi_o^2} + \frac{N_c k_B T}{2\alpha_z \alpha_x} (2\alpha_y - \frac{1}{\alpha_y}) - \frac{f_y}{\alpha_z \alpha_x} = 0 \quad (3.3b)$$

$$-\pi_z = \frac{k_B T}{v_s} (\chi - \frac{1}{2}) \frac{V}{\phi_o^2} + \frac{N_c k_B T}{2\alpha_x \alpha_y} (2\alpha_z - \frac{1}{\alpha_z}) = 0 \quad (3.3c)$$

Here, the quantities $f_x/\alpha_y\alpha_z$ and $f_y/\alpha_x\alpha_z$ correspond to the external stresses ($\tilde{\sigma}_x$ and $\tilde{\sigma}_y$, respectively) exerted normally on the gel surface in the x- and y-

directions. Since $\tilde{\sigma}_x=\tilde{\sigma}_y=0$ and $\pi_i=0$ are satisfied in the reference state ($\alpha_x=\alpha_y=\alpha_z=1$), we obtain

$$N_c = \frac{2\phi_o^2}{v_s}\left(\frac{1}{2}-\chi\right) \tag{3.4}$$

From Eqs. (3.3c) and (3.4), we have

$$\frac{1}{V^2}+\frac{1}{V}-\frac{2\alpha_z}{\alpha_x\alpha_y}=0 \tag{3.5}$$

When the strain is small, Eq. (3.5) is linearlized using the strain ε_i ($\varepsilon_i=\alpha_i-1$). Then, we obtain the relation between ε_x, ε_y and ε_z in equilibrium as follows.

$$\varepsilon_x+\varepsilon_y+5\varepsilon_z=0 \tag{3.6}$$

The linearlized expressions of $\tilde{\sigma}_x$ and $\tilde{\sigma}_y$ for the biaxial deformation are given by

$$\tilde{\sigma}_x=\frac{5}{2}G_o\,\varepsilon_x+\frac{1}{2}G_o\,(\varepsilon_y+\varepsilon_z) \tag{3.7a}$$

and

$$\tilde{\sigma}_y=\frac{5}{2}G_o\,\varepsilon_y+\frac{1}{2}G_o\,(\varepsilon_x+\varepsilon_z) \tag{3.7b}$$

The relation corresponding to Eq. (3.6) and the expression of $\tilde{\sigma}_x$ for the uniaxial deformation are obtained from Eqs. (3.6) and (3.7a) with $\varepsilon_y=\varepsilon_z$, respectively.

3.2.2 Governing Equations for Small Volume Element of Gel

We focus here a small volume element of the gel, which keeps its volume constant during the instantaneous deformation. This is equivalent to the condition that initial Poisson's ratio (μ_o) of the element is 1/2. The stress and strain acting on the small element in the gel ($\boldsymbol{s}$ and $\boldsymbol{u}$) are respectively written by the sum of the external ones ($\tilde{\boldsymbol{s}}$ and $\tilde{\boldsymbol{u}}$) and those induced by the osmotic swelling ($\boldsymbol{s}_{os}$ and $\boldsymbol{u}'$) as

$$\boldsymbol{s} = \tilde{\boldsymbol{s}} + \boldsymbol{s}_{os} \tag{3.8}$$

and

$$\boldsymbol{u} = \tilde{\boldsymbol{u}} + \boldsymbol{u}' \tag{3.9}$$

The expression of $\boldsymbol{s}_{os}$ was obtained by Tanaka *et al.*[8,9] as

$$\boldsymbol{s}_{os} = 2G_o\,(\boldsymbol{u}' - \frac{1}{3}\,\mathrm{tr}(\boldsymbol{u}')\boldsymbol{I}) + K_{os}\,tr(\boldsymbol{u}' - \boldsymbol{u}'_\infty)\boldsymbol{I} \tag{3.10}$$

Here, $\boldsymbol{u}'_\infty$ corresponds to $\boldsymbol{u}'$ at equilibrium, $\boldsymbol{I}$ the unit tensor, K_{os} the osmotic bulk modulus related to the osmotic pressure, and $tr(\boldsymbol{u}')$ means the trace of $\boldsymbol{u}'$, *i.e.*, $tr(\boldsymbol{u}') = u'_{xx} + u'_{yy} + u'_{zz}$. The external stress $\tilde{\boldsymbol{s}}$ for an incompressible material is described by the elasticity theory[10] as follows.

$$\tilde{\boldsymbol{s}} = 2G_o\,\tilde{\boldsymbol{u}} + p\boldsymbol{I} = 2G_o\,(\boldsymbol{u} - \boldsymbol{u}') + p\boldsymbol{I} \tag{3.11}$$

where p is the internal pressure. It is clear from a thermodynamic consideration that the observable stress in experiments is $\tilde{\boldsymbol{s}}$. From the incompressibility of the volume element,

$$tr(\tilde{\boldsymbol{u}}) = tr(\boldsymbol{u} - \boldsymbol{u}') = 0 \tag{3.12}$$

holds at any t. This equation means that the volume of small volume element is not changed by the external deformation. Equation (3.12) generates the relation $tr(\boldsymbol{u})=tr(\boldsymbol{u}')$ implying that the volume change of small volume element is caused only by the swelling. The strain tensor, $\boldsymbol{u}$ and $\boldsymbol{u}'$ are defined by the corresponding displacement vectors $\boldsymbol{v}$ and $\boldsymbol{v}'$ as $u_{ij}=1/2(\partial v_j/\partial i+\partial v_i/\partial j)$ and $u_{ij}'=1/2(\partial v_j'/\partial i+\partial v_i'/\partial j)$. Here, $\boldsymbol{v}$ and $\boldsymbol{v}'$ are specified in the reference (non-deformed) frame. Although we deal here with the case of $\mu_o=1/2$, the constitutive equation corresponding to Eq. (3.11) for the case of $\mu_o\neq1/2$ is expressed by

$$\tilde{\boldsymbol{s}} = 2G_o\,(\boldsymbol{u} - \boldsymbol{u}') + (K_o - \frac{2}{3}\,G_o)\,tr(\boldsymbol{u} - \boldsymbol{u}')\boldsymbol{I} \tag{3.13}$$

where K_o is the bulk modulus related to the compressibility of gel element itself.

The vector v must obey the equation of motion shown by Tanaka *et al.*[8,9] as

$$\zeta \frac{dv}{dt} = div\ s \tag{3.14}$$

where ζ is the friction coefficient between the polymer network and solvent molecule. The time dependence of $\boldsymbol{u}$ is obtained from Eq. (3.14). Although the swelling kinetics can be described by Eq. (3.14), the phenomenon must be written by the combination of s_{os} and v' (or $\boldsymbol{u}'$) because the external deformation does not affect the swelling. Then, we have

$$\zeta \frac{dv'}{dt} = \text{div}\ s_{os} \tag{3.15}$$

Equation (3.15) characterizes the time dependence of the strain-induced swelling. The time dependence of $\tilde{s}$ for the general deformation can be determined by the set of Eqs. (3.14) and (3.15).

It was shown that the equation of motion (Eqs. (3.14) and (3.15)) is generally separated into the two types of the diffusion equations, *i.e.*, the equations of the longitudinal and transverse modes.[5,6] The diffusion equation of the longitudinal mode for $\boldsymbol{u}$ is given by

$$\frac{\partial}{\partial t} tr(\boldsymbol{u}) = D_L\ \nabla^2\ tr(\boldsymbol{u}) \tag{3.16}$$

where D_L is the diffusion coefficient for the longitudinal mode and $D_L=(K_{os}+4/3G_o)/\zeta$. The diffusion equation of the transverse mode for $\boldsymbol{u}$ is given by

$$\frac{\partial}{\partial t} rot(\boldsymbol{v}) = D_T\ \nabla^2\ rot(\boldsymbol{v}) \tag{3.17}$$

where D_T is the diffusion coefficient for the transverse mode and $D_T=G_o/\zeta$. As is clear from the definition of Eqs. (3.16) and (3.17), the longitudinal mode controls the volume change for the small volume elements, while the transverse mode governs the shape change without the volume change.

3.2.3 Time Dependence of Strain-Induced Swelling

As described in the later sections, the time dependence of μ, and the process of the stress relaxation and creep are controled by the time dependence of the strain-induced swelling ($\boldsymbol{u}'(t)$). Here, we employ the two methods (zero-th and first order approximation) in order to obtain $\boldsymbol{u}'(t)$. We consider the thin rectangular disk of which thickness is much smaller than its widths for the biaxial deformation, and the long rectangular rod whose widths are much smaller than its height for the uniaxial deformation.

3.2.3.1 Zero-th Order Approximation. This approximation assumes the isotropic process for the strain-induced swelling, irrespective of the gel geometry. This assumption means that $u'_{xx}(t) = u'_{yy}(t) = u'_{zz}(t) = (1/3)tr(\boldsymbol{u}')$. Accordingly, the time dependence of $\boldsymbol{u}'$ is equivalent to that of $tr(\boldsymbol{u}')$. The time dependence of $tr(\boldsymbol{u}')$ is obtained by solving Eq. (3.16) with the appropriate initial and boundary conditions. For the biaxially stretched gels, since the sizes in the stretching directions (x- and y-directions) are so long compared to the thickness (in the z-direction), the diffusions in the x- and y-directions are negligible. Then, Eq. (3.16) must be solved as the $1D$ (z-direction) diffusion problem. The initial condition is given by

$$tr(\boldsymbol{u}') = 0 \qquad \text{at } t=0. \tag{3.18}$$

The boundary condition can be written as follows.

$$tr(\boldsymbol{u}') = tr(\boldsymbol{u}'_\infty) \qquad \text{at boundaries.} \tag{3.19}$$

Equation (3.19) means that the osmotic stress acting on the small element at the boundaries is zero at any $t(>0)$. The value of $tr(\boldsymbol{u}'_\infty)$ is determined by the degree of swelling at equilibrium, depending on the deformation mode, and will be shown later. The solution of Eq. (3.16) satisfying the above conditions is

$$tr(\boldsymbol{u}') = tr(\boldsymbol{u}'_\infty)\{\sum_{l}^{\text{odd}} A_l \sin\frac{l\pi}{a_r} z \exp(-k_l t) + 1\} \tag{3.20}$$

Here, a_r is the size of gel in the z-direction in the reference state, and A_l and k_l are the constants given by $A_l=-4/l\pi$ and $k_l=D_L\pi l^2/a_r^2=l^2/\tau_L$, where τ_L is the longest characteristic time of the longitudinal mode and l an odd integer.

In the case of uniaxial (x-direction) deformation, Eq. (3.16) can be solved as a $2D$ diffusion problem because the diffusional motion in the x-direction is negligible. The solution of Eq. (3.16) satisfying the Eqs. (3.18) and (3.19) for an uniaxially stretched gel is

$$tr(\boldsymbol{u}') = tr(\boldsymbol{u}'_\infty)\{\sum_{m}^{\text{odd}}\sum_{n} B_{mn} \sin\frac{m\pi}{a_r} y \sin\frac{n\pi}{a_r} z \exp(-k_{mn} t) + 1\} \tag{3.21}$$

Here, a_r is the size of gel in the y- and z-direction in the reference state, and B_{mn} and k_{mn} are $B_{mn}=-16/mn\pi^2$ and $k_{mn}=D_L\pi^2(m^2+n^2)/a_r^2=(m^2+n^2)/2\tau_L$, where m and n are odd integers.

3.2.3.2 First Order Approximation. Since the diffusions in the stretching directions (x- and y- directions) can be assumed not to occur in the case of the biaxial stretching, $\boldsymbol{v}'$ of a rectangular gel can be assumed by

$$v_x' = u'_{xx}(z)\, x \tag{3.22a}$$

$$v_y' = u'_{yy}(z)\, y \tag{3.22b}$$

$$v_z' = v_z'(z) \tag{3.22c}$$

and $u'_{xx}=u'_{yy}$ holds. From Eqs. (3.15) and (3.22a), the following equation is obtained.

$$\frac{\partial}{\partial t}u'_{xx} = D_T \nabla^2 u'_{xx} \tag{3.23}$$

The initial condition of Eq. (3.23) is given by

$$u'_{xx} = 0 \qquad \text{at } t = 0. \tag{3.24}$$

The boundary condition is expressed as follows.

$$u'_{xx} = u'_{xx\infty} = \frac{1}{3} tr(\boldsymbol{u}'_{\infty}) \qquad \text{at boundaries.} \tag{3.25}$$

Here, $u'_{xx\infty}$ corresponds to u'_{xx} at $t\to\infty$. Equation (3.23) has the following solution.

$$u'_{xx} = \frac{1}{3} tr(\boldsymbol{u}'_{\infty})\{\sum_{l}^{\text{odd}} A_l \sin\frac{l\pi}{a_r} z \ \exp(-k'_l t) + 1\} \tag{3.26}$$

Here, $k'_l=D_T\pi l^2/a_r^2 = l^2/\tau_T$, where τ_T is the longest characteristic time of the transverse mode.

Since the diffusion in the x-direction is negligible, $\boldsymbol{v}'$ in the uniaxial (x-direction) deformation is assumed by

$$v'_x = u'_{xx}(y,z)\, x \tag{3.27a}$$

$$v'_y = v'_y(y,z) \tag{3.27b}$$

$$v'_z = v'_z(y,z) \tag{3.27c}$$

The solution of Eq. (3.23) for the uniaxial deformation is written as follows.

$$u'_{xx} = \frac{1}{3} tr(\boldsymbol{u}'_{\infty})\{\sum_{m\ n}^{\text{odd}} B_{mn} \sin\frac{m\pi}{a_r} y \ \sin\frac{n\pi}{a_r} z \ \exp(-k'_{mn} t) + 1\} \tag{3.28}$$

where $k'_{mn}=D_T\pi^2(m^2+n^2)/a_r^2 = (m^2+n^2)/2\tau_T$.

3.3 Time Dependence of Poisson's Ratio of Gels

Here, we derive the t dependence of μ for the uniaxially stretched gels in solvent during and after elongation at a constant strain rate ($\dot{\varepsilon}$). The global value of Poisson's ratio ($\overline{\mu}$) for the uniaxially stretched gel is defined using the global strain ε as

$$\overline{\mu} = -\frac{\varepsilon_{\perp}}{\varepsilon_{\parallel}} \tag{3.29}$$

where $\varepsilon_{\parallel}$, and $\varepsilon_{\perp}$ are the global strains paralell and perpendicular to the stretching direction, respectively.

3.3.1 Two Types of Limiting Values of Poisson's Ratio

Poisson's ratio μ of gels is a t-dependent quantity, and the two limiting values of μ (μ_o and μ_∞) are defined corresponding to the two limiting case. One is the case where the strain-induced swelling does not occur ($t \to 0$). The other is the case where the equilibrium of the strain-induced swelling is achieved ($t \to \infty$). The initial Poisson's ratio μ_o reflects the compressibility of gel itself, and is related to the other elastic constants as[10]

$$\mu_o = \frac{3K_o - 2G}{2(3K_o + G)} \tag{3.30}$$

where K_o is the bulk modulus of gel itself, and G is the shear modulus. The equilibrium Poisson's ratio μ_∞ reflects the osmotic compressibility of the gel system comprising of the polymer network and the surrounding solvent, and has the following relation:

$$\mu_\infty = \frac{3K_{os} - 2G}{2(3K_{os} + G)} \tag{3.31}$$

where K_{os} is the osmotic bulk modulus for the gel system. Since G in Eqs. (3.30) and (3.31) is considered to be same, the qualitative difference between μ_o and μ_∞ is equivalent to that between K_o and K_{os}.

3.3.2 Time-Dependent Poisson's Ratio

The each component of $\boldsymbol{u}$ in process of uniaxial (x-directional) elongation is obtained from Eq. (3.9) as follows.

$$u_{xx} = \dot{\varepsilon}\, t \tag{3.32a}$$

$$u_{yy} = u_{zz} = -\mu_0 \dot{\varepsilon}\, t + \frac{1}{2} tr(\boldsymbol{u}') \tag{3.32b}$$

Here, $u_{xx} = \dot{\varepsilon}\, t$, and $\boldsymbol{u}' = (1/3)tr(\boldsymbol{u}')$ were used. The t dependence of $tr(\boldsymbol{u}')$ is given by Eq. (3.21). The global strain $\varepsilon_\perp$ is obtained by averaging u_{yy} over the y-z plane,

$$\varepsilon_\perp(t) = \frac{\int u_{yy}\, dS'}{\int dS'} \cong \frac{\int u_{yy}\, dS}{\int dS} = \frac{1}{a_r^2} \int_0^{a_r} dy \int_0^{a_r} dz \left(-\mu_0 \dot{\varepsilon}\, t + \frac{1}{2} tr(\boldsymbol{u}')\right) \tag{3.33}$$

where $dS'=(1+u_{yy}+u_{zz})dS$ and $dS=dydz$. The strain $\varepsilon_\perp(t)$ can be also written on the basis of the Boltzmann superposition principle with employing a response function ($m(t-t')$) and $\dot{\varepsilon}$ as

$$\varepsilon_\perp(t) = \int_0^{t''} m(t-t')\, \dot{\varepsilon}\, dt' \tag{3.34}$$

and $\varepsilon_\parallel$ is expressed as

$$\varepsilon_\parallel(t) = \int_0^{t''} \dot{\varepsilon}\, dt' \tag{3.35}$$

The time t'' is the time interval in which strain is imposed, and $t''=t$ corresponds to the elongational process, while $t''=t_0$=const to the swelling process after the completion of the imposition of x-directional strain. The explicit form of $m(t-t')$ is given by comparing Eq. (3.34) with Eqs. (3.21) and (3.33) as follows.

$$m(t-t') = \frac{1}{2a_r^2} \int_0^{a_r} dy \int_0^{a_r} dz \left\{ \sum_{m\ n}^{\text{odd}} \frac{-32(\mu_0 - \mu_\infty)}{mn\pi^2} \right.$$

$$\left. \times \sin\frac{m\pi}{a_r} y\ \sin\frac{n\pi}{a_r} z\ \exp[-k'_{mn}(t-t')] - 2\mu_\infty \right\} \tag{3.36}$$

3.4 Stress Relaxation of Gels

3.4.1 Equibiaxial Case

Let us discuss the stress relaxation of the gel stretched globally with $\varepsilon_x=\varepsilon_y=\varepsilon_o$ at $t=0$. The quantity, ε, is the global strain, while $\boldsymbol{u}$, $\boldsymbol{u}'$ and $\bar{\boldsymbol{u}}$ are local strains defined for small volume element. In the case of the equibiaxial deformation ($u_{xx}=u_{yy}=\varepsilon_o$), we have $u_{zz}-u'_{zz}=-2(\varepsilon_o-u'_{xx})$ from the relation $tr(\bar{\boldsymbol{u}})=0$. From Eq. (3.11) and $\hat{s}_z=0$, $\hat{s}_x$ ($=\hat{s}_y$) can be written by

$$\hat{s}_x = \hat{s}_y = 6G_o\,(\varepsilon_o - u'_{xx}) \tag{3.37}$$

The quantity, $\boldsymbol{s}$, is the local stress related to the small volume element. The t dependence of global (average) external stress, $\tilde{\sigma}_x(t)(=\tilde{\sigma}_y(t))$, can be expressed by

$$\tilde{\sigma}_x(t) = \frac{\int \hat{s}_x \; dz'}{\int dz'} \cong \frac{\int \hat{s}_x \; dz}{\int dz} = \frac{6G_o}{a_r}\int_0^{a_r} (\varepsilon_o - u'_{xx})\, dz \tag{3.38}$$

where $dz'=(1+u_{zz})dz$. In the 0-th order approximation, u'_{xx} is substituted by $(1/3)tr(\boldsymbol{u}')$, which is represented by Eq. (3.20), while in the 1st order approximation, Eq. (3.26) is applied to u'_{xx}.

3.4.2 Strip-Biaxial Case

Let us consider here the stress relaxation of the gel stretched with $\varepsilon_x=\varepsilon_o$ and $\varepsilon_y=0$ at $t=0$. From Eq. (3.12) and $u_{yy}=0$, we get $u_{zz}-u'_{zz}=-(\varepsilon_o-2u'_{xx})$. From Eq. (3.11) and $\hat{s}_z=0$, $\hat{s}_x$ and $\hat{s}_y$ can be respectively written by

$$\hat{s}_x = 4G_o\,(\varepsilon_o - \frac{3}{2}u'_{xx}) \quad \text{and} \quad \hat{s}_y = 2G_o\,(\varepsilon_o - 3u'_{xx}) \tag{3.39}$$

The global external stress, $\tilde{\sigma}_x(t)$ and $\tilde{\sigma}_y(t)$, can be obtained in the same way as Eq. (3.38). In the 0-th and 1st order approximations, the time dependence of u'_{xx} is calculated by using Eqs. (3.20) and (3.26), respectively.

3.4.3 Uniaxial Case

The uniaxially stretched gel with $\varepsilon_x=\varepsilon_o$ at $t=0$ is discussed here. From Eq. (3.12), we get $u_{yy}-u'_{yy}=-(1/2)(\varepsilon_o-u'_{xx})$. From Eq. (3.11) and $\hat{s}_y=\hat{s}_z=0$, $\hat{s}_x$ can be written by

$$\hat{s}_x = 3G_o\,(\varepsilon_o - u'_{xx}) \tag{3.40}$$

The quantity, $\tilde{\sigma}_x(t)$, can be expressed by

$$\tilde{\sigma}_x(t) = \frac{\int \hat{s}_x\, dS'}{\int dS'} \cong \frac{\int \hat{s}_x\, dS}{\int dS} = \frac{3G_o}{a_r^2}\int_0^{a_r} dy \int_0^{a_r} dz\,(\varepsilon_o - u'_{xx}) \tag{3.41}$$

Equations (3.21) and (3.28) is used for the time dependence of u'_{xx} in the 0-th and 1st order approximations, respectively.

3.5 Creep Behavior of Gels

3.5.1 Equibiaxial Case

We now discuss the creep behavior of the gel under constant stresses of $\tilde{\sigma}_x=\tilde{\sigma}_y=\sigma_o$ at $t>0$. The equation $tr(\tilde{\boldsymbol{u}})=0$ gives $2u_{xxo}+u_{zzo}=0$, where u_{xxo} and u_{zzo} correspond to u_{xx} and u_{zz} at $t=0$, respectively. The t dependent local strains, $u_{xx}(t)(=u_{yy}(t))$ and $u_{zz}(t)$ can be expressed from Eq. (3.9) as follows.

$$u_{xx}(t) = u_{yy}(t) = u_{xxo} + u'_{xx} \tag{3.42a}$$

$$u_{zz}(t) = -\,2u_{xxo} + u'_{zz} \tag{3.42b}$$

The t dependent global (average) strain, $\varepsilon_x(t)$ $(=\varepsilon_y(t))$ and $\varepsilon_z(t)$ can be expressed respectively as

$$\varepsilon_x(t) = \frac{\int u_{xx}(t)\, dz'}{\int dz'} \cong \frac{\int u_{xx}(t)\, dz}{\int dz} = \frac{1}{a_r}\int_0^{a_r} (u_{xxo} + u'_{xx})\, dz \tag{3.43a}$$

$$\varepsilon_z(t) \cong \frac{\int u_{zz}(t)\, dz}{\int dz} = \frac{1}{a_r}\int_0^{a_r} (-2u_{xxo} + u'_{zz})\, dz \tag{3.43b}$$

In the 0-th order approximation, u'_{xx} and u'_{zz} are replaced by $(1/3)tr(\boldsymbol{u}')$, which is shown by Eq. (3.20). In the 1st order approximation, the time dependence of u'_{xx} has been given by Eq. (3.26), and u'_{zz} is given from Eqs. (3.20) and (3.26) by

$$u'_{zz} = tr(\boldsymbol{u}'_{\infty})\{\sum_{l}^{\text{odd}} A_l \sin\frac{l\pi}{a_r} z \exp(-k_l t) - \frac{2}{3}\sum_{l}^{\text{odd}} A_l \sin\frac{l\pi}{a_r} z \exp(-k_l' t) + \frac{1}{3}\} \tag{3.44}$$

Equation (3.44) shows that the time dependence of u'_{zz} is governed by longitudinal and transverse modes. It should be noted that in both the 0-th and 1st order approximations, the time dependence of u_{zz} in the stress relaxation experiment where u_{xx} (and u_{yy}) is fixed is governed by only the longitudinal mode, regardless of the deformation mode.

3.5.2 Strip-Biaxial Case

Let us discuss here the creep behavior of the gel under constant stress $\tilde{\sigma}_x = \sigma_o$ holding $\varepsilon_y=0$ at $t>0$. Differing from the case of equibiaxial and uniaxial deformation, u_{yy} and u_{zz} are time dependent, while $\tilde{u}_{xx}=u_{xxo}$ is time independent. This results from that $u_{yy}=0$ and $u'_{yy}\neq 0$, and means that the stress relaxation occurs in y-direction. The relation that $u_{zz}=-u_{xxo}+u'_{yy}$ is obtained from $tr(\tilde{\boldsymbol{u}})=0$. From Eq. (3.6), $u_{xx}(t)$, $u_{yy}(t)$ and $u_{zz}(t)$ can be expressed by

$$u_{xx}(t) = u_{xxo} + u'_{xx} \tag{3.45a}$$

$$u_{yy}(t) = \tilde{u}_{yy} + u'_{yy} = 0 \tag{3.45b}$$

$$u_{zz}(t) = u_{zz} + u'_{zz} = -u_{xxo} + u'_{xx} + u'_{zz} \tag{3.45c}$$

The global strain, $\varepsilon_x(t)$ and $\varepsilon_z(t)$, can be calculated in the same way as Eq. (3.43). The treatments of u'_{xx} and u'_{zz} in the 0-th and 1st order

approximations are the same as in the case of the equibiaxial deformation except the value of $tr(\boldsymbol{u}'_\infty)$.

3.5.3 Uniaxial Case

Now let us consider the creep behavior of the gel under constant stress $\tilde{\sigma}_x=\sigma_0$ at $t>0$. In the case of uniaxial deformation, $tr(\tilde{\boldsymbol{u}})=0$ corresponds $u_{xxo}+2u_{yyo}=0$. From Eq. (3.6), $u_{xx}(t)$ and $u_{yy}(t)$ $(=u_{zz}(t))$ can be written by

$$u_{xx}(t) = u_{xxo} + u'_{xx} \tag{3.47a}$$

$$u_{yy}(t) = u_{zz}(t) = -\frac{1}{2}u_{xxo} + u'_{yy} \tag{3.47b}$$

The calculation of $\varepsilon_x(t)$ and $\varepsilon_y(t)$ $(=\varepsilon_z(t))$ is indentical with Eq. (3.33). In the 0-th order approximation, u'_{xx} and u'_{yy} are substituted by $(1/3)tr(\boldsymbol{u}')$ using Eq. (3.21). In the first approximation, the time dependence of u'_{xx} is described by Eq. (3.28), and that of u'_{yy} is obtained by using Eq. (3.21) and (3.28) as follows.

$$u'_{yy} = tr(\boldsymbol{u}'_\infty)\{\frac{1}{2}\sum_{m\ n}^{\text{odd}} B_{mn}\sin\frac{m\pi}{a_r}y\sin\frac{n\pi}{a_r}z\exp(-k_{mn}t)$$

$$-\frac{1}{6}\sum_{m\ n}^{\text{odd}} B_{mn}\sin\frac{m\pi}{a_r}y\sin\frac{n\pi}{a_r}z\exp(-k'_{mn}t) + \frac{1}{3}\} \tag{3.48}$$

The longitudinal and transverse modes are involved in the time dependence of u'_{yy} and u'_{zz} under uniaxial deformation as well as that of u'_{zz} under biaxial deformation.

3.6 Numerical Results and Discussion

3.6.1 Time Dependence of Poisson's Ratio

The t dependence of $\bar{\mu}$ is given by Eqs. (3.29) and (3.34)-(3-36). Figure 3-2 shows the t-dependence of the reduced value of $\bar{\mu}$ calculated for the $\dot{\varepsilon}\tau_L$ values of 0.01, 0.1, 1, and 10. In calculations, the strain imposed (ε_0) was fixed to be 0.1, and μ_0=1/2 was used. The value of μ_∞ used was 1/6, and was obtained from thermodynamic calculation for the degree of swelling of uniaxially stretched gel systems.[5] The curves show the discontinuous change in the slope at the time when elongation stops; the value of $\bar{\mu}$ shows the steep decrease at t''_0. It is clearly seen that the curves form the envelopes. We drew here the upper envelope as the t-dependence curve for $\dot{\varepsilon}\tau_L$=0.001, and the lower one as the curve for $\dot{\varepsilon}\tau_L$=10000. These are shown by solid curves in the figure. The upper envelope corresponds to the t-dependence for the elongational process, and the lower the swelling after uniaxial deformation. The difference between the two envelopes is due to whether the effect of μ_0 during the increasing deformation is simultaneously introduced in the time dependence of $\bar{\mu}$. Namely, $\bar{\mu}$ obtained in the elongational process is determined by both of the osmotic swelling and the increasing external deformation of the gel, but $\bar{\mu}$ in the swelling under a constant deformation depends only on the osmotic swelling process. This results in the higher value of $\bar{\mu}$ in the elongational process than that in the swelling after deformation in an intermediate time region. The two envelopes, however, coincide with each other at the short and long time limits.

3.6.2 Stress Relaxation of Gels

Equations (3.6) and (3.7) give the equilibrium stress and the equlibrium degree of strain-induced swelling for the gel deformed by an arbitrary biaxial

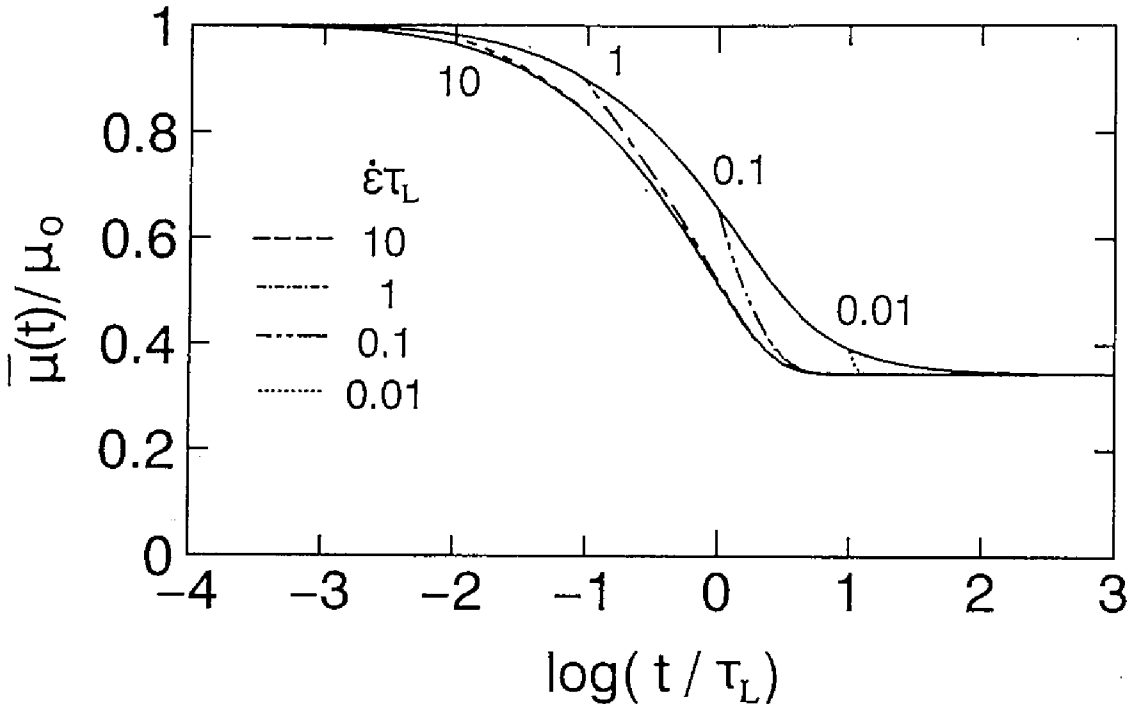

Figure 3-2. The time (t) dependence of Poisson's ratio ($\bar{\mu}$) for various $\dot{\varepsilon}\,\tau_L$. t is reduced by the longest characteristic time for longitudinal mode (τ_L) and $\bar{\mu}$ by the value at the short time limit (μ_o). The numerals in the figure stand for the value of $\dot{\varepsilon}\,\tau_L$.

deformation. Table 3-1 summarizes the numerical results with respect to the initial and equilibrium stress, the magnitude of stress reduction, and the degree of strain-induced swelling for the gel under the equi-, strip-biaxial and uniaxial deformation.

Figure 3-3 shows the stress relaxation curves under various deformation modes. In the figure, t and $\tilde{\sigma}$ are respectively reduced by τ_L and $\tilde{\sigma}_0$ corresponding to $\tilde{\sigma}$ at t=0. The dashed and solid curves indicate the results calculated on the basis of the 0-th and 1st order approximations, respectively. As is evident from the treatment, the stress relaxation processes in the 0-th and 1st order approximations are governed by the longitudinal and transverse modes, respectively. In the 1st order approximation, $\tau_T=(5/2)\tau_L$ was assumed.[6] The solid curves for transverse mode are shifted to long time region compared with the dashed curves for longitudinal mode, but the shape of the solid and dashed curves is similar to each other. As can be seen in Fig. 3-3, the magnitude of stress reduction at $t\to\infty$ under each deformation mode is much different. The order of the magnitude of the stress reduction is

$\Delta\tilde{\sigma}_y$ (strip biaxial) > $\Delta\tilde{\sigma}_x$ (equibiaxial) > $\Delta\tilde{\sigma}_x$(strip biaxial) > $\Delta\tilde{\sigma}_x$(uniaxial)

The magnitude of the stress reduction is controlled by the value of $tr(\boldsymbol{u}'_\infty)$. The anisotropy in magnitude of stress reduction in strip-biaxial deformation results from the anisotropy in the deformation itself, which is represented by the coefficients of u'_{xx} different in x- and y-directions in Eq. (3.39).

The stress relaxation curves under various deformation modes are shown in Fig. 3-4. The quantities, t and σ are respectively reduced by τ_L and the initial stress $6G_0\varepsilon_0$ in equibiaxial deformation. In Fig. 3-4, the absolute value of stress in imposing a strain ε_0 in each deformation mode can be compared with each other. The dashed and solid curves indicate the calculation results for the longitudinal and transverse modes, respectively.

Table 3-1. Degree of volume increase, equilibrium stress, and the degree of stress reduction of the gels under the constant strain by equi-, strip-biaxial and uniaxial deformations.

	Degree of Volume Increase	Initial Stress	Equilibrium Stress	Degree of Stress Reduction
	$(\Delta V/V_o)$[1]	$(\tilde{\sigma}_{io})$	$(\tilde{\sigma}_{i\infty})$	$(\Delta\tilde{\sigma}_i)$[2]
Equibiaxial	$\frac{8}{5}\varepsilon_o$	$6G_o\varepsilon_o$	$\frac{14}{5}G_o\varepsilon_o$	~0.53
Strip-biaxial (x)	$\frac{4}{5}\varepsilon_o$	$4G_o\varepsilon_o$	$\frac{12}{5}G_o\varepsilon_o$	~0.40
(y)		$2G_o\varepsilon_o$	$\frac{2}{5}G_o\varepsilon_o$	~0.80
Uniaxial	$\frac{2}{3}\varepsilon_o$	$3G_o\varepsilon_o$	$\frac{7}{3}G_o\varepsilon_o$	~0.22

1) $\Delta V/V_o = \mathrm{tr}(\boldsymbol{u}_\infty)$ 2) $\Delta\tilde{\sigma}_i = \dfrac{\tilde{\sigma}_{io} - \tilde{\sigma}_{i\infty}}{\tilde{\sigma}_{io}}$

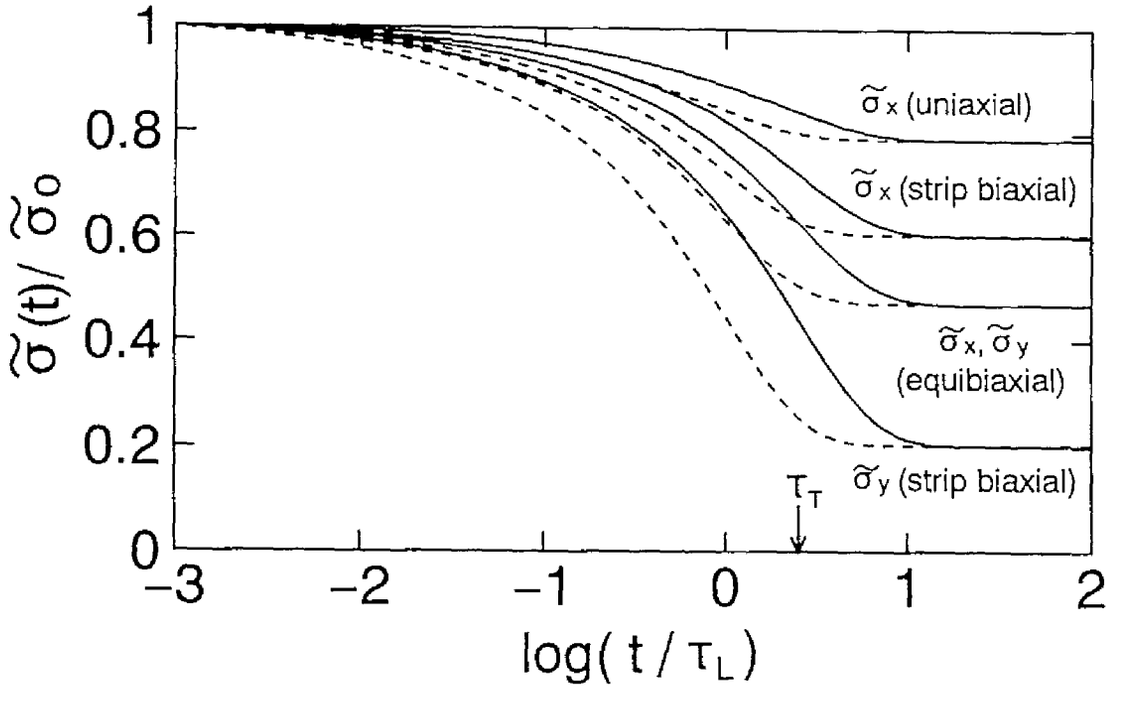

Figure 3-3. Stress relaxation curves under uniaxial, equibiaxial and strip biaxial deformations. Dashed and solid curves indicate the results for the 0-th and 1st order approximations, respectively. Time t and stress $\sigma(t)$ are respectively reduced by the longest characteristic time of longitudinal mode τ_L and the initial stress σ_0 for each deformation mode.

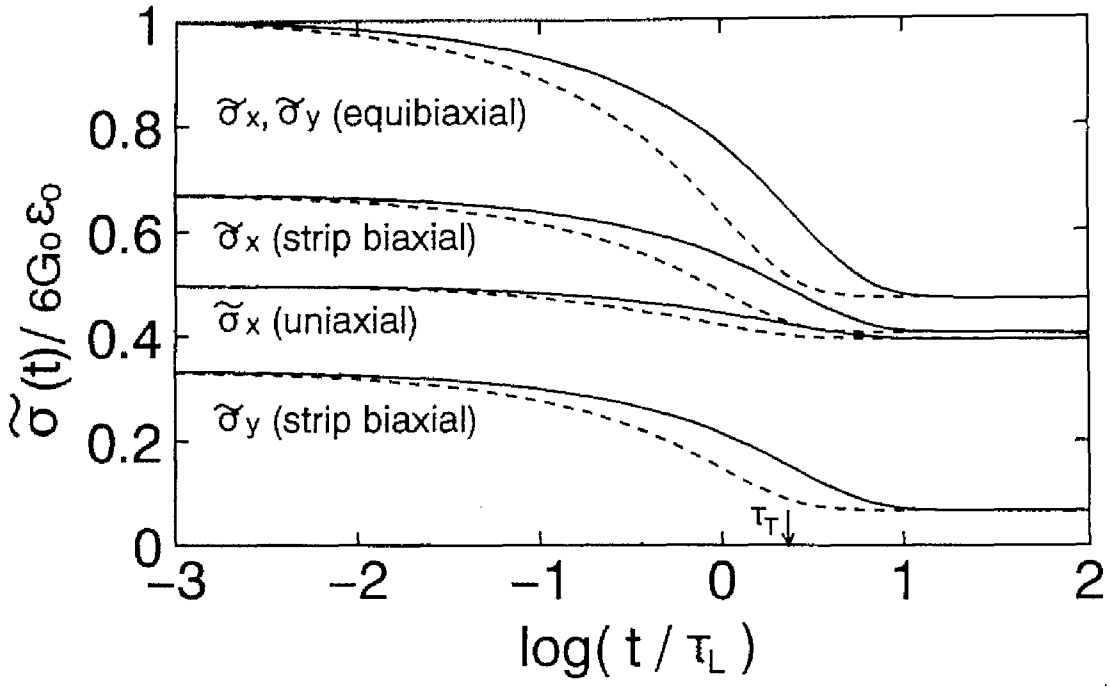

Figure 3-4. Time (t) dependence of stress $\sigma(t)$ under uniaxial, equibiaxial and strip biaxial deformations. Dashed and solid curves indicate the results for the 0-th and 1st order approximations, respectively. t and $\sigma(t)$ are reduced by the longest characteristic time of longitudinal mode τ_L and $6G_0\varepsilon_0$(G_0; shear modulus, ε_0; initial strain), respectively.

The ratio of the stress at t=0 for each deformation mode is 6 : 4 : 3 : 2. The ratio at equilibrium moves to 42 : 36 : 35 : 6. It is interesting that the equilibrium value of $\tilde{\sigma}_x$ in strip-biaxial deformation is almost the same as that in the uniaxial deformation, while the magnitude of the stress reduction for $\tilde{\sigma}_y$ is fairly large reaching ~80%. This means that the difference in mode of deformation between uniaxial and strip biaxial deformations diminishes as swelling proceeds, and the fixation of sample in y-direction has little effect on the stress in x-direction at equilibrium.

3.6.3 Creep Behavior of Gels

The magnitude of creep for the gel under each deformation mode is obtained from Eqs. (3.6) and (3.9). The results are tabulated in Table 3-2 together with the initial and equilibrium strain, and the equilibrium degree of strain-induced swelling.

Figure 3-5 shows the creep curves in x- and y-directions under the uniaxial deformation. ε_x, ε_y and t are reduced by ε_{xo}, ε_{yo} and τ_L, respectively. Here, ε_{xo} and ε_{yo} is the initial values of ε_x and ε_y. The creep curves are calculated by using the two methods. The creep behavior in any direction in the 0-th order approximation is governed by the longitudinal mode. In the case of the 1st approximation, the creep behavior in x- (loaded) direction is determined by the transverse mode, as can be seen in Eq. (3.28). On the other hand, and the creep process in y- and z- (load-free) directions is influenced by longitudinal and transverse modes, as shown in Eqs. (3.48). The calculation results for the 0-th and 1st order approximations are described by dashed and solid curves, respectively. As the swelling proceeds, the strain in the tensile direction, ε_x, increases and the absolute value of ε_y ($=\varepsilon_z<0$) in the direction perpendicular to the tensile axis decreases. At

Table 3-2. Degree of volume increase, equilibrium strain and the magnitude of creep of the gels under the constant stress under equi-, strip-biaxial and uniaxial deformations

	Degree of Volume Increase ($\Delta V/V_o$)	Initial Strain (ε_{io})	Equilibrium Strain ($\varepsilon_{i\infty}$)	Magnitude of Creep ($\Delta\varepsilon_i$)[1]
Equibiaxial (x,y)	$\frac{2}{3}\varepsilon_o$	ε_o	$\frac{15}{7}\varepsilon_o$	~2.1
(z)		$-2\varepsilon_o$	$-\frac{6}{7}\varepsilon_o$	~0.43
Strip-biaxial (x)	$\frac{12}{11}\varepsilon_o$	ε_o	$\frac{15}{11}\varepsilon_o$	~1.4
(z)		$-\varepsilon_o$	$-\frac{3}{11}\varepsilon_o$	~0.27
Uniaxial (x)	$\frac{6}{7}\varepsilon_o$	ε_o	$\frac{9}{7}\varepsilon_o$	~1.3
(y,z)		$-\frac{1}{2}\varepsilon_o$	$-\frac{3}{14}\varepsilon_o$	~0.43

1) $\Delta\varepsilon_i = \frac{\varepsilon_{i\infty}}{\varepsilon_{io}}$

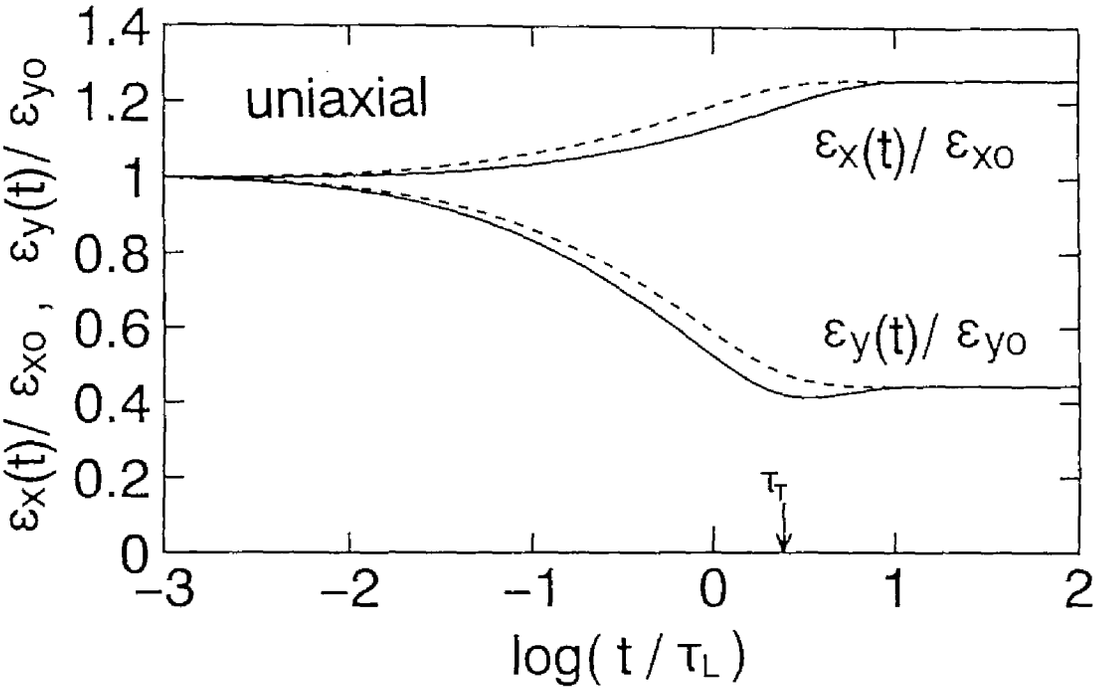

Figure 3-5. Time (t) dependence of strain $\varepsilon(t)$ under uniaxial deformation. Dashed and solid curves indicate the results for the 0-th and 1st order approximations, respectively. t and $\varepsilon_i(t)$ are reduced by the longest characteristic time of longitudinal mode τ_L and the initial strain ε_{io}, respectively.

equilibrium, $\varepsilon_x/\varepsilon_{xo}$ and $\varepsilon_y/\varepsilon_{yo}$ amount to ~130% and ~43%, respectively. The large difference in ε_x between two curves is not seen except the shift of solid curve to the long time side. On the other hand, the minimum appears in the behavior of the relative strain ($\varepsilon_y/\varepsilon_{yo}$) in load-free direction in the 1st order approximation, while $\varepsilon_y/\varepsilon_{yo}$ in the 0-th order approximation decreases monotonously. The ratio, $\varepsilon_y/\varepsilon_{yo}$, in the 1st order approximation has the minimum value of ~0.41 at $t/\tau_L \cong 3.4$. The undershoot of $\varepsilon_y/\varepsilon_{yo}$ results from the coupling of longitudinal and transverse modes. The mechanism for the undershoot of $\varepsilon_y/\varepsilon_{yo}$ is described in the end of this section.

Figure 3-6 shows the reduced creep curves under strip-biaxial deformation. The strain ε_x increases and the absolute value of $\varepsilon_z(<0)$ decreases with the increase of time. The values of $\varepsilon_{x\infty}/\varepsilon_{xo}$ and $\varepsilon_{z\infty}/\varepsilon_{zo}$ are respectively ~140% and ~27%, and there are no large differences in both values compared with those under uniaxial deformation. The calculation results in the 0-th and 1st order approximations are represented by the dashed and the solid curves, respectively. As well as in the case of uniaxial deformation, the behavior of relative strain ($\varepsilon_z/\varepsilon_{zo}$) in load-free direction in the 1st order approximation shows the undershoot originating from the coupling of longitudinal and transverse modes. The magnitude of undershoot is a little larger than that under uniaxial deformation. The minimum value of $\varepsilon_z/\varepsilon_{zo}$ is ~0.23 and located at $t/\tau_L \cong 3.3$.

The reduced creep curves under the equibiaxial deformation are shown in Fig. 3-7. The dashed and solid curves stand for the results for the 0-th and 1st order approximations, respectively. The strain ε_x ($=\varepsilon_y$) increases and the absolute value of $\varepsilon_z(<0)$ decreases as the swelling proceeds. As can be seen from Fig. 3-7, $\varepsilon_{x\infty}/\varepsilon_{xo}$ is ~210%, and $\varepsilon_{z\infty}/\varepsilon_{zo}$ ~43%. It is noticed that ε_x reaches the value twice as large as ε_{xo} at equilibrium. This is because the

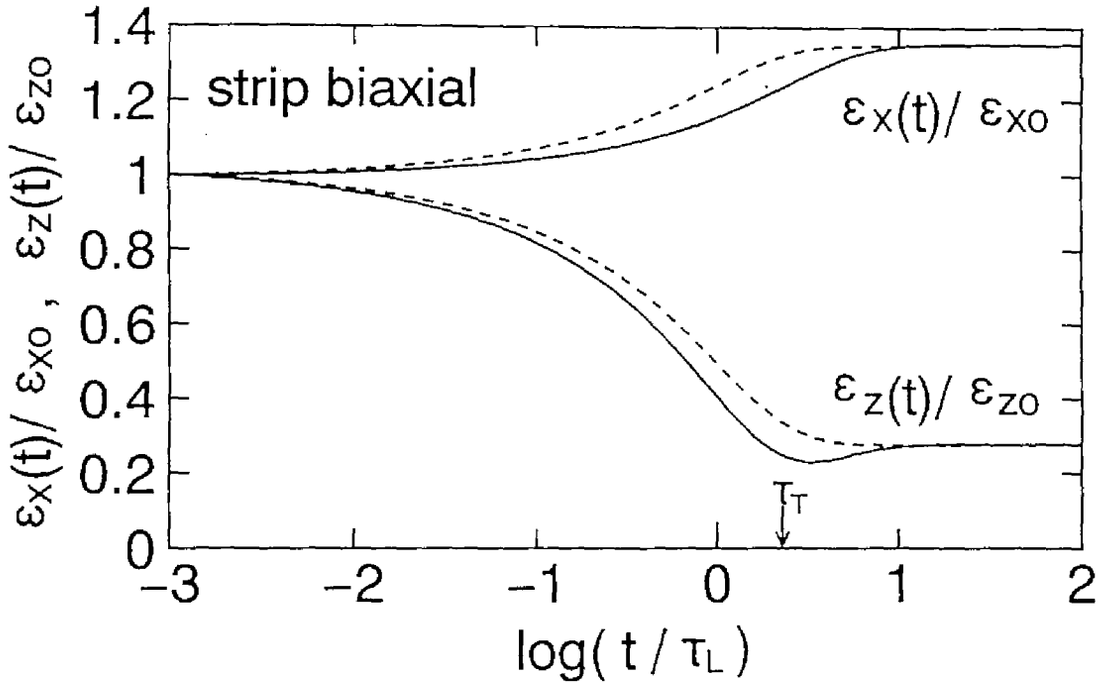

Figure 3-6. Time (t) dependence of strain $\varepsilon(t)$ under strip-biaxial deformation. Dashed and solid curves indicate the results for the 0-th and 1st order approximations, respectively. t and $\varepsilon_i(t)$ are reduced by the longest characteristic time of longitudinal mode τ_L and the initial strain ε_{io}, respectively.

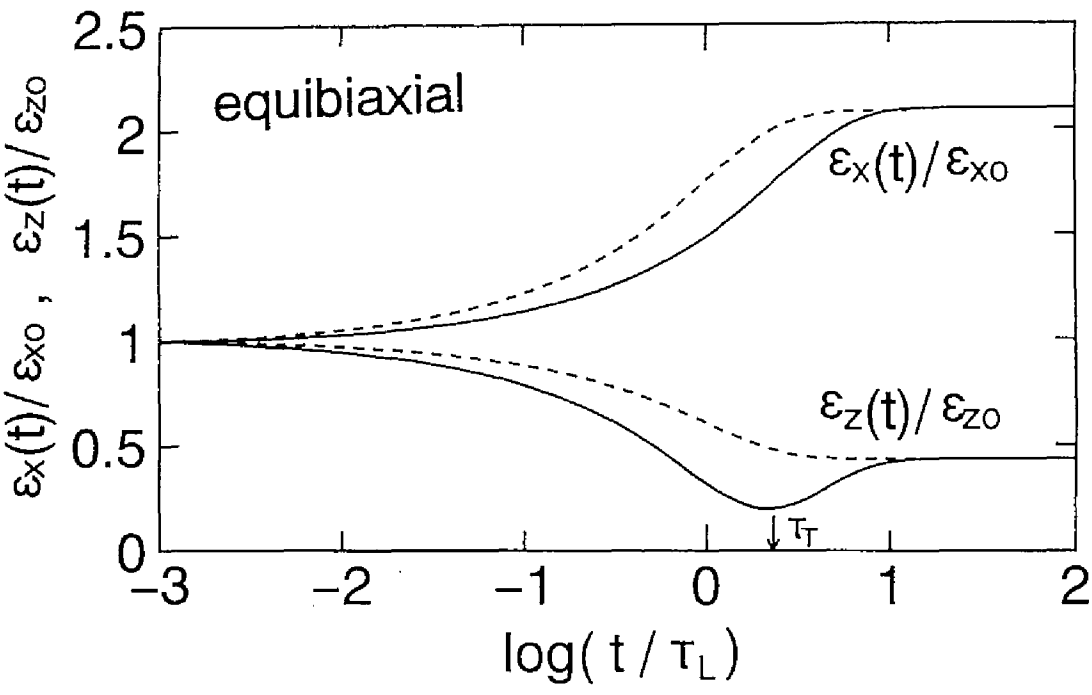

Figure 3-7. Time (t) dependence of strain $\varepsilon(t)$ under equibiaxial deformation. Dashed and solid curves indicate the results for the 0-th and 1st order approximations, respectively. t and $\varepsilon_i(t)$ are reduced by the longest characteristic time of longitudinal mode τ_L and the initial strain ε_{io}, respectively.

volume change caused by swelling under biaxial deformation is fairly large, while $\varepsilon_{z\infty}/\varepsilon_{z0}$ is the same as that in the uniaxial deformation. Actually, the value of $tr(\boldsymbol{u}'_\infty)$ under the equibiaxial deformation is four times larger than that in the uniaxial deformation. In the 1st order approximation, the time profile of ε_z is determined by longitudinal and transverse modes, while that of ε_x ($=\varepsilon_y$) by the transverse mode. The creep curve in z- (load-free) direction in the 1st order approximation also shows the clear minimum and the magnitude of undershoot is larger than those under uniaxial and strip-biaxial deformation. The minimum is located at the short time region compared with those under uniaxial and strip-biaxial deformations. The minimum value of $\varepsilon_z/\varepsilon_{z0}$ is ~0.20, which is located at $t/\tau_L \cong 2.2$.

The mechanism of the undershoot of $\varepsilon_i/\varepsilon_{i0}$ in the load-free direction under the 1st order approximation, which is seen in Figs. 3-5 - 3-7, is described as follows. At first, it should be noted that the value of ε_i in the load-free direction is negative at any t. Hence, the undershoot of $\varepsilon_i/\varepsilon_{i0}$ means that the overshoot of the size in the load-free direction. The size in the load-free direction increases with the increase of t at the initial stage, and reaches a maximum, and then, decreases to an equilibrium value. Figure 3-8 shows the schematic representation for this process. The overshoot behavior of the size in the load-free direction originates from its time dependence governed by the two types of the characteristic time (τ_L and τ_T) different in the character and the length. As can be seen in Eqs. (3.16) and (3.17), the longitudinal mode controls the volume change, and the transverse mode governs the shape change without volume change. The relation between τ_L and τ_T is expressed as $\tau_L=(5/2)\tau_T$, which implies that the volume change is completed faster than the shape change. Accordingly, in the time region $\tau_L < t < \tau_T$, the shape of gel is not similar to that at initial state, although the total change of volume is

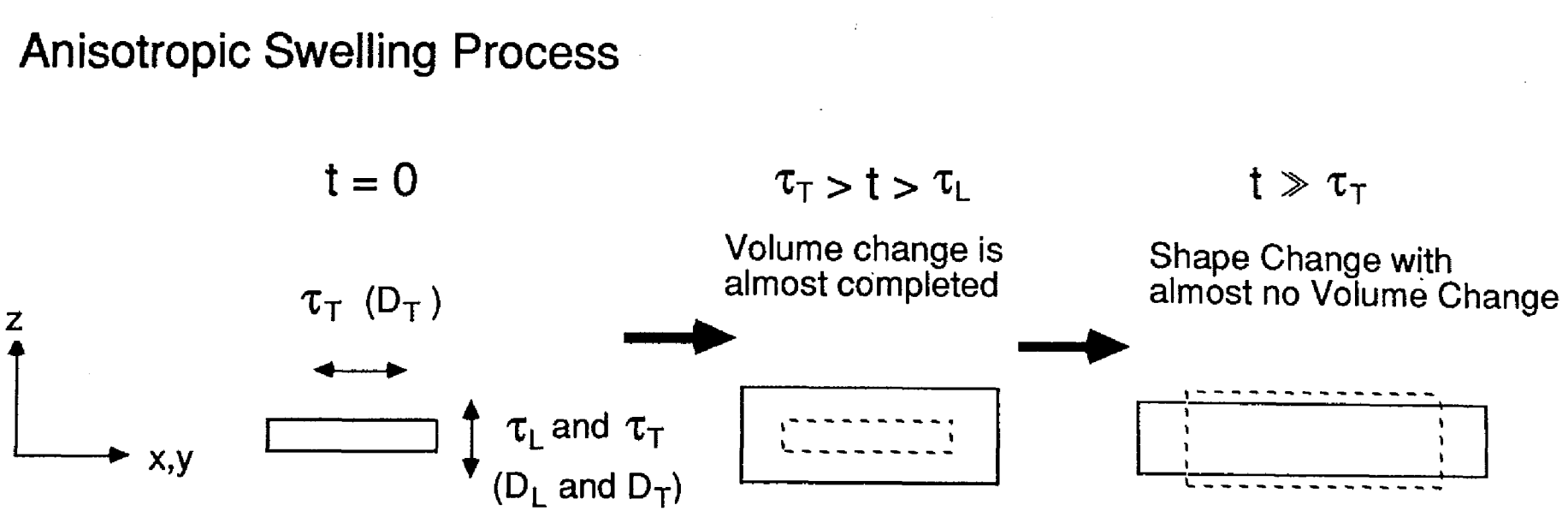

Figure 3-8. Schematic representation for the anisotropic swelling process of the biaxially stretched gel under the constant stresses $\tilde{\sigma}_{xx} = \tilde{\sigma}_{yy} = \tilde{\sigma}_o$.

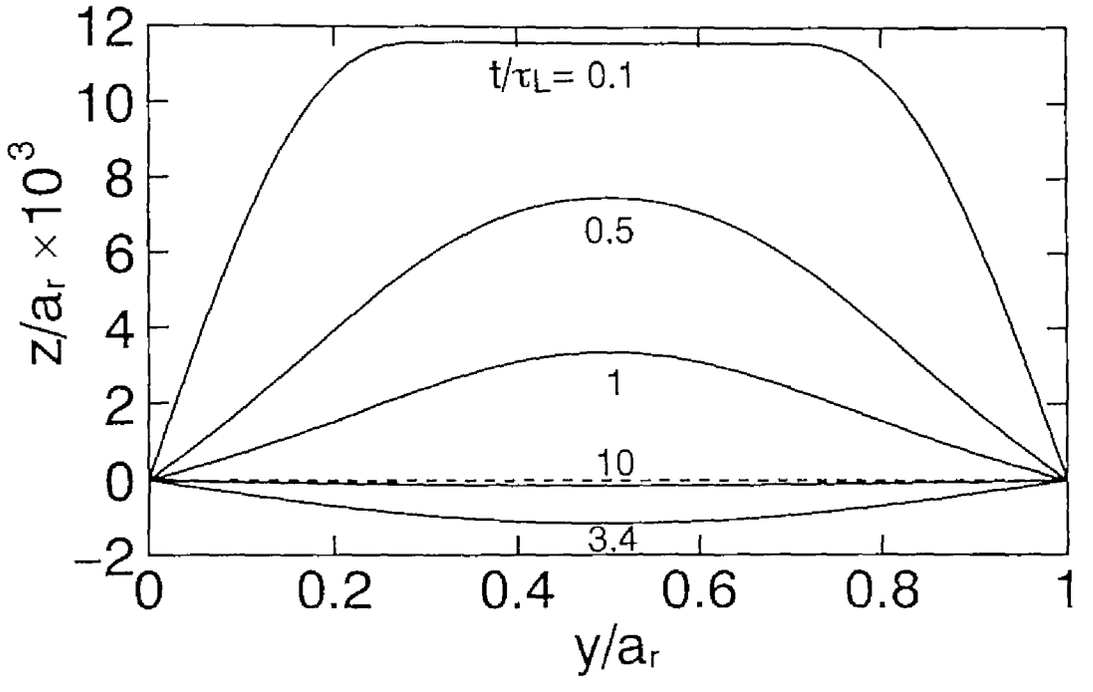

Figure 3-9. Time (t) profile of the boundary ($0 \le y \le a_r$, $z=0$) in the creep under uniaxial deformation in the 1st order approximation. Numerals in the figure indicate the values of t/τ_L.

almost completed. At this stage, the size in the loaded direction, whose time dependence is controled by τ_T, does not reach the equilibrium value. In the time region $t>\tau_T$, only the shape change occurs with keeping the volume constant, which results in the decrease of the size in the load-free direction together with the increase of the size in the loaded direction. The magnitude of undershoot and the location of the minimum for $\varepsilon_i/\varepsilon_{io}$ in the load-free direction are determined by the relative intensity of the transverse mode to the longitudinal one in the strain term in Eqs. (3.44) and (3.48). The relative intensity is governed by the dimensionality of diffusion and the type of deformation mode.

Here, we should mention that the strain focused here is a kind of average one. The time profile of boundary ($0\leq y\leq a_r$, $z=0$) in the creep under uniaxial deformation is shown in Fig. 3-9. The actual boundary has an arched shape during the transient process of swelling.

3.7 Conclusion

The degree of the strain-induced swelling and the resulting mechanical relaxation for the gel deformed under equi-, strip-biaxial and uniaxial deformation were evaluated on the basis of the thermodynamics for the swelling of constrained gels. The magnitude of mechanical relaxation was found to be strongly dependent on the deformation mode. The degree of the stress reduction for the equibiaxially stretched gel was estimated to be ~53%, while that for the uniaxially stretched gel to be ~22%. The ratio of the equilibrium strain to the initial one in the tensile direction for the creep under equibiaxial deformation is ~210%, while those under the uniaxial and the strip-biaxial deformations remain at ~130 and ~140%, respectively.

Poisson's ratio for the uniaxially stretched gel during and after the elongation, the stress in the stress relaxation and the strain in the creep under each deformation mode were obtained as a function of time by combining the constitutive equations of gels with a diffusion equation of polymer network. In the case where the experimental time scale for elongation is comparable to the characteristic time for the swelling, the value of Poisson's ratio was found to be intermediate between the two limiting values of Poisson's ratio which are the initial and equilibrium Poisson's ratio. The width of gel is decreased by the elongation, and simultaneously starts to increase by the swelling, which resulting in an intermediate value beween the initial and equilibrium Poisson's ratio.

The stress relaxation and creep curves were calculated by employing two methods. One is based on the assumption that the swelling occurs isotropically (zero-th order approximation) independently of the gel geometry, and the other is obtained by introducing the anisotropic swelling process (first-order approximation) which originates from the anisotropy in the gel shape. The stress relaxation processes in the 0-th and 1st order approximations are governed by the longitudinal and transverse modes, respectively. In the 0-th order approximation, the creep behavior in any direction under each deformation mode is controlled by longitudinal mode. In the 1st order approximation, the creep in the loaded direction, in which the diffusion is assumed not to occur, is determined by the transverse mode, and that in the load-free direction, in which the diffusion occurs, is determined by longitudinal and transverse modes. According to the 1st order approximation, it is expected that the overshoot of the size in the load-free direction occurs as a result of the coupling of longitudinal and transverse modes. The magnitude of the overshoot and the time showing the peak are

dependent on the deformation mode. The equibiaxially stretched gel shows the larger magnitude of overshoot, and has the peak located at the shorter time, in comparison with the gel under uniaxial and strip-biaxial deformation.

References

1. Nishinari, K., Watase, M., Ogino, K. and Nambu, M., *Polym. Commun.*, **24**, 345 (1983).
2. Cha, W.-I., Hyon, S.-H. and Ikada, Y., *Macromol. Chem.*, **193**, 1913 (1992).
3. Takigawa, T., Kashihara, H. and Masuda, T., *Polym. Bull.*, **24**, 613 (1990).
4. Takigawa, T., Kashihara, H., Urayama, K. and Masuda, T., *Polymer*, **33** 2335 (1992).
5. Takigawa, T., Urayama, K., Morino Y. and Masuda, T., *Polym. J.*, **25**, 929 (1993).
6. Takigawa, T., Urayama, K. and Masuda, T., *Polym. Gels & Networks*, **2**, 59 (1994).
7. Hirotsu, S. and Onuki, A., *J. Phys. Soc., Jpn.*, **58**, 1508 (1989).
8. Tanaka, T., Hocker, L. O. and Benedek, G. B., *J. Chem. Phys.*, **59**, 5151 (1973).
9. Tanaka, T. and Fillmore, D. J., *J. Chem. Phys.*, **70**, 1214 (1979).
10. Landau, L. D. and Lifshitz, E. M., "*Theory of Elasticity*", The 4th Ed., Nauka, Moscow, 1987.

Chapter 4
Stress-Strain Behavior of Typical Polymer Networks Under Pure Shear Deformation

4.1 Introduction

In Chapter 3 the mechanical behavior of polymer networks in swollen state is treated. In this chapter, the rubber elasticity of polymer networks in the bulk state is considered. The strain energy density function (W) has been considered as a basic quantity to describe elastic properties of materials. As reviewed by Kawabata and Kawai,[1] many studies have been made to investigate the functional form of W of rubber-like materials. Most of the experimental studies were carried out under uniaxial deformation, while experiments under biaxial deformation[2-6] have been limited although they give important information on the functional form of W of real elastomers. It has been shown that the elastic properties of real elastomers can be basically described by the classical theory[7] of rubber elasticity.[1] Various molecular theories[8-14] have been proposed to improve the classical theory of rubber elasticity, and have been compared with experiments by Gottlieb and Gayload.[15] They indicated that none of these molecular theories describe the experimental results quantitatively, and especially, the descrepancies are considerable in small deformation region. These molecular theories focus basically on the entropic elasticity, although some of the theories take intermolecular interaction by entanglement into accounts. It has been also pointed out that the intermolecular interactions originating from intermolecular force must be taken into account for the elasticity of real elastomers in order to explain the elastic behavior at small deformations.[5,16,17] However, the origin of the intermolecular interactions occurring in real

elastomers is not unclear at present. Poisson's ratio (μ_o) of rubber-like materials has been assumed to be 1/2, as the value at incompressible limit, but the values for the real elastomers are not identical exactly to 1/2.[5,18,19] There is one possibility that the origin of the intermolecular interaction is related to a volume change of materials. In this case, real elastomers must be treated as compressible materials. In this chapter, we eliminate the assumption of μ_o=1/2, and investigate the elastic behavior of real elastomers at small strains under pure shear deformation using the experimental value of μ_o. The stress-strain relations for the three types of segmented polyurethaneureas (SPUs) under pure shear deformation are measured. The experimental results are compared with theoretical predictions proposed here on the basis of a phenomenological elasticity theory for compressible materials. The values of μ_o for SPUs are measured by the method described in Chapter 2. The experimental results at small strains under pure shear deformation for isoprene rubber[5] (IR) reported by Kawabata *et al.*, and styrene-butadiene rubber[6] (SBR), nitrile-butadiene rubber[6] (NBR) and butadiene rubber[6] (BR) by Fukahori *et al.*, are also compared with the theoretical predictions.

4.2 Theory

4.2.1 Elasticity Theory

Elastic properties of rubber-like materials can be analyzed by the infinitesimal elasticity theory as far as applied strains are small enough.[20] The assumption of incompressibility has usually been applied to rubber-like materials. We eliminate here this assumption and treat the rubbery materials as a compressible one. According to the infinitesimal elasticity theory for compressible materials, that is, the Poisson ratio of the material (μ_o) is not

equal to 1/2, one can define the three invariants (J_i;i=1,2,3) using components of the strain tensor (ε) as follows.

$$J_1 = \varepsilon_1 + \varepsilon_2 + \varepsilon_3 \tag{4.1a}$$

$$J_2 = \varepsilon_1\varepsilon_2 + \varepsilon_2\varepsilon_3 + \varepsilon_3\varepsilon_1 \tag{4.1b}$$

$$J_3 = \varepsilon_1\varepsilon_2\varepsilon_3 \tag{4.1c}$$

Here, ε_p (p=1,2,3) stands for the principal strain in the p-direction. The strain energy density function (W) is written in terms of J_i on the basis of the infinitesimal elasticity theory as follows.

$$W = \left[\frac{K}{2} + \frac{2G}{3}\right] J_1^2 - 2GJ_2 \tag{4.2}$$

Here, K and G are respectively the bulk and shear moduli. The principal stress in the p-th direction (σ_p) is given by

$$\sigma_p = 2G\varepsilon_p + \left[K - \frac{2G}{3}\right] J_1 \tag{4.3}$$

In order to describe a stress-strain behavior of the materials at large strains, W is conventionally regarded as a function of the three invariants (I_i;i=1,2,3) for a deformation tensor. Using principal stretch ratio (λ_p;p=1,2,3), which is related to the principal strain (ε_p) as $\lambda_p=\varepsilon_p+1$, I_i is given by

$$I_1 = \lambda_1^2 + \lambda_2^2 + \lambda_3^2 \tag{4.4a}$$

$$I_2 = \lambda_1^2\lambda_2^2 + \lambda_2^2\lambda_3^2 + \lambda_3^2\lambda_1^2 \tag{4.4b}$$

$$I_3 = \lambda_1^2\,\lambda_2^2\,\lambda_3^2 \tag{4.4c}$$

The principal engineering stress, which we also assign here as σ_p, is generally expressed by

$$\sigma_p = 2\lambda_p\left[\frac{\partial W}{\partial I_1} + \left(\lambda_q^2 + \lambda_r^2\right)\frac{\partial W}{\partial I_2} + \lambda_q^2\,\lambda_r^2\,\frac{\partial W}{\partial I_3}\right] \tag{4.5}$$

where p,q,r=1,2,3. The partial derivative of W with respect to I_i ($\partial W/\partial I_i$;i=1,2,3) can be calculated by using a set of σ_p and λ_p (p=1,2,3).

4.2.2 Pure Shear Deformation

Pure shear (strip-biaxial) deformation is one of the common deformation mode among biaxial deformations. The schematic representation for the pure shear deformation is given in Fig. 3-1. We designate the elongational direction as x_1, sustaining direction as x_2, and the direction in free motion as x_3 for pure shear deformation. The derivatives $\partial W/\partial I_i$ in the case of pure shear deformation are obtained from Eq. (4.5), $\lambda_2=1$ and $\sigma_3=0$ as follows.

$$\frac{\partial W}{\partial I_1} = \frac{\sigma_1 \lambda_1^3}{2(\lambda_1^2 - \lambda_3^2)(\lambda_1^2 - 1)} - \frac{\sigma_2}{2(1 - \lambda_3^2)(\lambda_1^2 - 1)} \tag{4.6a}$$

$$\frac{\partial W}{\partial I_2} = \frac{-\sigma_1 \lambda_1}{2(\lambda_1^2 - \lambda_3^2)(\lambda_1^2 - 1)} + \frac{\sigma_2}{2(1 - \lambda_3^2)(\lambda_1^2 - 1)} \tag{4.6b}$$

$$\frac{\partial W}{\partial I_3} = \frac{\sigma_1 \lambda_1 + \sigma_2}{4 \lambda_1^2 \lambda_3^2} - \frac{\lambda_1^2 + 1}{2 \lambda_1^2 \lambda_3^2} \frac{\partial W}{\partial I_1} - \frac{2\lambda_1^2 + \lambda_1^2 \lambda_3^2 + \lambda_3^2}{2 \lambda_1^2 \lambda_3^2} \frac{\partial W}{\partial I_2} \tag{4.6c}$$

As can be seen in Eq. (4.6), when $\mu_o \neq 1/2$, not only the values of λ_1 and λ_2 but also the value of λ_3 is required for the numerical calculation of the value of $\partial W/\partial I_i$. Since direct measurement of λ_3 in the pure shear experiment is usually difficult, λ_3 is estimated by calculation. In this case, the value of μ_o is required. At small deformations, λ_3 (or, equivalently ε_3) is easily obtained from Eq. (4.3). For ε_3 we have

$$\varepsilon_3 = -\frac{\mu_o}{1 - \mu_o} \varepsilon_1 \tag{4.7}$$

because $\varepsilon_2=0$ and $\sigma_3=0$ for pure shear deformation. It should be noted that the stress ratio (σ_2/σ_1) gives μ_o as

$$\mu_o = \frac{\sigma_2}{\sigma_1} \tag{4.8}$$

In order to calculate the value of λ_3 at large strains, we modify Eq. (4.7) to

$$\lambda_3 = \lambda_1^{-\mu_o/(1 - \mu_o)} \tag{4.9}$$

This equation, of course, coincides with Eq. (4.7) at small strains. When μ_0 is known, we can calculate the value of λ_3 at both small and large strains by using Eq. (4.9).

4.2.3 Limiting Values of Partial Derivatives of W

As strain decreases, $\partial W/\partial I_i$ at large strains approaches its limiting value predicted by the infinitesimal elasticity theory. The value at zero strain limit can be estimated by using the derivative of W with respect to J_i ($\partial W/\partial J_i$; i=1,2,3) at zero strain limit. The quantity $\partial W/\partial J_i$ is related to $\partial W/\partial I_i$ as

$$\frac{\partial W}{\partial J_i} = \frac{\partial W}{\partial I_1}\frac{\partial I_1}{\partial J_i} + \frac{\partial W}{\partial I_2}\frac{\partial I_2}{\partial J_i} + \frac{\partial W}{\partial I_3}\frac{\partial I_3}{\partial J_i}, \quad (i=1,2,3) \tag{4.10}$$

and the values of the derivatives at zero strain limit ($J_i \rightarrow 0$) are given by

$$\frac{\partial W}{\partial J_1} \rightarrow 0 \tag{4.11a}$$

$$\frac{\partial W}{\partial J_2} \rightarrow -2G \tag{4.11b}$$

$$\frac{\partial W}{\partial J_3} \rightarrow 0 \tag{4.11c}$$

assuming that W can be expressed by Eq. (4.2) at small strain limit. The relations between J_i and I_i are as follows.

$$I_1 = J_1^2 + 2J_1 - 2J_2 + 3 \tag{4.12a}$$

$$I_2 = 2J_1^2 + J_2^2 + 2J_1J_2 - 2J_3J_1 + 4J_1 - 6J_3 + 3 \tag{4.12b}$$

$$I_3 = (1 + J_1 + J_2 + J_3)^2 \tag{4.12c}$$

From Eqs. (4.10)-(4.12), we have the values of $\partial W/\partial I_i$ at zero strain limit ($I_1, I_2 \rightarrow 3$ and $I_3 \rightarrow 1$) as follows:

$$\frac{\partial W}{\partial I_1} \rightarrow \frac{5G}{8} \tag{4.13a}$$

$$\frac{\partial W}{\partial I_2} \rightarrow -\frac{G}{8} \tag{4.13b}$$

$$\frac{\partial W}{\partial I_3} \rightarrow -\frac{3G}{8} \tag{4.13c}$$

It should be noted that the limiting values of $\partial W/\partial I_2$ and $\partial W/\partial I_3$ are negative, while $\partial W/\partial I_1$ has the positive value at zero strain limit.

4.3 Experimental

4.3.1 Material

Three types of SPUs used in this study were supplied as dimethylformamide solutions from Toyobo Co., Japan. The three types of prepolymers of the SPUs differing in the molecular weight of poly(tetramethylene glycol) (PTMG) were prepared from the mixed solutions of methylene diisocyanate (MDI) and PTMG. The solvent used was N,N'-dimethylacetate (DMAc). The prepolymers were chain-extended by using 1,2-diaminopropane (DAP). The number-average molecular weight of PTMG (M_s), weight fraction of PTMG (W_s), number-and weight-average molecular weights of SPUs (M_n and M_w, respectively), and the ratio of M_w to M_n (M_w/M_n) are listed in Table 4-1, together with the sample name. Here, M_n and M_w are reduced molecular weights to polystyrene. Film specimens for mechanical tests were prepared by solution-cast method.

4.3.2 Uniaxial and Biaxial Elongation

Uniaxial elongation of SPU film was made to estimate μ_o by using an Orientec tensile tester (RTM-250) at a crosshead speed of 50mm/min. The width and thickness of the specimens were respectively 5mm and 100-200μm. The crosshead distance at rest was *ca.* 20mm. Poisson's ratio (μ_o) was determined by the method described in Chapter 2. The values of μ_o were estimated from

$$\mu_o = -\frac{\log \lambda_2}{\log \lambda_1} \tag{4.14}$$

Table 4-1. Sample codes, number-average molecular weights of poly(tetramethyleneglycol) (PTMG)(M_s), weight fractions of PTMG (W_s), number-and weight-average molecular weights of SPU (M_n and M_w; reduced to molecular weights of polystyrene), and the ratios of M_w to M_n.

Sample	M_s	W_s	M_n	M_w	M_w/M_n
SPU850	870	0.60	42000	127000	3.0
SPU1650	1700	0.74	59000	155000	2.6
SPU3000	3100	0.84	68000	192000	2.8

The stretch ratio in the stretched direction (λ_1) was calculated from distance between two marked points of the film surface, and the stretch ratio perpendicular to the stretched direction (λ_2) was calculated from the width in the central region of the specimen. The distance and width during uniaxial elongation process were recorded by using a video-tape recorder.

The stress-strain curves of the SPU under pure shear deformation were obtained by using a specially designed biaxial elongation apparatus (Iwamoto Seisakusho Co.). The shape of the film specimens used was square with thickness of 100-200μm. The distance between cramps at rest was 50mm and elongation speed was 0.83mm/sec.

4.4 Results and Discussion

4.4.1 Poisson's Ratio of SPUs

Figure 4-1 shows the plots of $-\log\lambda_2$ against $\log\lambda_1$ obtained in the uniaxial elongation experiment of SPU850. All the data points are approximated by a single line of slope 0.442, and we assign the slope of line as Poisson's ratio (μ_o). The value of λ_1 examined here ranged from 1.035 to 1.468. The stress-strain curve of SPU850 under uniaxial elongation was linear in the region of λ_1 lower than about 1.2, and the curve showed the nonlinear relation at larger stretch ratios, although we do not show the curve here. The linear relation between $-\log\lambda_2$ and $\log\lambda_1$ over a wide range of λ_1 indicates that μ_o is independent of the magnitude of the applied strain: the value of μ_o in the nonlinear stress-strain region is the same as that in the linear elasticity region. Similar behavior has been observed for μ_o of poly(vinyl alcohol) (PVA) gels as described in Chapter 2. SPU1650 and SPU3000 also showed the nonlinear stress-strain behavior at large stretch ratios, but they also showed the linear relation in the $-\log\lambda_2$ *vs.* $\log\lambda_1$ plots

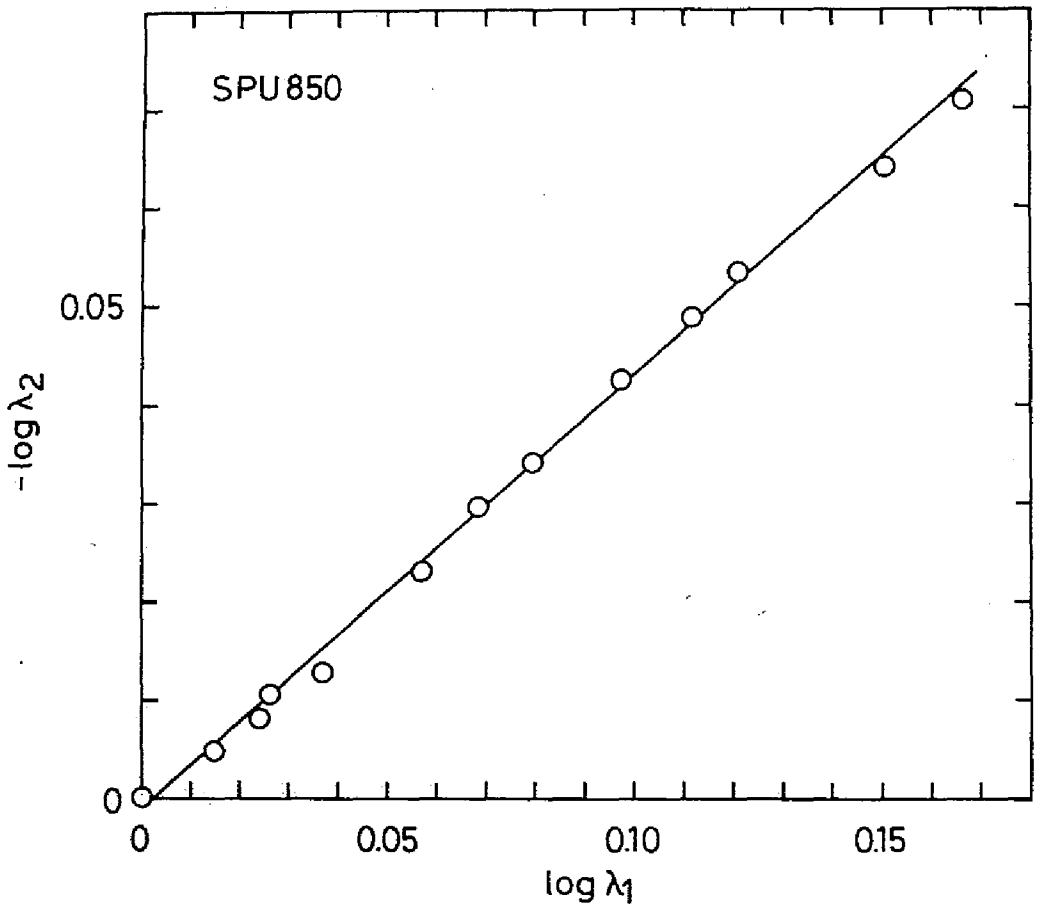

Figure 4-1. Plots of $-\log\lambda_2$ *vs.* $\log\lambda_1$ for SPU850.

Table 4-2. Poisson's ratios obtained from uniaxial elongation experiment (μ_o) and from stress ratio under pure shear deformation (μ_o'), and shear modulus (G) for SPUs.

Sample	μ_o	μ_o'	G /MPa
SPU850	0.442	0.400	12.1
SPU1650	0.471	0.425	5.2
SPU3000	0.494	0.447	2.9

in the whole range of λ_1. The values of μ_o for SPUs are listed in Table 4-2. The value of μ_o for the SPUs increases with increasing M_s. SPUs have the two-phase structure and the phase separation becomes clearer as M_s increases.[21] The clear phase separation will make the materials close to ideal cross-linked rubbers, resulting in the closer value of μ_o to 1/2 with increasing M_s.

In Fig. 4-2, the stresses (σ_1 and σ_2) under pure shear deformation are plotted against the stretch ratio (λ_1) for SPU850. The stresses σ_1 and σ_2 increase monotonically with increasing λ_1, but the inflection point is observed around λ_1=1.5 on each stress-strain curve. We measured the stress-strain curves of three specimens of SPU850 in order to check the reproducibility of the stress-strain curves. The data obtained in each experiment are well coincided with one another. Scattering was observed for the data at strains lower than about 10%, but the deviation was very small. SPU1650 and SPU3000 showed almost the same stress-strain behavior as SPU850 shown in the figure. We also found the good reproducibility of the stress-strain curves for SPU1650 and SPU3000. The stress level in both elongational and sustaining directions became lower as M_s increases.

According to Eq. (4.8), the stress ratio (σ_2/σ_1) gives Poisson's ratio. Figure 4-3 shows the plots of σ_2/σ_1 against λ_1 for the three SPUs. The data are limited to those at relatively small stretch ratios. The stress ratio increases with increasing λ_1 for the three SPUs. The extrapolated value to the zero strain limit, which is assigned here as μ_o', is tabulated in Table 4-2. The value of μ_o' increases with increasing M_s, and the value is lower than that of μ_o obtained from the uniaxial experiment. As far as the infinitesimal elasticity theory holds, the stress ratio (σ_2/σ_1) under pure shear deformation must be constant and it also gives the Poisson ratio of material. We do not

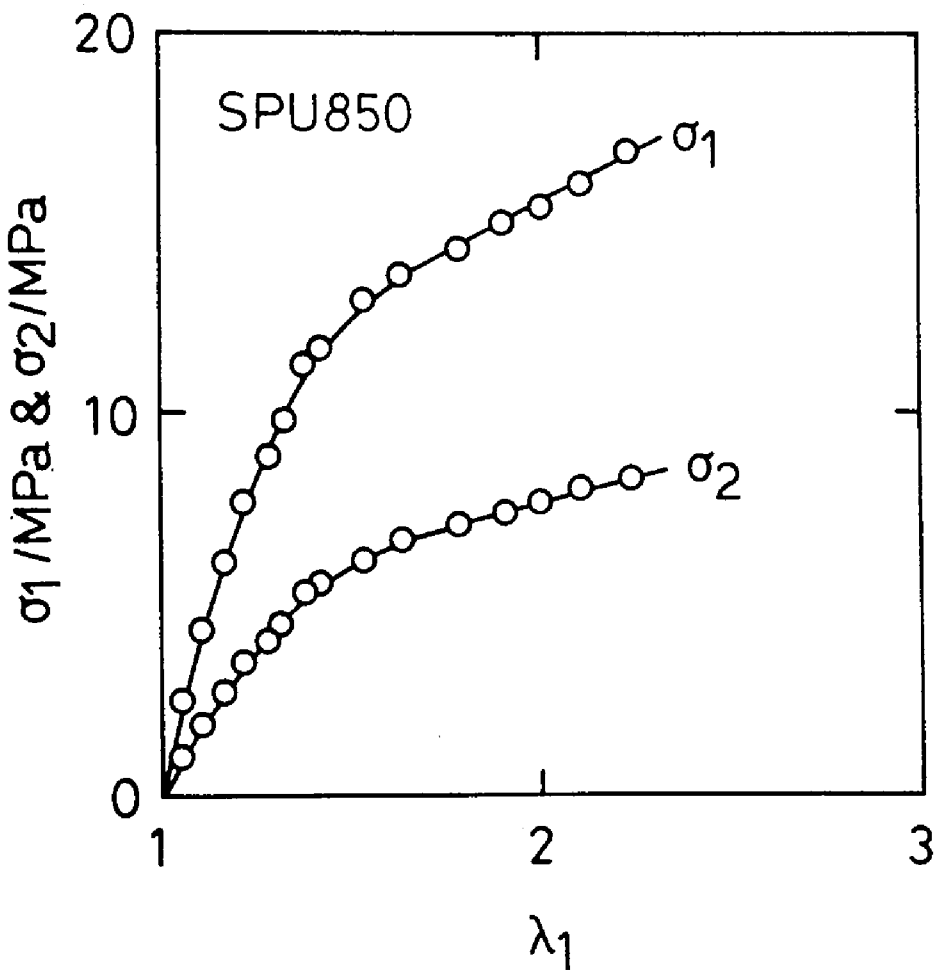

Figure 4-2. Stresses (σ_1 and σ_2) plotted against stretch ratio (λ_1) for SPU850 under pure shear deformation. σ_1 stands for the stress in the stretched direction and σ_2 for the stress in the sustaining direction.

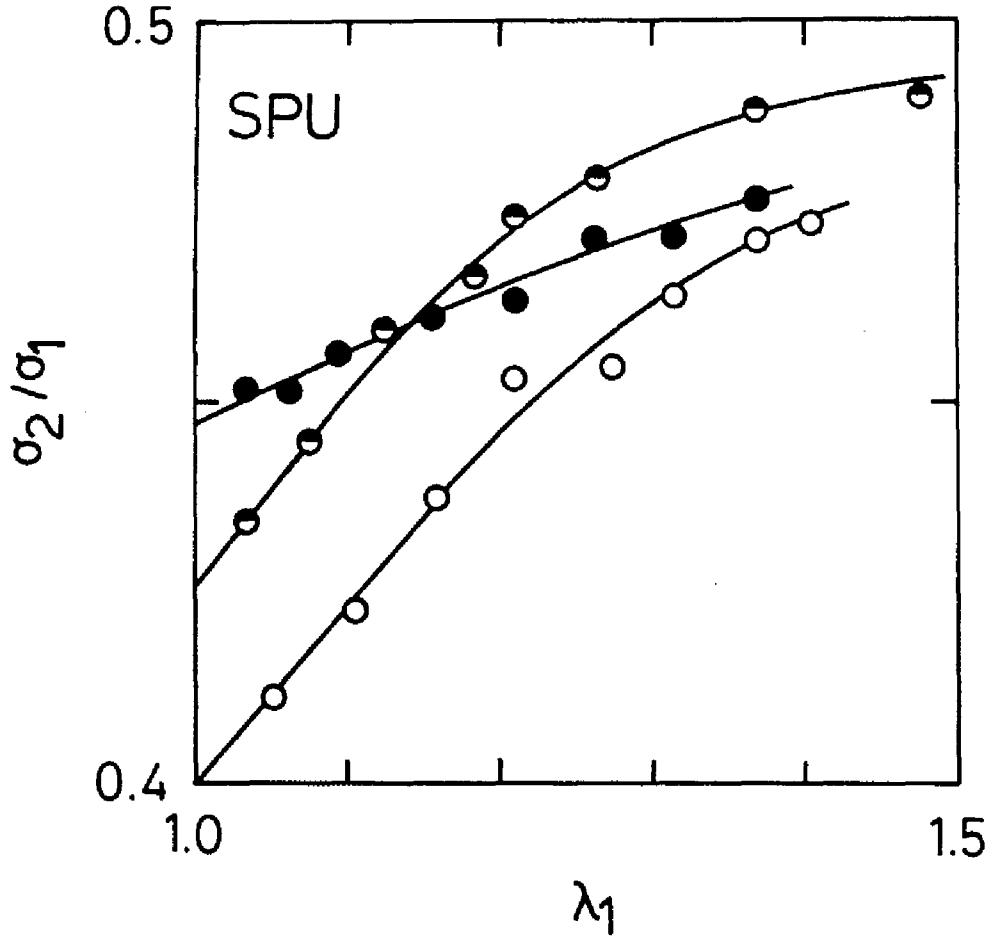

Figure 4-3. The stress ratio (σ_2/σ_1) against stretch ratio for SPUs. Symbols: (O) SPU850; (◓) SPU1650; (●) SPU3000.

know at present why μ_o' from pure shear deformation (from Eq. (4.8)) is smaller than μ_o from uniaxial deformation (from Eq. (4.14) for SPUs, although both the values must basically coincide with each other. However, the fact that μ_o as well as μ_o' is not identical to 1/2 clearly indicates that the SPUs are compressible and volume change occurs during deformation. The linear stress-strain relation was observed up to stretch ratio of about 1.2 for uniaxial elongation of all the SPUs, but the stress ratio is I_1-dependent over the range of I_1 including small I_1 region. This suggests that the region of strain, where the linear elasticity holds, is very narrow for pure shear deformation compared with the linear region for uniaxial elongation.

4.4.2 Shear Modulus of SPUs, SBR, NBR, BR and IR

As can be seen from Eq. (4.13b), $(-1/2)(\partial W/\partial J_2)$ at zero strain limit gives the shear modulus (G). Figure 4-4 shows the plots of $(-1/2)(\partial W/\partial J_2)$ against I_1 for the three SPUs. The values of $(-1/2)(\partial W/\partial J_2)$ for SPUs were calculated by the combination of a set of $\partial W/\partial I_i$ and J_i (i=1,2,3), since $(-1/2)(\partial W/\partial J_2)$ is given from Eqs. (4.10) and (4.12) by

$$-\frac{1}{2}\frac{\partial W}{\partial J_2} = \frac{\partial W}{\partial I_1} - (J_1 + J_2)\frac{\partial W}{\partial I_2} - (1 + J_1 + J_2 + J_3)\frac{\partial W}{\partial I_3} \qquad (4.15)$$

Data shown in the figure are limited to those at I_1 smaller than 5. The solid curve in the figure is the best-fit curve for each SPU. The three curves show the monotonical decrease with increasing I_1. The vertical level of the curve becomes lower as M_s increases. We estimate G for the SPUs as a limiting value of the curve at I_1=3. The value of G for SPUs is listed in Table 4-2. The value decreases with increasing M_s.

Figures 4-5 - 4-8 show the plots of $(-1/2)(\partial W/\partial J_2)$ against I_1 for IR, SBR, NBR and BR, respectively. Since the number of the data for SBR, NBR and BR are not enough in the small I_1 region, the data in the large I_1 region

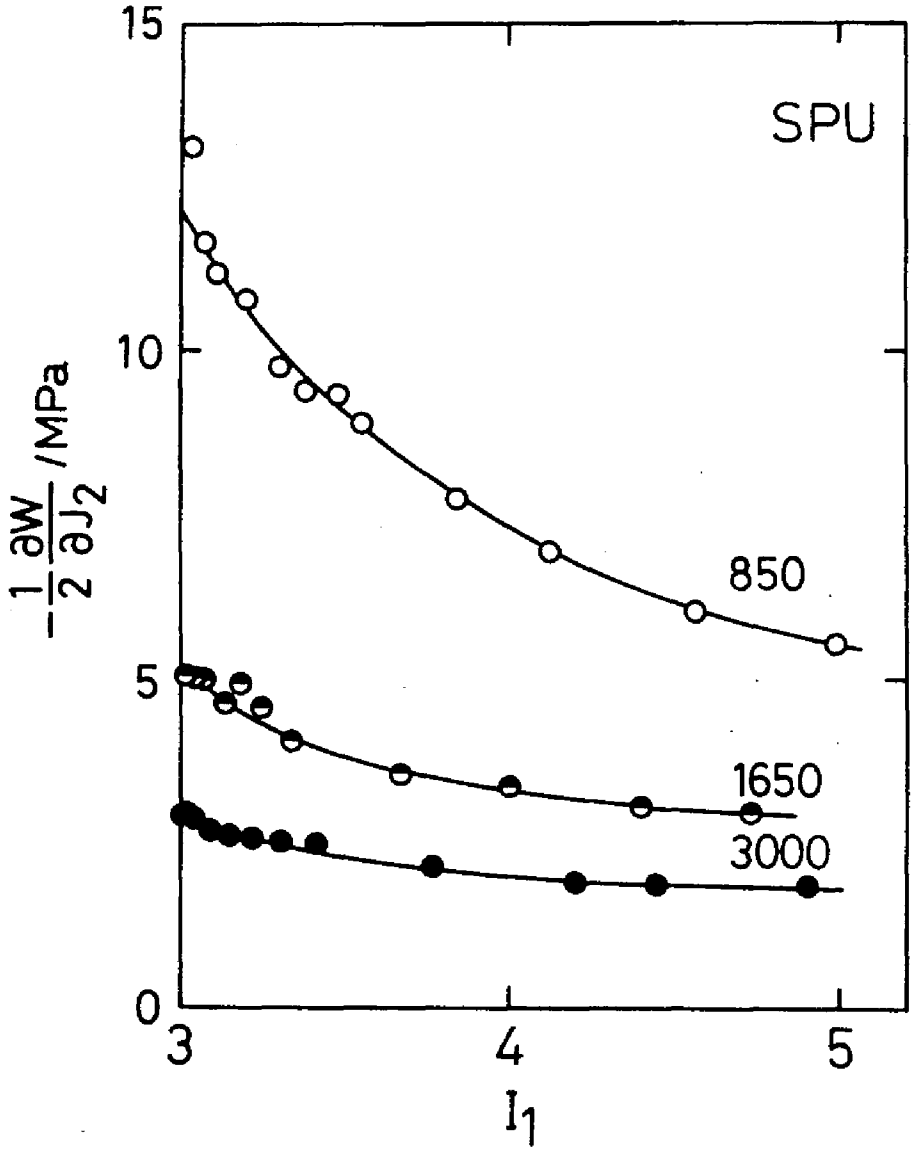

Figure 4-4. Plots of (-1/2)($\partial W/\partial J_2$) against I_1 for SPUs. Symbols are the same as Fig. 4-3.

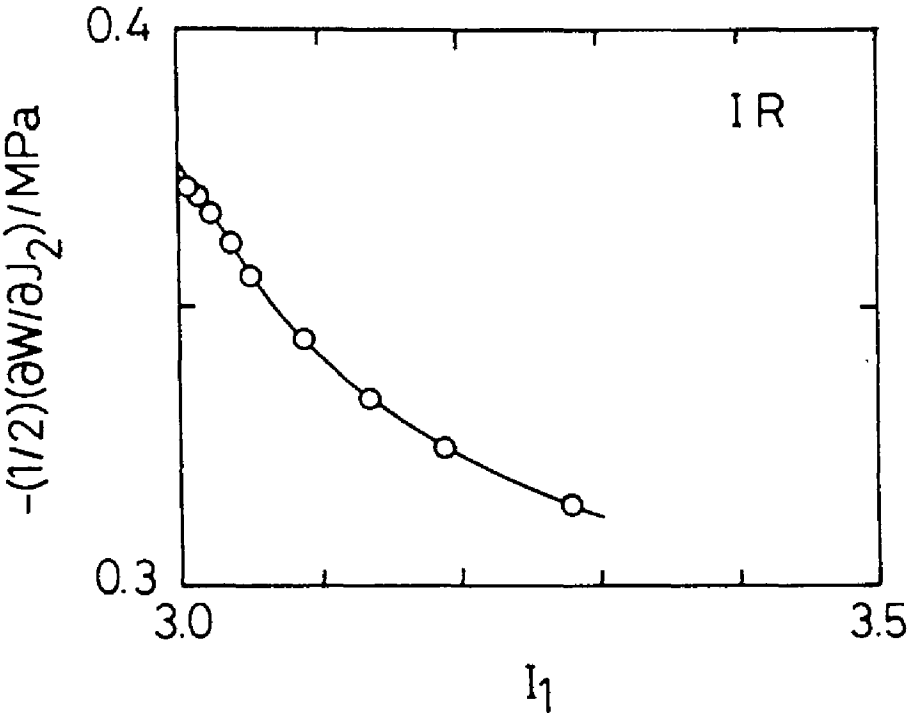

Figure 4-5. Plots of $(-1/2)(\partial W/\partial J_2)$ against I_1 for IR.

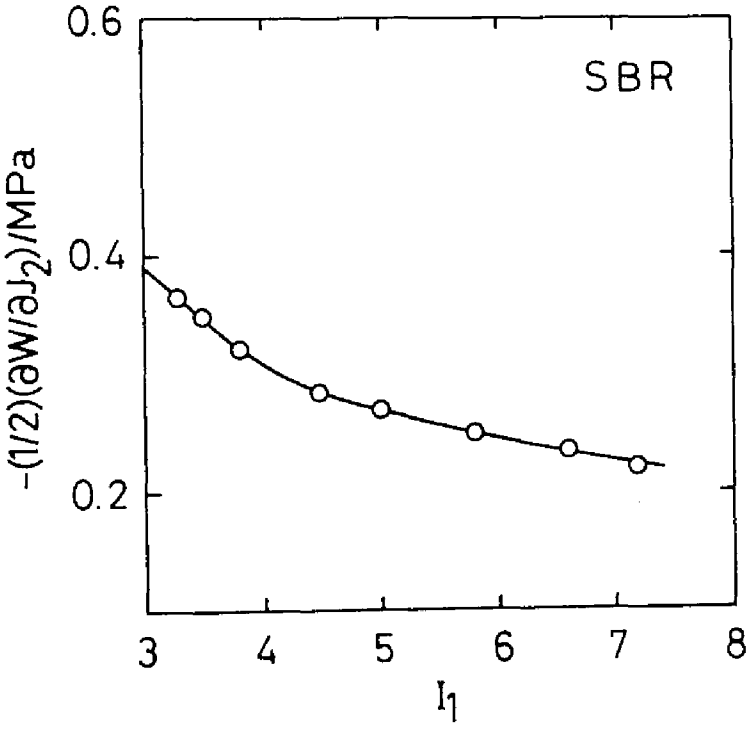

Figure 4-6. Plots of $(-1/2)(\partial W/\partial J_2)$ against I_1 for SBR.

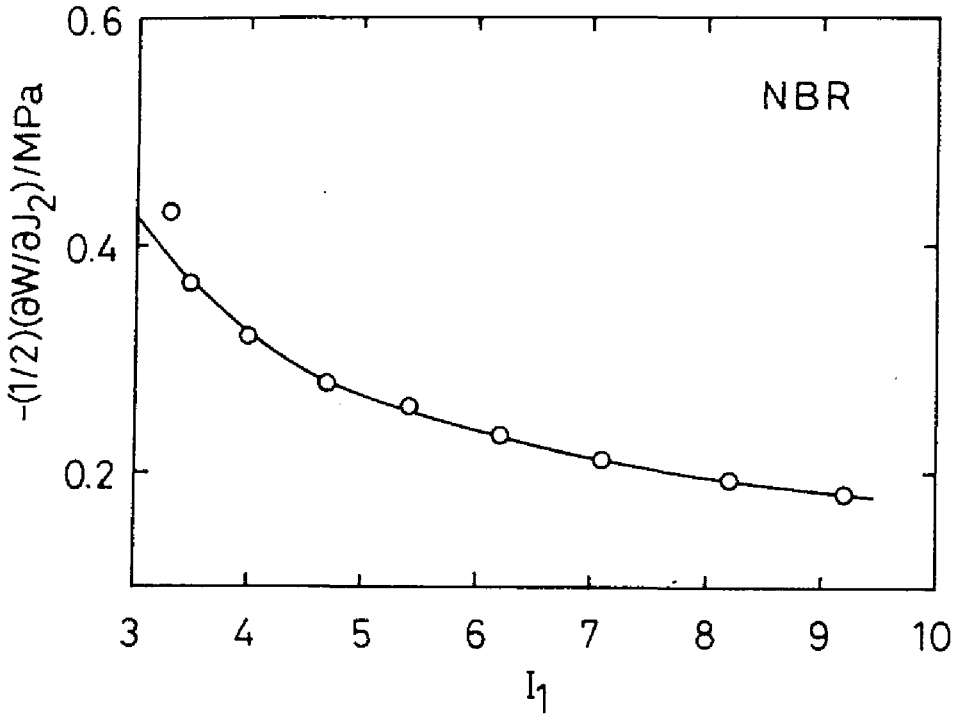

Figure 4-7. Plots of $(-1/2)(\partial W/\partial J_2)$ against I_1 for NBR.

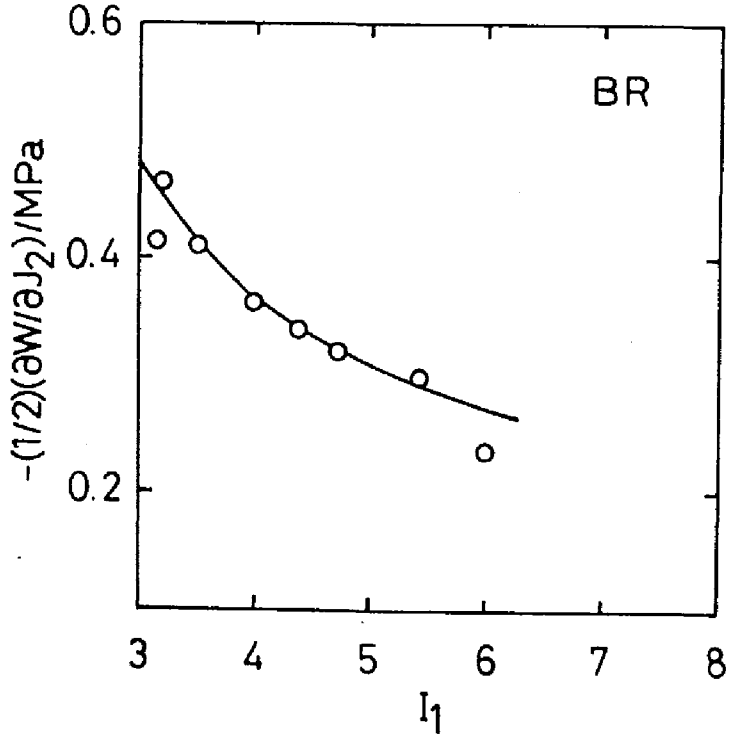

Figure 4-8. Plots of $(-1/2)(\partial W/\partial J_2)$ against I_1 for BR.

Table 4-3. Poisson's ratios used for the calculation (μ_o) and shear moduli (G) for IR, SBR, NBR and BR.

Sample	μ_o	G /MPa
IR	0.499916[a]	0.375
SBR	0.49983[b]	0.39
NBR	0.49983[b]	0.43
BR	0.49983[c]	0.48

[a] obtained by Kawabata *et al.* (Ref. 5)

[b] assumed to be equal to μ_o of BR

[c] obtained by Holownia (Ref. 19)

are included. The curves show a monotonous decrease with increasing I_1 , as in the case of SPUs in Fig. 4-4. The values of G were obtained by extrapolating the curve to I_1=3, and are listed in Table 4-3.

4.4.3 Partial Derivatives of W for SPUs

The values of Poisson's ratio (both μ_o and μ_o') for SPUs were rather close to 0.5 but were not exactly identical to 0.5 (Table 4-2), meaning that SPUs are better to be treated as compressible materials. Figure 4-9 shows the I_1 dependence of $\partial W/\partial I_i$ (i=1,2,3) for SPU850. The value of Poisson's ratio used for the calculation of $\partial W/\partial I_i$ was 0.442 which is the value of μ_o, although we had two values for Poisson's ratio, namely, μ_o and μ_o'. We chose μ_o as Poisson's ratio for the calculation because μ_o is in accordance with its definition. The data points shown in Fig. 4-9a are those at I_1 larger than 3.5. The derivatives $\partial W/\partial I_1$ and $\partial W/\partial I_2$ are positive in this region of I_1 shown in Fig. 4-9a and are decreasing functions of I_1. The value of $\partial W/\partial I_2$ is very small compared with that of $\partial W/\partial I_1$. The value of $\partial W/\partial I_3$ is negative in the region of I_1 shown here, and $\partial W/\partial I_3$ increases with increasing I_1. At large I_1, the absolute value of $\partial W/\partial I_3$ is much smaller than that of $\partial W/\partial I_1$. In Fig. 4-9b, the data at I_1 smaller than 3.5 are shown. The derivative, $\partial W/\partial I_1$, increases very rapidly as I_1 approaches three from the larger side of I_1, while $\partial W/\partial I_2$ shows a maximum around I_1=3.4 and the values in the smaller I_1 region are negative. The derivative $\partial W/\partial I_3$ shows a rather broad minimum around I_1=3.2, and then it increases steeply as I_1 decreases further. The I_1 dependence is observed for the three derivatives over the entire region of I_1 investigated here, but the dependence is weaker in the large I_1 region (Fig. 4-9a) than in the small I_1 region (Fig. 4-9b). As stated previously, we examined stress-strain behavior for three specimens of SPU850. We also calculated the

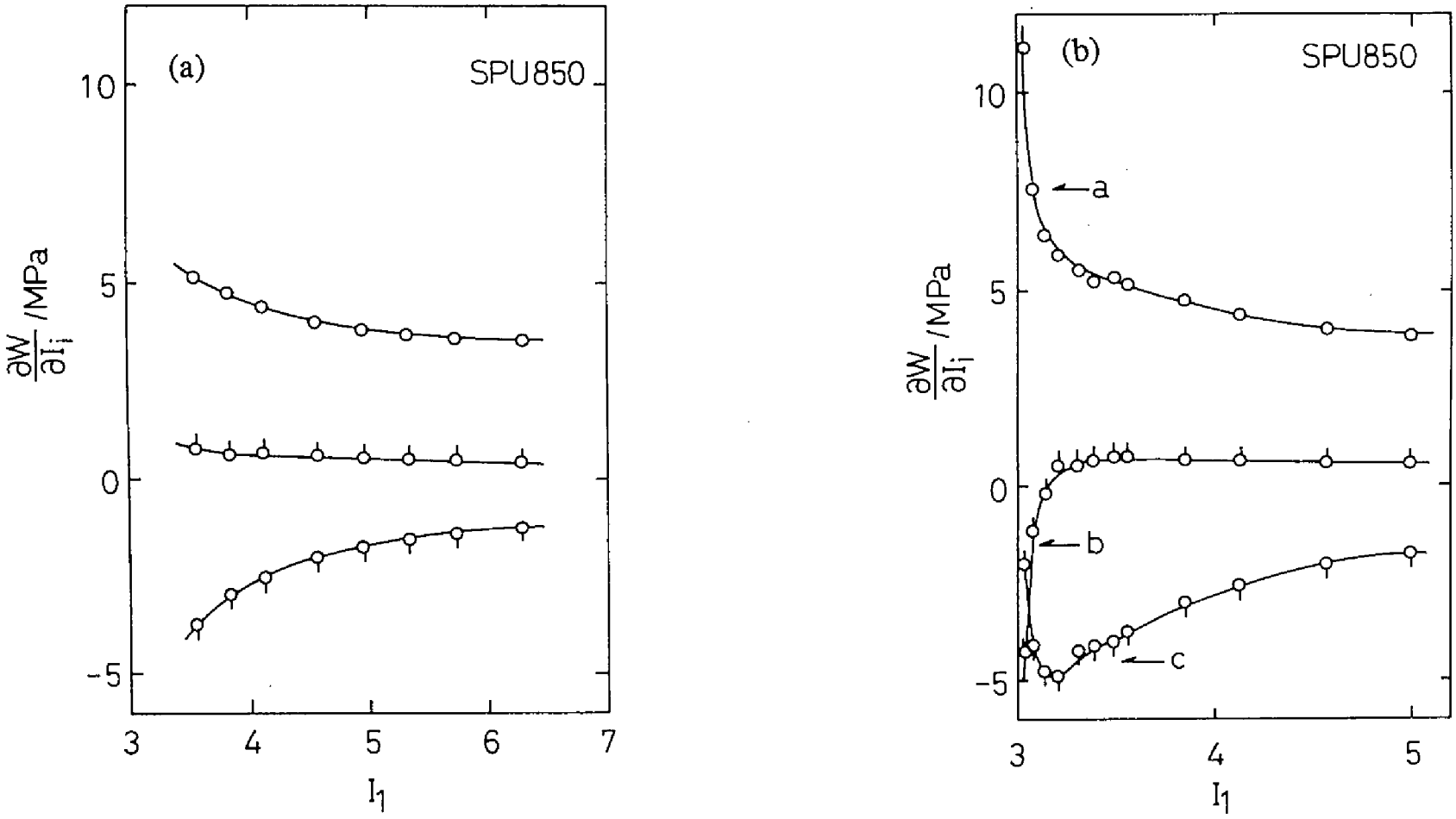

Figure 4-9. (a) Plots of $\partial W/\partial I_i$ against I_1 for SPU850 for large I_1 region. (b) Plots of $\partial W/\partial I_i$ against I_1 for SPU850 for small I_1 region. Symbols: (O) data points for $\partial W/\partial I_1$; (Ȯ) for $\partial W/\partial I_2$; (Ǫ) for $\partial W/\partial I_3$. The arrows *a*, *b* and *c* represent the theoretical predictions for $\partial W/\partial I_1$, $\partial W/\partial I_2$ and $\partial W/\partial I_3$ at zero strain limit, respectively.

I_1 dependence of $\partial W/\partial I_i$ (i=1,2,3) using the stress-strain data for each specimen. The $\partial W/\partial I_i$ *vs.* I_1 curves for the three specimens were almost identical to one another for i=1, 2 and 3. This indicates that the stronger I_1 dependence of the three derivative truely occurs at small strains.

Figures 4-10 and 4-11 respectively show the similar plots for SPU1650 and SPU3000. Here, the values of the Poisson ratio used were 0.471 for SPU1650 and 0.494 for SPU3000, which are the experimental values of μ_o for the SPUs. Figures 4-10a and 4-11a represent the I_1 dependence of the derivatives in the large I_1 region, while Figs. 4-10b and 4-11b are the data at small strains (or small I_1). As can be seen from Figs. 4-10a and 4-11a, the absolute values of $\partial W/\partial I_2$ and $\partial W/\partial I_3$ are smaller compared with that of $\partial W/\partial I_1$ for both SPUs, as in the case of SPU850. In the small region of I_1 (Figs. 4-10b and 4-11b), the shapes of the derivatives for the SPUs are also almost identical to that for SPU850; $\partial W/\partial I_1$ of the SPUs increases steeply and $\partial W/\partial I_2$ decreases rapidly, as I_1 approaches three from the right side of the I_1 axis. The derivative, $\partial W/\partial I_3$, shows the broad minimum at smaller I_1, and then it shows the sharp increase as I_1 decreases further. The three derivatives of SPU1650 as well as SPU3000 show the relatively weak I_1 dependence at large I_1, as is the case of SPU850.

In Figs. 4-9b, 4-10b and 4-11b, there are three arrows, each of which is specified as *a*, *b* and *c*. The vertical position of the arrow *a* indicates the limiting value of $\partial W/\partial I_1$, and those of the arrows *b* and *c* correspond to the limiting values of $\partial W/\partial I_2$ and $\partial W/\partial I_3$, respectively. The limiting values were calculated from Eqs. (4.13a)-(4.13c), using the value of G listed in Table 4-2. For SPU850, the limiting values of the derivatives shown by the arrows are a little different from those estimated from experiment; the vertical level of the arrow *a* is almost identical to the experimental value at the second lowest I_1.

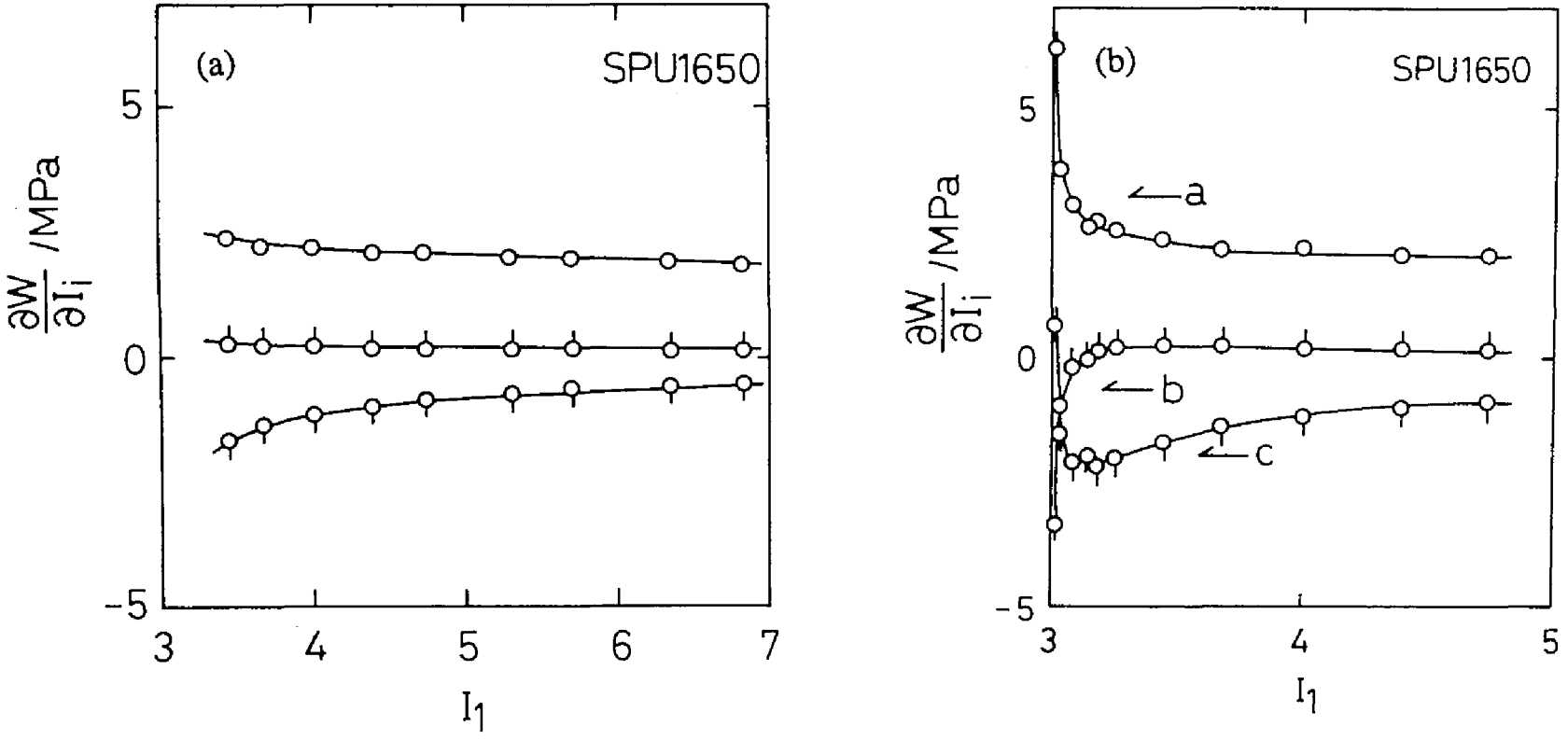

Figure 4-10. (a) Plots of $\partial W/\partial I_i$ against I_1 for SPU1650 for large I_1 region. (b) Plots of $\partial W/\partial I_i$ against I_1 for SPU1650 for small I_1 region. Symbols: (O) data points for $\partial W/\partial I_1$; (Ȯ) for $\partial W/\partial I_2$; (O̤) for $\partial W/\partial I_3$. The arrows *a*, *b* and *c* represent the theoretical predictions for $\partial W/\partial I_1$, $\partial W/\partial I_2$ and $\partial W/\partial I_3$ at zero strain limit, respectively.

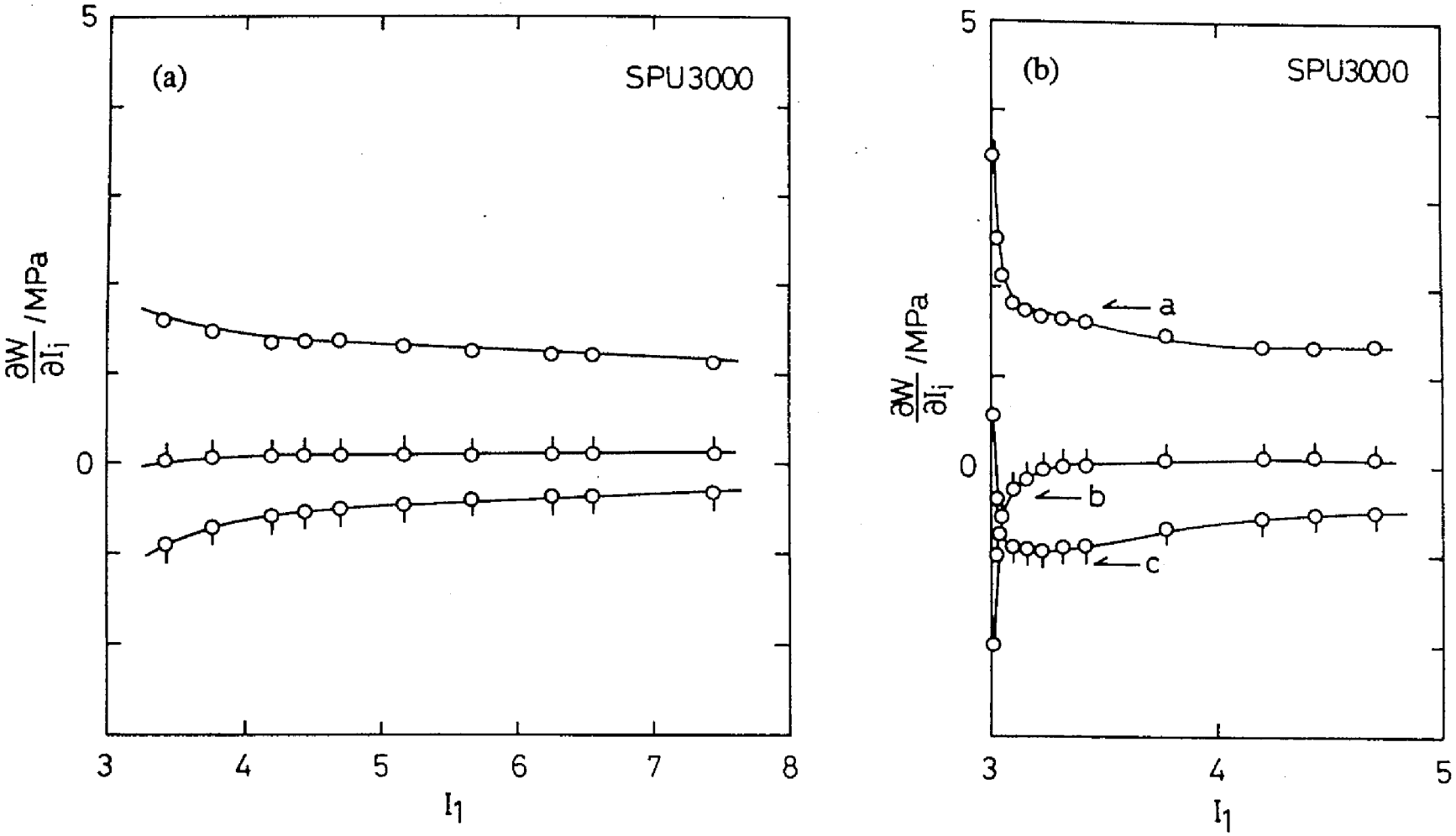

Figure 4-11. (a) Plots of $\partial W/\partial I_i$ against I_1 for SPU3000 for large I_1 region. (b) Plots of $\partial W/\partial I_i$ against I_1 for SPU3000 for small I_1 region. Symbols: (O) data points for $\partial W/\partial I_1$; (Ȯ) for $\partial W/\partial I_2$; (Ǫ) for $\partial W/\partial I_3$. The arrows *a*, *b* and *c* represent the theoretical predictions for $\partial W/\partial I_1$, $\partial W/\partial I_2$ and $\partial W/\partial I_3$ at zero strain limit, respectively.

The arrows *b* and *c* are also close to the corresponding experimental value at that I_1. Although there remains a small deviation of the limiting values of the derivatives between theoretical prediction and experiment, the theoretical predictions appear to show the basic features of the experimental data at small I_1 limit. The quantitative agreement between theoretical predictions and experiment for SPU1650 and SPU3000 is not so good compared with the case of SPU850, but the theoretical prediction could qualitatively explain the asymptotic behavior of the derivatives at small I_1 limit. As mentioned previously, the reproducibility of the $\partial W/\partial I_i$ *vs.* I_1 (i=1,2,3) curves was fairly good, but a small scattering was observed at small strains for the SPUs. The deviation in the limiting values between theory and experiment will originate from the experimental errors at small strains, because the limiting values determined by experiment is sensitive to the experimental errors.

The I_1 dependence of the derivatives was also investigated for three kinds of SPUs by employing the assumption that the material is incompressible (*i.e.*, I_3=1) for comparison. In this case, only $\partial W/\partial I_1$ and $\partial W/\partial I_2$ are the quantities of interest. For pure shear deformation of incompressible material, I_1 is identical to I_2. The $\partial W/\partial I_i$ *vs.* I_1 (i=1,2) curves for each SPU was almost identical to the corresponding curves shown here (Figs. 4-9, 4-10, 4-11 for SPU850, SPU1650, SPU3000, respectively). This suggests that $\partial W/\partial I_i$ *vs.* I_1 (i=1,2) curves are unchanged whether or not the volume change during deformation occurs. According to the classical theory of rubber elasticity for incompressible material, $\partial W/\partial I_1$ is independent of I_1 and is identical to $G/2$, and $\partial W/\partial I_2$ is also constant to be zero. At large strains, $\partial W/\partial I_1$ for SPUs showed lower values than $G/2$, which were weakly dependent on I_1. The derivative $\partial W/\partial I_2$ also showed slight I_1 dependence, although the value is close to zero at large strains. These features at large

strains appear to resemble the results expected by the classical theory of rubber elasticity for incompressible material. However, the strong I_1 dependence of the two derivatives at small strains can not be described by the classical theory. In addition, the classical theory can also not explain the negative limiting value of $\partial W/\partial I_2$. The theoretical predictions for $\partial W/\partial I_2$ shown in Sec. 4.2.3 is $-G/8$, which is negative. This qualitatively agrees with the experimental results for the SPUs. The classical theory predicts that the limiting value of $\partial W/\partial I_1=G/2$, while our prediction gives $\partial W/\partial I_1=5G/8$. The limiting values of the derivative by experiment (see, Figs. 4-9b, 4-10b and 4-11b) appear to be higher than $5G/8$ for the three SPUs. For the SPUs our prediction ($5G/8$) is closer to the experimental value than $G/2$ (the predicted value from the classical theory), although the difference between two predictions is rather small.

4.4.4 Partial Derivatives of W for IR

Figure 4-12 shows the plots of $\partial W/\partial I_i$ against I_1 for isoprene rubber (IR) under pure shear deformation reported by Kawabata *et al.*[5] Figures 4-12a and 4-12b represent the data at large I_1 and at small I_1, repectively. Their data were re-calculated by using μ_o=0.499916, the mean value of μ_o reported by the authors. The $\partial W/\partial I_i$ *vs.* I_1 (i=1,2) curves obtained here were almost identical to the corresponding original curves shown in Figure 10 of their paper[5], which were calculated by assuming the incompressibility of the material. As can be seen from Fig. 4-12a, the absolute values of $\partial W/\partial I_2$ and $\partial W/\partial I_3$ are very small compared with that of $\partial W/\partial I_1$ at large I_1, and the three derivatives are also weakly dependent on I_1. The experimental data in Fig. 4-12b show that the three derivatives are strongly dependent on I_1 at small strains. We can also see that the limiting values of $\partial W/\partial I_2$ and $\partial W/\partial I_3$ are

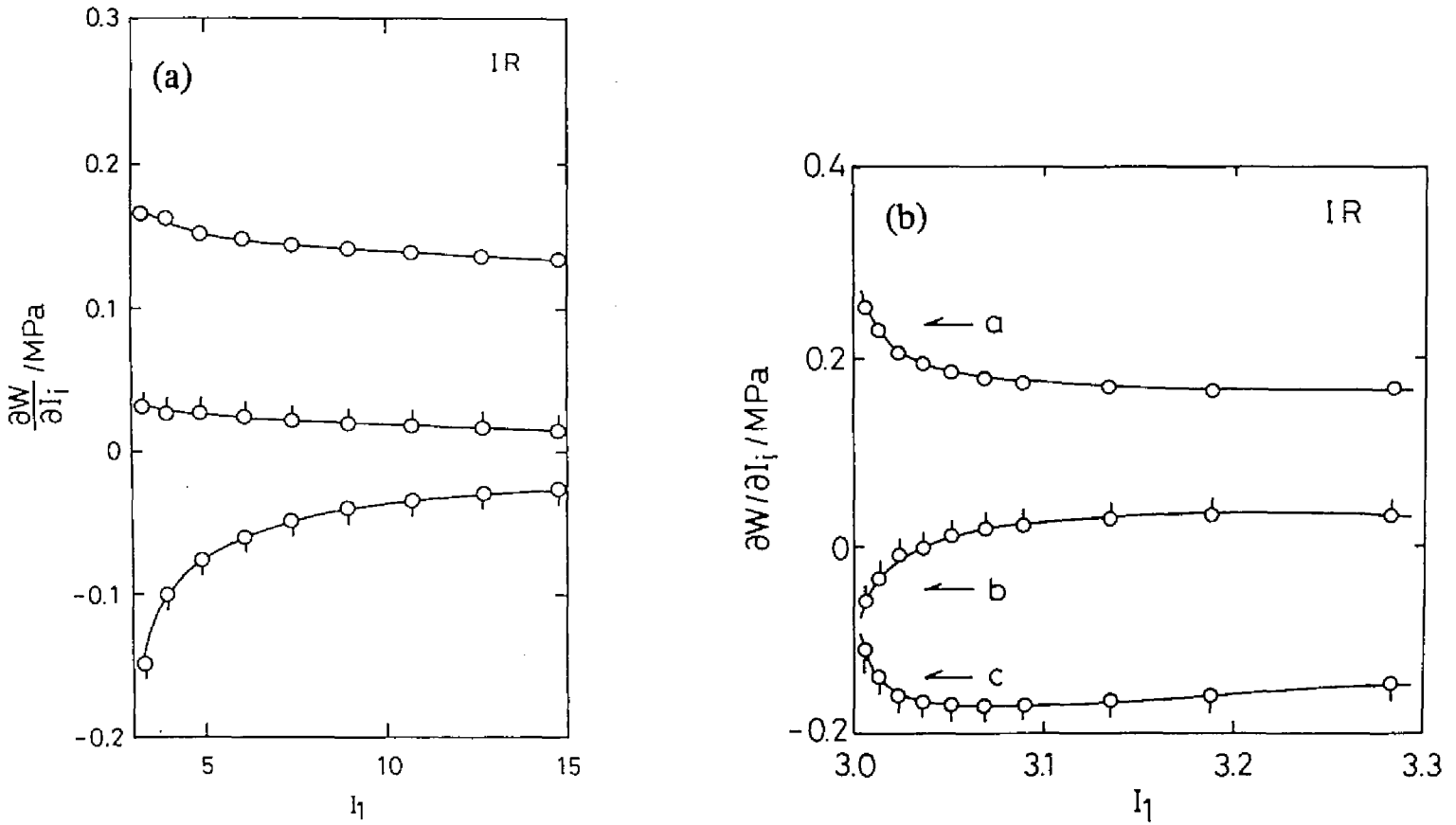

Figure 4-12. (a) Plots of $\partial W/\partial I_i$ against I_1 for IR for large I_1 region. (b) Plots of $\partial W/\partial I_i$ against I_1 for IR for small I_1 region. Symbols: (O) data points for $\partial W/\partial I_1$; (Ȯ) for $\partial W/\partial I_2$; (Ǫ) for $\partial W/\partial I_3$. The arrows *a*, *b* and *c* represent the theoretical predictions for $\partial W/\partial I_1$, $\partial W/\partial I_2$ and $\partial W/\partial I_3$ at zero strain limit, respectively.

negative and that of $\partial W/\partial I_1$ is positive for IR. There are also three arrows in the figure and the meaning of the arrows is the same as that in Figs. 4-9b, 4-10b and 4-11b. The value of G obtained from Fig. 4-5 was used for the calculation of the derivatives. The value of G is very close to the original value reported by Kawabata *et al.*[5] Each arrow appears to agree fairly well with the corresponding limiting value estimated from the experimental data. According to the classical theory of rubber elasticity for incompressible material, the limiting value of $\partial W/\partial I_1$ is given by $G/2$, as stated previously. The value of $G/2$ is 0.188MPa for IR, if we use G=0.375MPa. The value $G/2$ is much lower than the limiting value of $\partial W/\partial I_1$ determined by the experiment (Fig. 4-12b). It is also clear that the limiting value of $\partial W/\partial I_2$ estimated by experiment is negative, which is not in agreement with the prediction based on the classical theory for incompressible material, because the theory gives the limiting value of zero, as mentioned before. These mean that the classical theory of rubber elasticity for incompressible material can not correctly predict the limiting values of $\partial W/\partial I_1$ and $\partial W/\partial I_2$ for IR.

4.4.5 Partial Derivatives of W for SBR, NBR, BR

We calculate $\partial W/\partial I_i$ (i=1,2,3) for SBR, NBR and BR using the experimental data obtained by Fukahori *et al.*[6] The value of μ_o for BR was reported to be 0.49983,[19] and those for SBR and NBR are unknown. We used μ_o=0.49983 for the calculation of $\partial W/\partial I_i$ for three types of rubbers.

Figures 4-13 - 4-15 indicate the plots of $\partial W/\partial I_i$ *vs.* I_1 for SBR, NBR and BR, respectively. The I_1 dependence of $\partial W/\partial I_i$ for three types of rubbers is similar to each other, and resembles that for the SPUs and IR mentioned before: The $\partial W/\partial I_1$ is almost independent of I_1 at large I_1 region, and increases rapidly as I_1 approaches to three. The $\partial W/\partial I_2$ is almost constant and

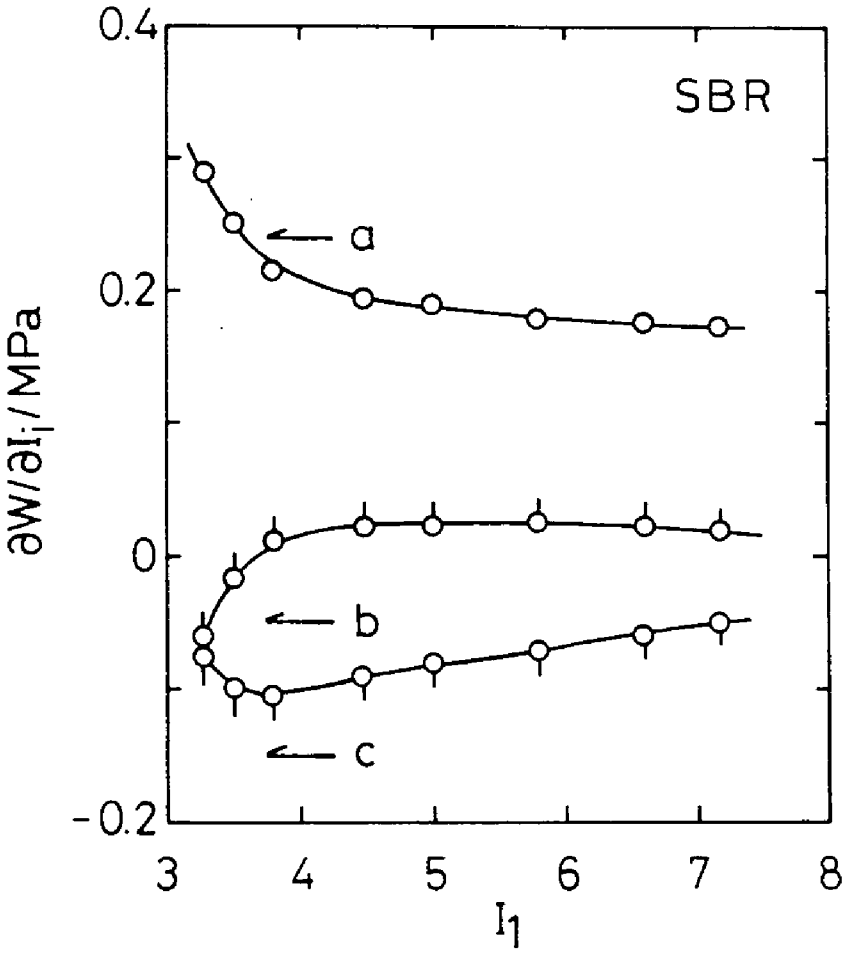

Figure 4-13. Plots of $\partial W/\partial I_i$ against I_1 for SBR. Symbols: (O) data points for $\partial W/\partial I_1$; (Ȯ) for $\partial W/\partial I_2$; (Ǫ) for $\partial W/\partial I_3$. The arrows *a*, *b* and *c* represent the theoretical predictions for $\partial W/\partial I_1$, $\partial W/\partial I_2$ and $\partial W/\partial I_3$ at zero strain limit, respectively.

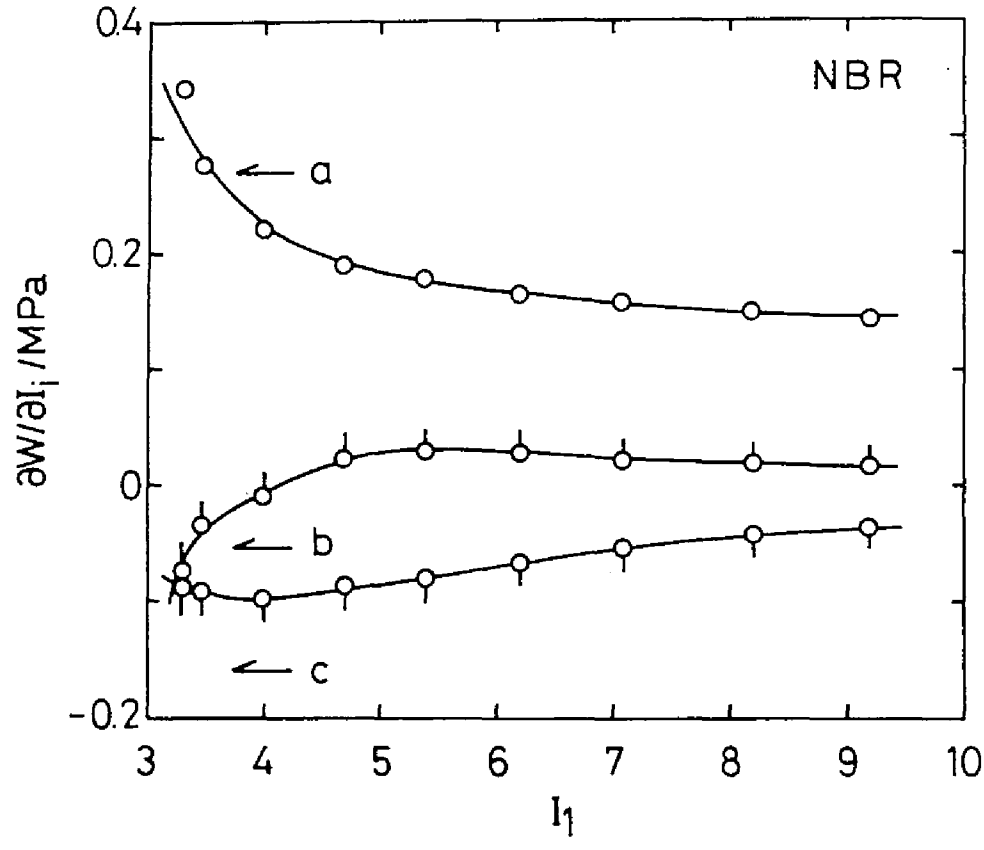

Figure 4-14. Plots of $\partial W/\partial I_i$ against I_1 for NBR. Symbols: (O) data points for $\partial W/\partial I_1$; (Ȯ) for $\partial W/\partial I_2$; (Ǫ) for $\partial W/\partial I_3$. The arrows *a*, *b* and *c* represent the theoretical predictions for $\partial W/\partial I_1$, $\partial W/\partial I_2$ and $\partial W/\partial I_3$ at zero strain limit, respectively.

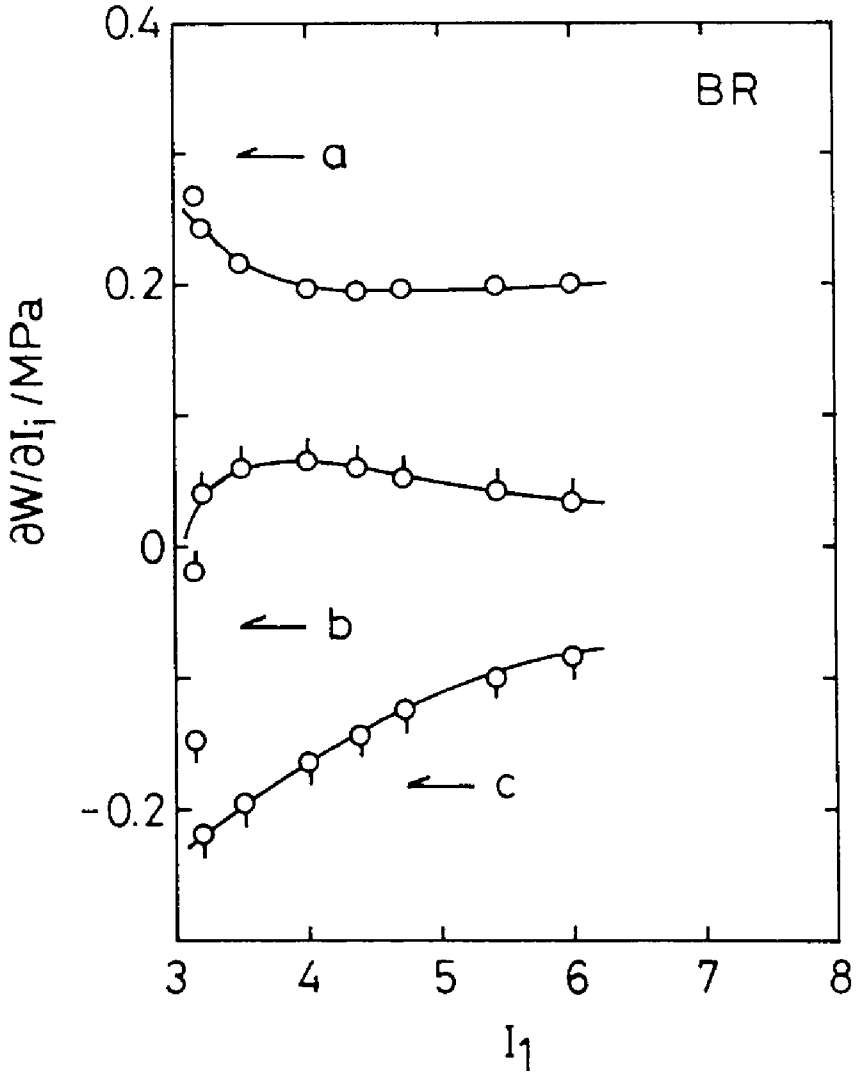

Figure 4-15. Plots of $\partial W/\partial I_i$ against I_1 for BR. Symbols: (O) data points for $\partial W/\partial I_1$; (O) for $\partial W/\partial I_2$; (O) for $\partial W/\partial I_3$. The arrows *a*, *b* and *c* represent the theoretical predictions for $\partial W/\partial I_1$, $\partial W/\partial I_2$ and $\partial W/\partial I_3$ at zero strain limit, respectively.

close to zero at large I_1 region, and decreases as I_1 decreses, and then becomes negative in the small I_1 region. The $\partial W/\partial I_3$ is negative over the whole I_1 region, and has a minimum in the small I_1 region.

The arrows *a-c* in Figs. 4-13 - 4-15 indicate the theoretical predictions for the limiting values of $\partial W/\partial I_i$ calculated from Eq. (4.13) with measured *G*. The agreement of the theoretical predictions with the experiments are not necesarrily perfect, but the theoretical values are not so far from the experiments, considering that the the values of $\partial W/\partial I_i$ in small deformation region is very sensitive to the experimental errors, and the number of experimental data points for SBR, NBR and BR is not enough in the small I_1 region .

The shapes of $\partial W/\partial I_i$ (i=1,2,3) *vs.* I_1 curves of three types of SPUs and four types of rubbery materials are similar to each other, suggesting that the shapes of the three derivatives shown here are common to real elastomers.

4.4.6 Some Comments on the Functional Form of W

The function W can be phenomenologically expressed in the following expansion form.[22]

$$W = \sum_{p,q,r} C_{pqr} (I_1 - 3)^p (I_2 - 3)^q (I_3 - 3)^r \qquad (4.16)$$

where C_{pqr} is the numerical constant and C_{000}=0. When the material is incompressible, Eq. (4.16) is reduced to

$$W = \sum_{p,q} C_{pq} (I_1 - 3)^p (I_2 - 3)^q \qquad (4.17)$$

with numerical constant C_{pq} and C_{00}=0. Mooney[23] approximated Eq. (4.17) as

$$W = C_{10} (I_1 - 3) + C_{01} (I_2 - 3) \qquad . \qquad (4.18)$$

The rubber materials dealt in this study is compressible. In this case, the approximated equation corresponding to Eq. (4.18) is given by

$$W = C_{100}(I_1 - 3) + C_{010}(I_2 - 3) + C_{001}(I_3 - 3) \quad . \quad (4.19)$$

Equation (4.19) means $\partial W/\partial I_1 = C_{100}$, $\partial W/\partial I_2 = C_{010}$ and $\partial W/\partial I_3 = C_{001}$. The I_1 dependence of $\partial W/\partial I_i$ (i=1,2,3) for rubbers investigated here is how $\partial W(I_1, I_2, I_3)/\partial I_1$ changes with I_1 on the trajectory $S(I_1, I_2, I_3)$ for pure shear deformation, where I_2 and I_3 vary as I_1 varies. In this case, the I_2 and I_3 dependece might also be involved in the plots of $\partial W/\partial I_1$ *vs.* I_1 for the experiments. Still, the I_1 dependence of $\partial W/\partial I_i$ for the real elastomers (Figs. 4-9 - 4-15) indicates that Eq. (4.19) is insufficient for the better description of W for the real elastomers at small strains, although Eq. (4.19) appears to approximate W of the real elastomers in the large I_1 region. The rapid change of $\partial W/\partial I_i$ at small strains will originate from the fact that $W(I_1, I_2, I_3)$ must have the asymptotic form shown in Eq. (4.2) at infinitesimal strains, although the functional form of $W(I_1, I_2, I_3)$ remains still unknown at present.

4.5 Conclusions

On the basis of the infinitesimal elasticity theory, the limiting values of the partial derivatives of W with respect to I_i (i=1,2,3) were evaluated. The limiting value of $\partial W/\partial I_1$ was found to be $(5G/8)$, while both $\partial W/\partial I_2$ and $\partial W/\partial I_3$ were respectively $(-G/8)$ and $(-3G/8)$. The Poisson ratios of the three types of SPUs different in M_s were measured by the experiments under uniaxial elongation (μ_o) and under pure shear deformation (μ_o'). The values of μ_o and μ_o' were smaller than 1/2, and increased with increasing M_s. The value of μ_o was larger than that of μ_o' for the SPUs. The limiting values of the derivatives ($\partial W/\partial I_i$; i=1,2,3) for SPUs were compared with the theoretical prediction. It was found that the theoretical prediction could explain the asymptotic behavior of the derivatives at small I_1 limit. The comparison of the limiting values was also made for the experimental results of isoprene

rubber (IR) reported by Kawabata *et al.*, styrene-butadiene rubber (SBR), nitrile-butadiene rubber (NBR) and butadiene rubber (BR) reported by Fukahori *et al.* The agreement of the limiting values between theory and experiment was also fairly well for these four types of rubbers.

References

1. Kawabata, S. and Kawai H., *Adv. Polym. Sci.*, **24**, 89 (1977).
2. Becker, G. W., *J. Polym. Sci., Part C*, **16**, 2893 (1967).
3. Jones, D. J. and Treloar, J. R. G., *J. Phys. D*, **8**, 1285 (1975).
4. James, A. G., Green, A., Simpson, G. M., *J. Appl. Polym. Sci.*, **19**, 2033 (1975).
5. Kawabata, S., Matsuda, M., Tei, K. and Kawai, H., *Macromolecules*, **14**, 154 (1981).
6. Fukahori, Y. and Seki, W., *Polymer*, **33**, 502 (1992).
7. Treloar, L. R. G., "*The Physics of Rubber Elasticity*", 3rd Ed., Clarendon Press, Oxford (1975).
8. Wall, F. T., *J. Chem. Phys.*, **11**, 527 (1943).
9. James, H. M. and Guth, E., *J. Chem. Phys.*, **15**, 669 (1947).
10. Edwards, S. F., *Br. Polym. J.*, **9**, 140 (1977).
11. Ball, R. C., Doi, M., Edwards, S. F. and Warner, M., *Polymer*, **22**, 1010 (1981).
12. Marrucci, G., *Macromolecules*, **14**, 434 (1981).
13. Flory, P. J. and Erman, B., *Macromolecules*, **15**, 800 (1982).
14. Gaylord, R. J., *Polym. Bull.*, **8**, 325 (1982); **9**, 181 (1983).
15. Gottlieb, M. and Gayload, R. J., *Macromolecules*, **20**, 130 (1987).
16. Matsuda, M., Kawabata, S. and Kawai, H., *Macromolecules*, **14**, 1688 (1981).
17. Matsuda, M., Kawabata, S. and Kawai, H., *Macromolecules*, **15**, 160 (1982).
18. Wood, L. A. and Martin, G. M., *Rubber Chem. Technol.*, **37**, 850 (1964).
19. Holownia, B. P., *Rubber Chem. Technol.*, **48**, 246 (1975).

20. Landau, L. D. and Lifshitz, E. M., "*Theory of Elasticity*", Nauka, Moscow, 1987.
21. Takahara, A., Tashita, J., Kajiyama, T. and Takayanagi, M., *J. Biomed. Mat. Res.*, **19**, 13 (1985).
22. Rivlin, R. S., *J. Appl. Phys.*, **18**, 444, 837 (1947).
23. Mooney, M., *J. Appl. Phys.*, **11**, 582 (1940).

Chapter 5
Effects of Polymer Concentration at Crosslinking on Swelling and Elastic Properties of End-Linked Poly(dimethylsiloxane) Networks

5.1 Introduction

The thermodynamics on swelling of polymer networks and the elastic properties have been experimentally and theoretically investigated for many years. However, in spite of tremendous efforts, several problems still remain unsolved. Especially, the vigorous discussions have been made on the effects of trapped entanglements on elastic modulus of polymer networks, and the treatment of reference state in the theory describing the equilibrium swelling of polymer networks crosslinked in solution. In this chapter and Chapter 6, the above two problems are focused, and the thermodynamics of equilibrium swelling as well as the elasticity for polymer networks crosslinked in solution are investigated.

Trapped entanglements are formed by the uncrossablility of network chains when crosslinks are introduced in the system. The contribution of trapped entanglements to elastic modulus has been disputed since the latter half of 1970's. The central subject of the dispute has been that trapped entanglements might contribute to elastic modulus together with chemical crosslinks[1-6] or not[7-10]. In order to settle this problem, the elastic moduli of "model polymer networks", which are prepared in bulk state by end-linking prepolymer having a definite molecular weight, have been measured as a function of the molecular weight of prepolymer (M_p).[3-7,9] However, in spite of considerable number of experiments following this line, the dispute still remains unsettled. In this thesis, as an alternative experiment aiming to solve

this problem, the elastic moduli of networks prepared by end-linking reaction in solution are measured as a function of preparation concentration, *i.e.*, polymer concentration at crosslinking. The prepolymer used has high molecular weight enough to form entanglement couplings in uncrosslinked state. As described later, preparation concentration dependence of elastic modulus in preparation state clarifies the effects of trapped entanglements on elastic modulus.

In respect to thermodynamics of swelling of polymer networks crosslinked in solution, there have been an unresolved problem regarding the treatment of reference state. Some researchers[12-16] have regarded a polymer volume fraction at preparation (ϕ_o) as a reference state. Others[17-21] have taken ϕ^* (the polymer volume fraction at which overlapping of network chains begins) as a reference state independently of ϕ_o (this is so-called the c^* theorem[17]). The classical theory regarding ϕ_o as a reference state had a weak point that it was based on Gaussian chain statistics and mean field theory, because concentration of gels usually belongs to semidilute concentration regime in which excluded volume effect and concentration fluctuation can not be neglected.[17,18] Recently, Panyuhov[15] proposed a scaling form in respect to the elasticity of gels considering excluded volume effect under the assumption of the affine displacement of crosslinks on swelling. Obukhov *et al.*[16] derived new theoretical predictions considering ϕ_o as a reference state by combining the Panyuhov's concept with the scaling theory taking an effect of the concentration fluctuation into account. On the other hand, the c^* theorem considers that polymer volume fraction of equilibrium swollen network (ϕ_e) is equivalent to ϕ^*.[17] The c^* theorem gives the familiar prediction for ϕ_e dependence of elastic modulus of equilibrium swollen networks (E_s) as follows.[17]

$$E_S \propto \phi_e^{3\nu/(3\nu-1)} \tag{5.1}$$

where ν is the excluded volume exponent. For instance, in respect to polymer networks swollen in a typical good solvent (ν=3/5), Eq. (5.1) gives $E_S \propto \phi_e^{9/4}$. The validity of the c^* theorem has often been believed on the basis of the experimental confirmation of Eq. (5.1).[17-21] The c^* theorem postulates the complete disinterpenetration of network chains in equilibrium swollen state.[17] However, as demonstrated later, Eq. (5.1) is also derived from a model in which crosslinks moves affinely in swelling.[22] Under the affine displacement of crosslinks in swelling, the number of network chains per unit volume occupied by a network chain is unchanged between before and after swelling, which means that the affine assumption does not satisfy the complete disinterpenetration of network chains at equilibrium. This implies that the confirmation of Eq. (5.1) is not complete support of the validity of the c^* theorem. The same logic holds with respect to the scaling relation for correlation length (ξ), $\xi \propto \phi_e^{\nu/(1-3\nu)}$, which has been confirmed by scattering experiments,[23-25] because ξ is related to E_S as $E_S \propto \xi^{-3}$.[17] Eventually, the ϕ_e dependence of physical quantities of equilibrium swollen networks does not give us any information about the interspersion state of network chains. As mentioned later, the differences between the theories are clearly seen in ϕ_o dependence of physical properties of equilibrium swollen networks. In order to obtain the definite theoretical description for equilibrium swollen networks, we must investigate physical properties through the ϕ_o dependence, together with the ϕ_e dependence.

It is worth while noting that the network samples in this study were prepared to have as small number of structural defects as possible. The molar ratio of the reaction sites in crosslinker to the reaction groups in prepolymer (r) was varied at each ϕ_o, and the value of r showing the maximum of ϕ_e

(r_{opt}) was regarded as the condition at which a model network having the least amount of structural defect is obtained. The details of this method will be described later. The experimental data for the network samples prepared at $r=r_{opt}$ were used for the analysis of ϕ_o dependence of ϕ_e, E_i and E_s. It should be noted that generally, r_{opt} is larger than the stoichiometric ratio ($r=1$),[6] and in the earlier studies for polymer networks crosslinked in solution,[18,26,27] the samples were prepared at $r=1$, *i.e.*, not under the optimal condition.

In this chapter, we prepare polymer networks by end-linking the polydimethylsiloxane (PDMS) whose molecular weight is higher than the critical molecular weight (M_c=16600)[28] for the formation of entanglements in uncrosslinked state. (The case in which the prepolymers are non-entangled in uncrosslinked state, *i.e.*, the molecular weight of prepolymer is lower than M_c, is treated in the next chapter.) The polymer networks are attempted to have as small amount of structural defect as possible. The degree of equilibrium swelling and initial Young's moduli of networks in both preparation and equilibrium swollen states are measured as a function of ϕ_o. The experimental results are compared with the theoretical predictions based on the affine model assuming ϕ_o as reference state, and the c^* theorem.

5.2 Theoretical Background

In this section, theoretical predictions for ϕ_o dependence of ϕ_e and E_s for end-linking type of networks prepared in solution are derived from the affine model and the c^* theorem, respectively.

5.2.1 Affine Model

The affine model employed here is based on the treatment by Obukhov *et al.*[16], to which we add the consideration about the concentration regime and

the contribution of trapped entanglements to elastic modulus. According to Flory and Rehner's assumption,[29] the free energy of swollen polymer network consists of osmotic term for the mixing of solution and the elastic term for the deformation of network. The scaling form of F_{mix} (the osmotic part of free energy per site occupied by a monomer) is[17]

$$\frac{F_{mix}}{k_B T} \approx \frac{\pi a^3}{k_B T} \approx \phi^{3\nu/(3\nu-1)} \tag{5.2}$$

where k_B and T is respectively the Boltzmann constant and the absolute temperature, and π is the osmotic pressure, and a^3 is the volume of a monomer, and ϕ is the polymer volume fraction, and ν is an excluded volume exponent.

Panyukov derived the scaling form of F_{el} (the elastic part of free energy per site occupied by a monomer), considering the thermal expansion effect of chains due to concentration difference between preparation and swollen state.[15]

$$\frac{F_{el}}{k_B T} \approx \frac{E a^3}{k_B T} \approx \frac{\phi}{N_{ef}} \lambda_s^2 \alpha_T^2 \tag{5.3}$$

where E is the elastic modulus, and N_{ef} is the length in polymerization index for elastic chains contributing to elastic modulus, and λ_s is the swelling coefficient defined as $\lambda_s=(\phi/\phi_o)^{-1/3}$, and α_T is the expansion coefficient defined as $\alpha_T = R_o/R$. Here, R_o is the root of mean square end-to-end distance of the connected prepolymer chain at ϕ_o and R is the end-to-end distance of the prepolymer chain in unconnected state in solution at ϕ. Equation (5.3) implies that the end-to-end distance of prepolymer chains in swollen state is equal to λR_o, which corresponds to the assumption of affine displacement of crosslinks. The theoretical descriprion for $N_{ef}(\phi_o)$ will be discussed in the end of this section. Here, we derive the scaling predictions for ϕ_e and E_s without giving the definite form of $N_{ef}(\phi_o)$.

The scaling theory predicts the ϕ dependence of R in semidilute regime ($\phi^* < \phi < \phi^{**}$) as follows.[17]

$$R(\phi) = R(1)\left(\frac{\phi}{\phi^{**}}\right)^{(2\nu-1)/(2-6\nu)} \tag{5.4}$$

Here, $R(1)$ corresponds to the end-to-end distance of prepolymer chain in melt, *i.e.*, the unperturbed state, and ϕ^* corresponds to the threshold value of ϕ where the overlap of polymer chains occurs, ϕ^{**} being the value of ϕ at the boundary for $R(\phi)$ between semidilute and the concentrated regime. In concentrated regime, $R(\phi)$ is equal to $R(1)$ due to full screening of excluded volume effect.

We consider here the two situations for swelling of polymer network prepared in good solvent: The case that ϕ_o and ϕ_e belong to semidilute regime, and the case that ϕ_o and ϕ_e belong to concentrated and semidilute regime, respectively. When networks are prepared in good solvent over the wide range of ϕ_o, the two situations above ($\phi_o < \phi^{**}$ and $\phi_o > \phi^{**}$) will be realized. The difference between the two situations is $R_o(\phi_o)$: $R_o(\phi_o)$ in the region $\phi_o < \phi^{**}$ is expressed by Eq. (5.4), while $R_o(\phi_o)$ in $\phi_o > \phi^{**}$ is equal to $R(1)$. The difference in $R_o(\phi_o)$ between the two situations leads to the difference in ϕ_o dependence of ϕ_e and E_s between the region $\phi_o < \phi^{**}$ and $\phi_o > \phi^{**}$ as shown below. From Eqs. (5.3) and (5.4), the scaling expression for E for each case is as follows.

$$\frac{F_{el}}{k_BT} \approx \frac{E\,a^3}{k_BT} \approx \frac{1}{N_{cf}(\phi_o)}\,\phi^{(9\nu-4)/(9\nu-3)}\phi_o^{1/(9\nu-3)} \qquad (\phi_o < \phi^{**}) \quad (5.5a)$$

$$\approx \frac{1}{N_{cf}(\phi_o)}\,\phi^{(9\nu-4)/(9\nu-3)}\,\phi^{**(2\nu-1)/(1-3\nu)}\phi_o^{2/3} \quad (\phi_o > \phi^{**}) \quad (5.5b)$$

The equilibrium swelling is achieved by the minimization of total free energy with respect to ϕ. It is found from Eqs. (5.2) and (5.5) that ϕ_e scales as

$$\phi_e \approx N_{cf}^{(3-9\nu)/4}\,\phi_o^{1/4} \qquad (\phi_o < \phi^{**}) \qquad (5.6a)$$

$$\approx N_{cf}^{(3-9\nu)/4}\,\phi^{**(3-6\nu)/4}\,\phi_o^{(3\nu-1)/2} \qquad (\phi_o > \phi^{**}) \qquad (5.6b)$$

The scaling prediction for E_s is derived from Eqs. (5.5) and (5.6) as follows.

$$\frac{E_s\,a^3}{k_B\,T} \approx N_{cf}^{-9\nu/4}\,\phi_o^{3\nu/(12\nu-4)} \qquad (\phi_o < \phi^{**}) \qquad (5.7a)$$

$$\approx N_{cf}^{-9\nu/4}\,\phi^{**(9\nu-18\nu^2)/(12\nu-4)}\,\phi_o^{3\nu/2} \qquad (\phi_o > \phi^{**}) \qquad (5.7b)$$

The relation between ϕ_e and E_s is easily obtained from Eqs. (5.6) and (5.7).

$$\frac{E_s\,a^3}{k_B\,T} \approx \phi_e^{3\nu/(3\nu-1)} \qquad (5.8)$$

Equation (5.8) was first derived from the c^* theorem assuming the complete disinterpenetration of network chains in equilibrium swelling state.[17] However, Eq. (5.8) has been derived here on the basis of the affine model which does not postulate the disinterpenetration of network chains in swelling. Actually, when the scaling form of F_{el} is expressed as $F_{el} \propto \phi_o^a\,\phi^b$, Eq. (5.8) is obtained irrespective of a and b, and the exponent for ϕ_e dependence of E_s is entirely determined by that for ϕ dependence of π in Eq. (5.1).[22] This means that Eq. (5.8) simply represents a balance between elastic force and osmotic pressure in equilibrium swelling. In other words, Eq. (2.6) is only an embodiment of the Flory-Rehner's assumption.

The full expressions for ϕ_o dependence of ϕ_e and E_s requires ϕ_o dependence of N_{cf}. The ϕ_o dependence of N_{cf} is directly related to ϕ_o dependence of elastic modulus in preparation state (E_i) as follows. The ϕ_o dependence of E_i is obtained from Eq. (5.3) with $\phi=\phi_o$ as

$$E_i(\phi_o) \approx \frac{\phi_o\,k_B\,T}{N_{cf}(\phi_o)\,a^3} \qquad (5.9)$$

This is identical with the conventional equation for elastic modulus from rubber elasticity theory.[30] As can be seen in Eq. (5.9), the ϕ_o dependence of E_i ($E_i \propto \phi_o^{\alpha}$) is directly related to ϕ_o dependence of N_{cf} ($N_{cf} \propto \phi_o^{x}$;$x=1-\alpha$). The value of x includes ϕ_o dependence of any effects of trapped entanglements on elastic modulus such as the role as additional crosslinks, and

the suppression effect of thermal fluctuation of crosslinks. The value of x is greatly influenced by the relative amount of trapped entanglement to chemical crosslink, and it depends on the details of network system concerned (such as molecular weight of prepolymer and functionality of crosslinks). In this sense, x is a phenomenological value depending on the network system used. In respect to the networks (as treated in this chapter) which has much more trapped entanglements than chemical crosslinks ($N_{ef} \simeq N_e$ where N_e is the length between neighboring trapped entanglements), the scaling form for $N_{ef}(\phi_o)$ will be analogous to that for $N_e(\phi_o)$. The theoretical prediction for concentration dependence of N_e has been reported by several authors,[17,30-33] and is still unsettled. The theoretical exponent for N_e ($N_e(\phi_o) \propto \phi_o^x$) was reported to be $x=-1$ by some authors,[30,31] while $x=1/(1-3\nu)$ ($=-5/4$ if $\nu=3/5$) was derived for good solvent system on the basis of the blob model.[17,32] Another authors argues that $x=-1$ holds in concentrated regime and $x=1/(1-3\nu)$ in semidilute regime.[33,34] The value of x has been obtained from the experiments[35-39] and the simulations[34] for rubbery plateau modulus of polymer solution. The reported values of x for good solvent vary from -1.0 to -1.4. It seems to be difficult at present to determine the correct theoretical value of x from available experimental data. Accordingly, we use here both $x=-1$ and $x=1/(1-3\nu)$ for the predictions for ϕ_o dependence of ϕ_e and E_s. The predicted exponents for ϕ_e and E_s ($\phi_e \propto \phi_o^y$, $E_s \propto \phi_o^z$) using $x=-1$ and $x=1/(1-3\nu)$ are shown in Table 5-1, respectively. Here, we used $\nu=0.57$ which is evaluated from the relationship between molecular weight and intrinsic viscosity for PDMS in toluene,[40] namely, $[\eta] \propto M^{3\nu-1}$. It can be seen from Table 5-1 that the theory predicts that the exponents for ϕ_e and E_s are higher in $\phi_o > \phi^{**}$ than in $\phi_o < \phi^{**}$.

Table 5-1. Exponents predicted by the affine model and the c^* theorem for the ϕ_o dependence of ϕ_e and E_s (y and z, respectively) according to the value of x. x is the exponent for the ϕ_o dependence of N_{cl}.

	x	y		z	
		$\phi_o < \phi_o^{**}$	$\phi_o > \phi_o^{**}$	$\phi_o < \phi_o^{**}$	$\phi_o > \phi_o^{**}$
affine model	-1^a	0.78	0.89	1.9	2.1
	-1.4^b	1.0	1.1	1.8	2.7
	-1.1^c	0.84	0.94	2.0	2.3
c^* theorem	-1^a	0.71		1.7	
	-1.4^b	0.99		2.4	
	-1.1^c	0.78		1.9	

[a] From the uniform network theory.

[b] From the scaling theory for good solvent system with ν=0.57.

[c] From the experimental result of the ϕ_o dependence of E_i in this study.

5.2.2 c Theorem*

According to the c^* theorem,[17] the polymer concentration of equilibrium swollen networks is identified with the overlapping concentration with respect to the network chains with polymerization index N. The c^* theorem predicts that ϕ_e scales as

$$\phi_e \approx \phi^* \propto N^{1-3\nu} \tag{5.10}$$

If N in Eq. (5.10) is regarded as the distance between chemical crosslinks, Eq. (5.10) gives an unrealistic prediction that ϕ_e is constant independently of ϕ_o for networks prepared by end-linking method. Candau *et al.*[18] argued that the c^* theorem is valid by substituting N_{cf} for N in Eq. (5.10), *i.e.*, treating trapped entanglements similarly as chemical crosslinks. Then, ϕ_e depends on ϕ_o through the ϕ_o dependence of N_{cf} as follows.

$$\phi_e \propto {N_{cf}}^{1-3\nu} \propto {\phi_o}^{x(1-3\nu)} \tag{5.11}$$

Using the relation $E_s \propto \phi_e / N_{cf}$ and Eq. (5.11), we obtain the relation between E_s and ϕ_e which is the same as Eq. (5.8). From Eqs. (5.8) and (5.11), the ϕ_o dependence of E_s is expressed as

$$E_s \propto {\phi_o}^{3\nu x} \tag{5.12}$$

The value of x in Eqs. (5.11) and (5.12) is related to ϕ_o dependence of E_i through Eq. (5.9).

The values of y and z predicted by the c^* theorem are obtained from Eqs. (5.11) and (5.12) according to x=−1 and −1.4, and are listed in Table 5-1. The difference in theoretical values of y and z by the affine model and the c^* theorem is not so large, but it should be noted that the c^* theorem does not predict the crossover in y and z in contrast to the affine model. This difference is due to the fact that the c^* theorem does not originally treat ϕ_o as an independent variable, and ϕ_o dependence of ϕ_e and E_s in Eqs. (5.11) and (5.12) is indirect one through ϕ_o dependence of N_{cf}.

5.3 Experimental

The molecular weight of vinyl-terminated PDMS (Chisso Co., Japan) is M_W=4.7×10^4, which was determined by light scattering measurement, and the value of M_W/M_n measured by gel permeation chromatography (GPC) is 1.6. Here, M_W and M_n is the weight and the number average molecular weight, respectively.

The gel samples were prepared by hydrosilylation in toluene between the vinyl groups at both ends of PDMS and silane hydrogens in tetrakisdimethysiloxysilane (TDMS). $H_2PtCl{\bullet}6H_2O$ dissolved in 2-propanol (the Spier's catalyst) was used as a catalyst for hydrosilylation.[41,42] The solutions were prepared at the seven kinds of polymer volume fraction (ϕ_o'), and r was varied at each ϕ_o'. The solution was casted into Teflon mold with sealing apparatus. The reaction was carried out at 100°C for 24h. In preliminary experiments, sol fraction for the samples with ϕ_o'=0.191 (the lowest ϕ_o' in this study) prepared under various reaction temperature was measured. The hydrosilylation reaction at low concentration involved difficulties at low reaction temperature, differing from that in bulk state. The samples with ϕ_o'=0.191 prepared below 100°C showed the larger sol fraction or no gelation. Though some types of side reaction in hydrosilylation reaction are known to occur at high temperature,[43,44] the sample prepared at 100°C were regarded as the network with the least amount of structural defect on the basis of the lowest value of sol fraction. The loss of toluene during the reaction process was prevented by sealing the mold. We confirmed that the loss amount of toluene was very small (less than 0.3 weight percent) by comparing the mold weight with sample between before and after the reaction.

The obtained gel samples were immersed in toluene until equilibrium of swelling was achieved. Toluene was properly renewed. The fully swollen gels were weighed, and then were kept drying in air to obtain fully deswollen networks. The weight of fully deswollen network was measured, and the value of ϕ_e and the weight fraction of soluble material for each sample was calculated. The sol fraction for each sample with $r=r_{opt}$ (where ϕ_e has the maximum in r dependence of ϕ_e) was less than eight weight percent. The values of ϕ_o were re-calculated by subtracting sol fraction from ϕ_o', taking the unreacted portion of prepolymer into account.

The original and the fully swollen networks prepared at each ϕ_o with $r=r_{opt}$ were used for mechanical measurements. The values of E_i and E_s at each ϕ_o were obtained by uniaxial elongational measurement. The values of ϕ_o, r_{opt}, ϕ_e, E_i and E_s at each ϕ_o' are summarized in Table 5-2.

5.4 Results and Discussion

5.4.1 r Dependence of ϕ_e at Each ϕ_o'

The r dependence of ϕ_e at ϕ_o'=0.191, 0.298, and 0.430 is shown in Fig. 5-1. The r dependence of ϕ_e at each ϕ_o' has the maximum, and the location of peaks is at $r\neq1$. The other samples have the similar r dependence of ϕ_e, and the data are not shown. The results in Fig. 5-1 qualitatively agree with those for the networks crosslinked in bulk state reported by Patel *et al.*[6] One of the reasons why the location of peak shifts to high r region is the unequal reactivity in the functional sites of tetrafunctional crosslinker. The reactivity of the fourth site of crosslinker with three reacted sites is much lowerd by steric hindrance.[6,45] The existence of dangling ends and structural defects should lead to decrease of ϕ_e.[6,46] The cyclization in end-linking of PDMS at low concentration was investigated by Vasiliev *et al.*[27] They

Table 5-2. Polymer volume fraction of the solution for preparation (ϕ_o'), polymer volume fraction and Young's modulus of the network in preparation state (ϕ_o and E_i, respectively) and in equilibrium swollen state (ϕ_e and E_s, respectively) and, the optimal ratio of silane hydrogen to vinyl group (r_{opt}).

ϕ_o'	ϕ_o	r_{opt}	$E_i \times 10^{-4}$(Pa)	$E_s \times 10^{-4}$(Pa)	ϕ_e
1.00	1.00	1.15	34	10	0.187
0.861	0.852	1.20	28	8.1	0.155
0.725	0.709	1.14	19	5.2	0.126
0.564	0.544	1.07	8.9	2.2	0.0933
0.430	0.411	1.24	5.8	1.4	0.0778
0.298	0.281	1.18	2.6	0.68	0.0549
0.191	0.179	1.20	0.89	0.28	0.0381

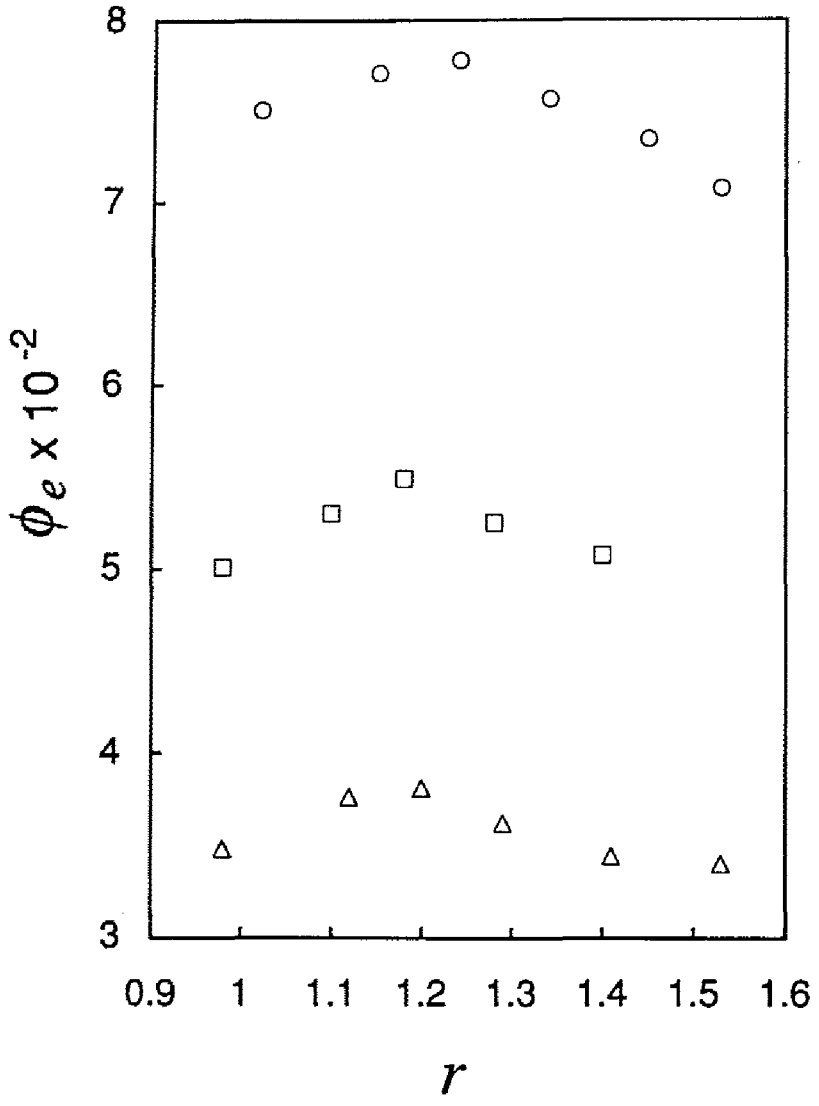

Figure 5-1. The ratio of silane hydrogens to vinyl groups (r) dependence of the polymer volume fraction of equilibrium swollen network (ϕ_e) for the samples prepared at ϕ_o' =0.191 (△); 0.298 (□); 0.430 (○). ϕ_o' is the polymer volume fraction in solution for sample preparation.

reported that the degree of cyclization in 10% solution decreases with increasing M of prepolymer, and that the formation of loop does not occur at M=1.1×10^4. The formation of loop defects should be negligible in this study because M of prepolymer in this study is much larger than 1.1×10^4. We regard the sample with r=r_{opt} as the network with the least amount of dangling end and the structural defect. The ϕ_o dependence of ϕ_e, E_i, and E_s in this study is for samples with r=r_{opt} at each ϕ_o.

5.4.2 ϕ_o Dependence of E_i

The ϕ_o dependence of E_i is shown in Fig. 5-2. The all data points fall on the straight line with the slope 2.1. If the elastic modulus is determined only by the number of chemical crosslinks (*i.e*, trapped entanglements do not give any contribution to elastic modulus), E_i is simply proportional to number density of prepolymer as

$$E_i \propto \phi_o^{1} \quad . \tag{5.13}$$

Equation (5.13) is also obtained from Eq. (5.9) with $N_{eff(\phi_o)} = N$ where N is the polymerization index of prepolymer. The relation $E_i \propto \phi_o^{2.1}$ is similar to concentration dependence of plateau modulus of polymer solutions, which suggests that trapped entanglements have dominant contribution to elastic modulus for all samples in this study. It is found from $E_i \propto \phi_o^{2.1}$ and Eq.(5.9) that $N_{eff(\phi_o)}$ scales as

$$N_{eff(\phi_o)} \propto \phi_o^{-1.1} \quad . \tag{5.14}$$

This exponent is within the results ($-1 \le x \le -1.4$) obtained from rubbery plateau modulus of polymer solution,[35-39] and is closer to the value from uniform network theory (x=-1)[30,31] than that from scaling theory[17,32] (x=$1/(3\nu-1)$=-1.4). Equation (5.14) holds in the wide range of ϕ_o ($0.178 \le \phi_o \le 1$), which is the similar result for rubbery plateau modulus of polymer

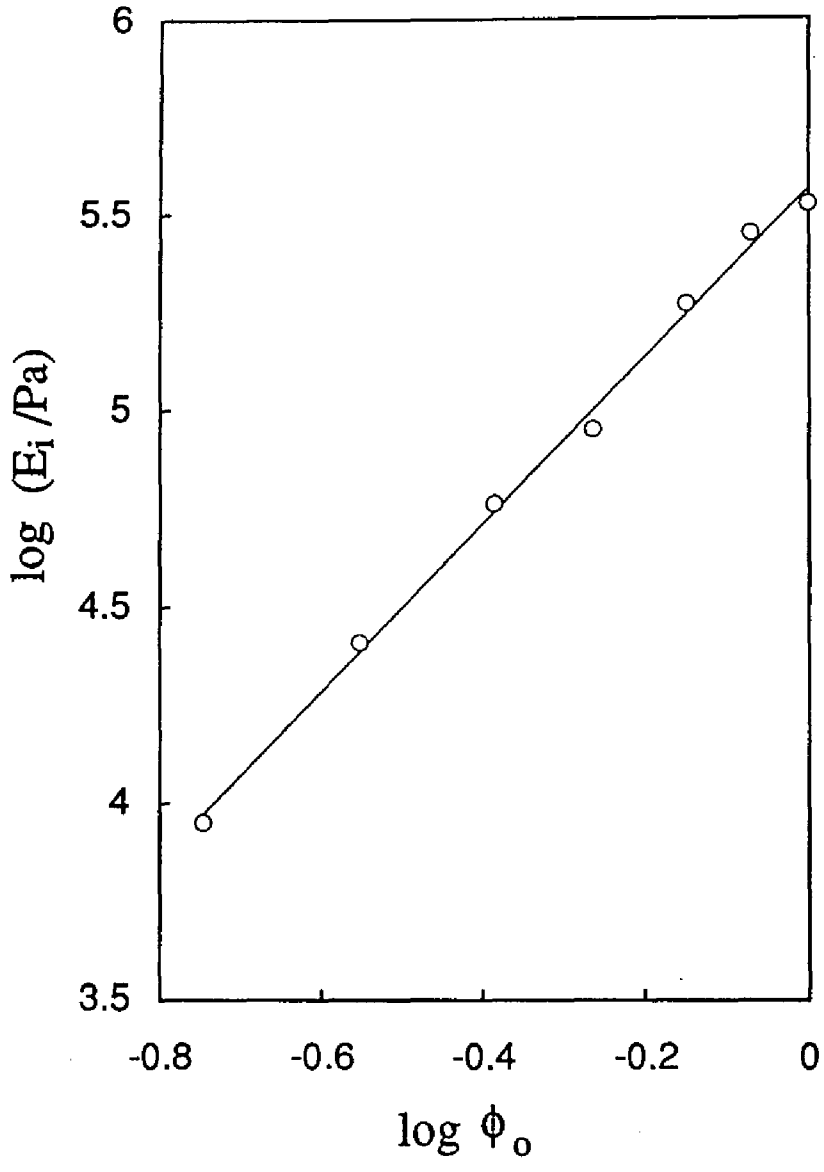

Figure 5-2. The ϕ_o dependence of E_i . ϕ_o is the polymer volume fraction of the network in preparation state, and E_i is the Young's modulus of the network in preparation state. The slope of the solid line is 2.1.

solution.[35-38] With regard to this point, Takahashi *et al.*[38] concluded that for the understanding of plateau modulus of polymer solutions the scaling concept of a semidilute region is not necessary, and the uniform network model (x=−1) is enough for the description of $N_{e(\phi_o)}$. Our experimental data ($\phi_o \geq 0.178$) seem to support their idea. The data for E_i of samples prepared at lower ϕ_o may be necessary in order to discuss strictly whether the crossover in ϕ_o dependence of E_i exists or not, but the elongation of samples with $\phi_o<0.178$ was very difficult due to the softness of material.

Here, the exponents of y and z predicted with the experimental result x=−1.1 are added to the third and sixth row of Table 5-1. This *ad hoc* procedure would be significant under present situation that the definite theoretical description for $N_{e(\phi_o)}$ is not established. The prediction with x=−1.1 gives the somewhat higher exponents than that with x=−1.

5.4.3 ϕ_o *Dependence of* ϕ_e and E_s

The ϕ_o dependence of ϕ_e is shown in Fig. 5-3. The ϕ_o dependence of ϕ_e showed the crossover: $\phi_e \propto \phi_o^{0.82}$ in low ϕ_o region, and $\phi_e \propto \phi_o^{1.1}$ in high ϕ_o region. The exponents were determined by the least square method for the four data points in each region. The value of ϕ_o at the boundary is estimated to be *ca.* 0.58.

The theoretical evaluation of ϕ_o^{**} is given by the following equation.[47]

$$\phi_o^{**} \approx (T-\Theta)/\Theta \qquad (5.15)$$

where Θ is the Θ temperature. The value of ϕ_o^{**} is evaluated to be 0.22 by using Eq. (5.15) with T=298K and Θ=234K for PDMS in toluene.[48] However, Adachi *et al.* showed that the value of ϕ_o^{**} predicted by Eq. (5.15) is quite different from the experimental value of ϕ_o^{**} obtained from concentration dependence of R of *cis*-polyisoprene in good solvent by means

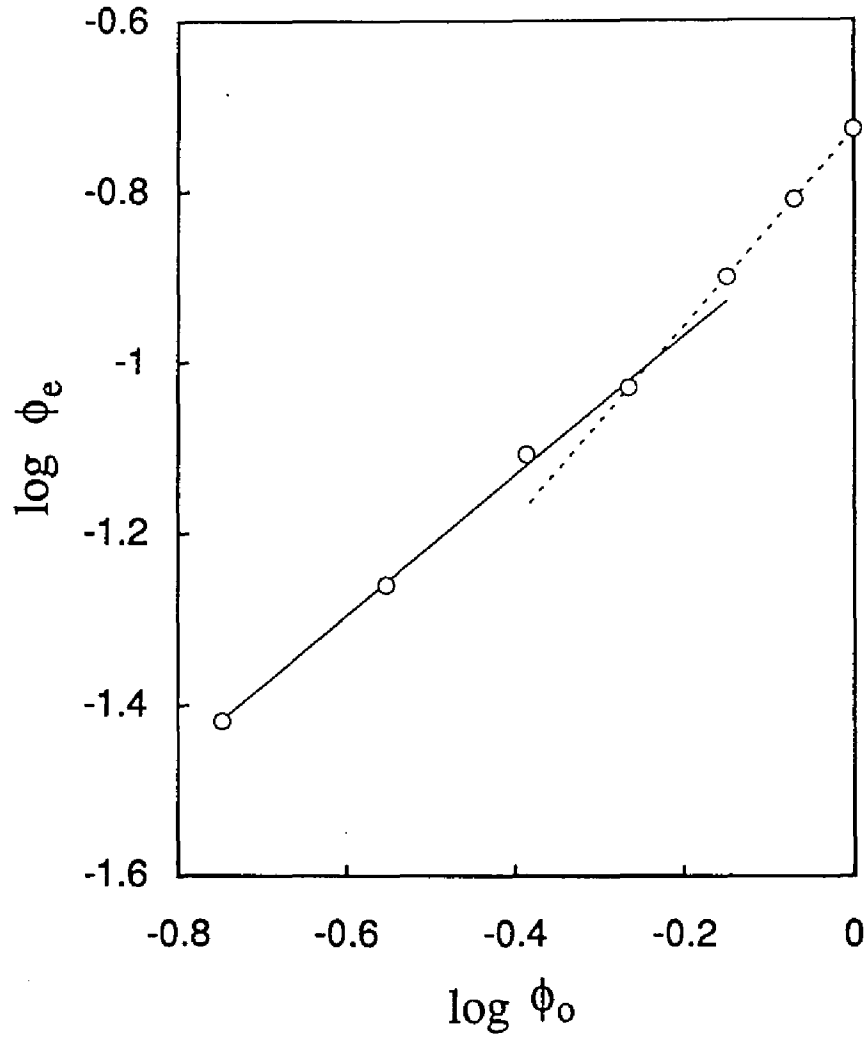

Figure 5-3. The ϕ_o dependence of ϕ_e. ϕ_o and ϕ_e is the polymer volume fraction of the network in the preparation state and the fully swollen state, respectively. The slope of the solid and the broken line is 0.82 and 1.1, respectively. The crossover point is estimated to be $\phi_o \approx 0.58$.

of dielectric spectroscopy.[49] The dielectric spectroscopy has been the only method to measure R directly.[49,50] The measurement is possible only on the so-called type-A polymers having the dipole moment aligned parallel in the same direction along chain contour.[50] (Poly(dimethyl siloxane) does not correspond to type-A polymer.) According to their study,[49] the crossover concentration for R of *cis*-polyisoprene in benzene between semidilute and concentrated regime was evaluated to be 0.55g/cm^3, which is converted into 0.60 in polymer volume fraction with the density of *cis*-polyisoprene (0.913g/cm^3). The value of ν for *cis*-polyisoprene in benzene was reported to be 0.578,[49] which is close to ν=0.57 for the system in this study. Assuming that ϕ_o^{**} is dominated by the affinity between the polymer and the solvent,[51,52] their result (ϕ_o^{**} = 0.60) would be considered as a rough estimation of ϕ_o^{**} for the system in this study. The crossover point in Fig. 5-3 is close to their result (ϕ_o^{**} = 0.60), suggesting that the crossover of ϕ_o dependence of ϕ_e occurs at ϕ_o^{**}.

As can be seen from Table 5-1, the experimental value of y in the region $\phi_o < \phi_o^{**}$ is close to those expected by the affine model with x=−1 or x=−1.1, while the dependence in $\phi_o > \phi_o^{**}$ is stronger than the predictions with x=−1 or x=−1.1. The prediction by the affine model with x=−1.4 is higher than the experimental exponent in low ϕ_o region, while that is in good agreement with the experiment in high ϕ_o region. On the other hand, the theoretical exponent by the c^* theorem with x=−1 or x=−1.1 is close to the experimental one in $\phi_o < \phi_o^{**}$, but the c^* theorem does not explain the crossover in ϕ_o dependence of ϕ_e in the experiment.

The results in earlier studies[18,26,27] for ϕ_o dependence of ϕ_e in good slovent were rather different from our results. In Ref. 18, the exponent was 0.71 and 0.75, and the crossover was not observed. This discrepancy may be

due to three reasons: Their samples were prepared at $r \neq r_{opt}$ and did not have much trapped entanglements due to low molecular weight of PDMS prepolymer (M=9700), and the data in low ϕ_o region below ϕ_o^{**} were lacking (the lowest ϕ_o was 0.458). The exponent from the data in Refs. 26 and 27 yields 0.71 and 0.54-1.1, respectively. However, the exponents are estimated from a small number of data, and their samples were not prepared at $r=r_{opt}$.

We indicate ϕ_o dependence of E_s in Fig. 5-4. The crossover in ϕ_o dependence of E_s is observed, and the change of slope occurs more clearly, compared with that in the ϕ_o dependence of ϕ_e. The value of ϕ_o at crossover point is estimated to be *ca.* 0.53, which is close to that for ϕ_o dependence of ϕ_e and also ϕ_o^{**}=0.60 reported by Adachi *et al.*[49] The crossover point for ϕ_o dependence of E_s would be considered as ϕ_o^{**}. The ϕ_o dependence of E_s in each region is as follows: $E_s \propto \phi_o^{1.9}$ in the region $\phi_o < \phi_o^{**}$; $E_s \propto \phi_o^{2.5}$ in $\phi_o > \phi_o^{**}$. The determining method for the exponent in each region is the same as that in ϕ_o dependence of ϕ_e. The prediction by the affine model with each value of x explains the experimental results in $\phi_o < \phi_o^{**}$, while the experimental exponent in $\phi_o > \phi_o^{**}$ is intermediate between the predictions with x=−1.1 and x=−1.4. As is the case in ϕ_o dependence of ϕ_e, the prediction by the c^* theorem shows the good agreement with the experiment in either $\phi_o < \phi_o^{**}$ or $\phi_o > \phi_o^{**}$, depending on the value of x employed. However, the crossover in ϕ_o dependence of E_s in the experiment is not explained by the c^* theorem.

In the earlier studies, the exponent for E_s was estimated to be 1.8,[18] 1.9[18] and 1.6-2.3,[27] and the crossover was not reported at all. The reason why their results are different from ours will be the same as that in the case of ϕ_o dependence of ϕ_e as mentioned before.

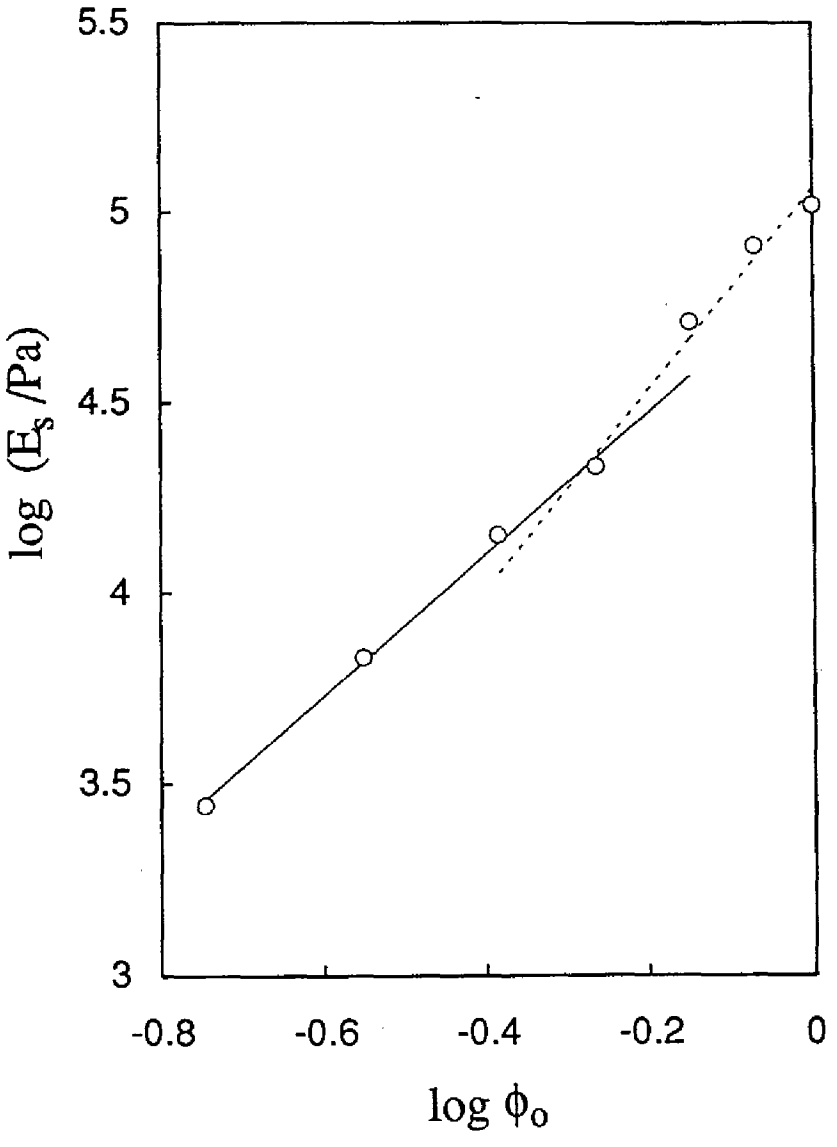

Figure 5-4. The ϕ_0 dependence of E_s. ϕ_0 is the polymer volume fraction of the network in preparation state, and E_s is the Young's modulus of the fully swollen network. The slope of the solid and the broken line is 1.9 and 2.5, respectively. The crossover point is evaluated to be $\phi_0 \approx 0.53$.

In the comparison of experimental results in Figs. 5-2 - 5-4 with the predictions by the affine model with three kinds of x value, the *ad hoc* procedure using $x=-1.1$ seems to be superior to the others in the quantitative description of experimental results, though the experimental results of y and z in $\phi_o > \phi_o^{**}$ are somewhat higher. The predictions with $x=-1.4$ succeeds in the description of y in $\phi_o > \phi_o^{**}$, but the employment of $x=-1.4$ would not be reasonable, because there is a noticeable difference between $x=-1.4$ and $x=-1.1$ obtained experimentally, and it seems to be unreasonable that the scaling concept for good solvent system is valid from semidilute regime to melt. The fairly good agreement of theoretical predictions by the *ad hoc* procedure with experimental results supports the validity of the affine assumption for the displacement of crosslinks on swelling and the treatment of trapped entanglements in this study, though the problem on the strict theoretical description of $N_{eff(\phi_o)}$ still remains.

The exponents for ϕ_e and E_s by the c^* theorem are close to those by the affine model, and this fortuitous coincidence made it somewhat difficult to discuss the difference between both theories. However, the crossover in ϕ_o dependence of ϕ_e and E_s observed experimentally is explained by the affine model, while it is not described by the c^* theorem. This result strongly suggests that ϕ_o need to be considered as the reference state for networks crosslinked in solution, and the displacement of crosslinks on swelling is affine.

5.4.4 ϕ_e Dependence of E_s

The plots of $\log E_s$ against $\log\phi_e$ are indicated in Fig. 5-5. The relation between $\log E_s$ and $\log\phi_e$ is represented by the straight line with slope 2.3. Equation (5.8) with $\nu = 0.57$ predicts the relation between E_s and ϕ_e as E_s

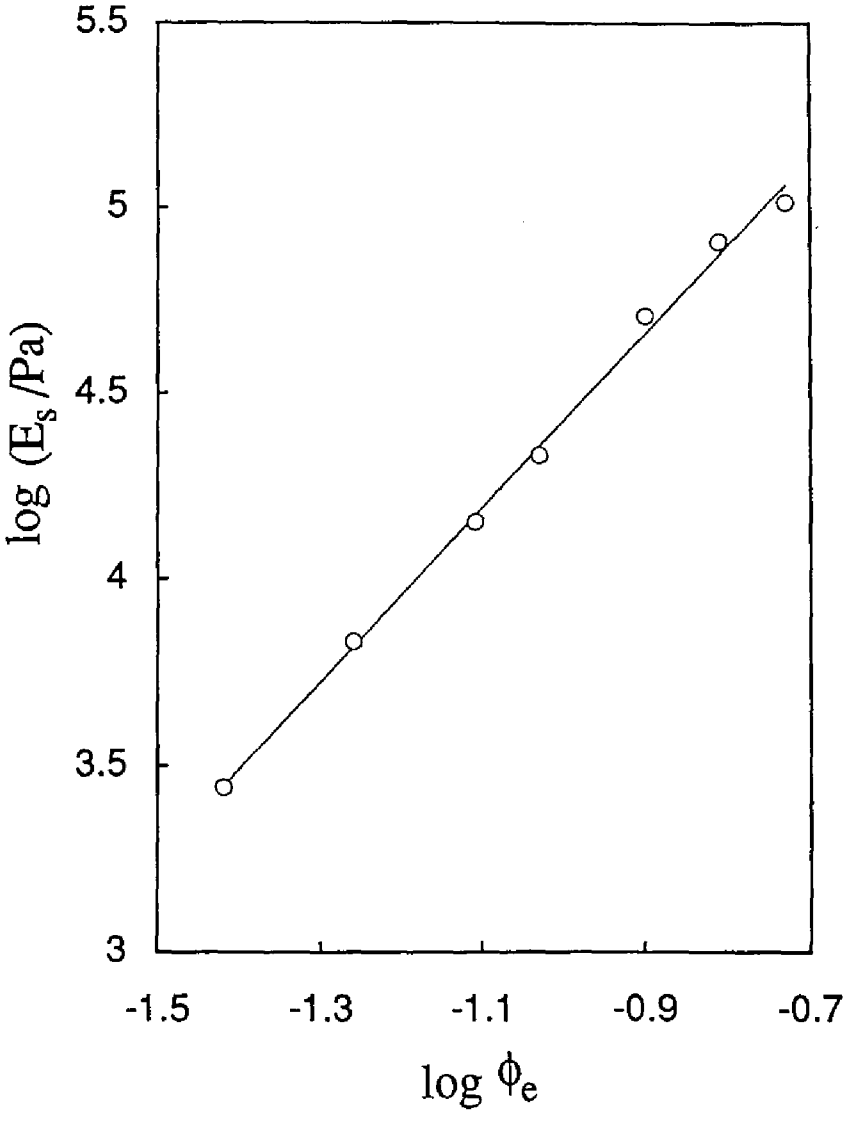

Figure 5-5. The ϕ_e dependence of E_s. ϕ_e and E_s is the polymer volume fraction and the Young's modulus of the equilibrium swollen network, respectively. The slope of the solid line is 2.3.

$\propto \phi_e^{2.4}$. The theoretical exponent is in good agreement with the experimental value. Equation (5.8) has been experimentally confirmed by many experiments for good solvent system.[17-21] Equation (5.8) is not influenced by the details of sample preparation and the amount of entanglements in the network, as described previously.

5.5 Conclusions

In this chapter, the degree of equilibrium swelling and the elastic modulus of equilibrium swollen networks were investigated as a function of preparation concentration. The polymer networks were prepared by end-linking the prepolymers with high molecular weight which are entangled in uncrosslinked state. The network samples were attempted to have as small amount of structural defects as possible. The preparation concentration dependence of elastic modulus in preparation state coincided with the concentration dependence of plateau modulus of polymer solutions, which suggests that trapped entanglements act similarly as chemical crosslinks, and those dominantly contribute to elastic modulus. The crossover in preparation concentration dependence was observed both for the volume fraction and the elastic modulus of equilibrium swollen networks. The crossover concentration for both cases coincided with each other, and corresponded to the concentration where full screening of excluded volume effect for polymer chains occurs. The theoretical predictions for preparation concentration dependence of swelling and elastic properties were derived on the basis of the affine model which regards preparation concentration as a reference state, and assumes the affine displacement of crosslinks on swelling. The experimental results quantitatively agreed with the predictions by the affine model, while the c^* theorem considering ϕ^* as a reference state did not

explain the crossover in preparation concentration dependence of the degree of equilibrium swelling and the elastic modulus of equilibrium swollen networks. The above results suggests that the displacement of crosslinks moves affinely on swelling, and the complete disinterpenetration of network chains does not occur in equilibrium swelling state when there is the high degree of overlapping of network chains in preparation state.

References

1. Langley, N. R. and Polmanteer, K. E., *J. Polym. Sci.; Polym. Phys. Ed.*, **12**, 1023 (1974).
2. Dossin, L. M. and Graessley, W. W., *Macromolecules*, **12**, 123 (1979).
3. Gottlieb, M., Macosko, C. W., Benjamin, G. S.,Meyers, K. O. and Merril, E. W., *Macromolecules*, **14**, 1039 (1981).
4. Valles, E. M., Rost, E. J. and Macosko, C. W., *Rubber Chem. Technol.*, **57**, 55 (1984)
5. Opperman, W.and Rennar, N., *Prog. Colloid Polym. Sci.* **75**, 49 (1987).
6. Patel, S. K., Malone, S., Cohen, C., Gillmor, J. R. and Colby, R. H., *Macromolecules*, **25**, 5241 (1992).
7. Mark, J. E. and Sullivan, J. L., *J. Chem. Phys.*, **66**, 1006 (1977).
8. Flory, P. J. and Erman, B., *Macromolecules*, **15**, 800 (1982).
9. Queslel, J. P. and Mark, J. E., *J. Polym. Sci.; Polym. Phys. Ed.*, **22**, 1201 (1984).
10. Soni, V. K. and Stein, R. S., *Macromolecules*, **23**, 5257 (1990).
11. Erman, B. and Mark, J. E., *Macromolecules*, **25**, 1917 (1992).
12. James, M. and Guth, E., *J. Chem. Phys.*, **15**, 669 (1947).
13. Dusek, K. and Prins, W., *Fortshr. Hochpolym. Forsh.*, **6**, 1 (1969).
14. Floelich, D., Crawford, D., Rozek, T. and Prins, W., *Macromolecules*, **5**, 100 (1972).
15. Panyukov, S. V., *Sov. Phys. JETP*, **71**, 372 (1990).
16. Obukhov, S. P., Rubinstein, M., and Colby, R. H., *Macromolecules*, **27**, 3191 (1994).
17. de Gennes, P. G., "*Scaling Concepts in Polymer Physics*", Cornell University Press, Ithaca, NY, 1979.
18. Candau, S., Peters, A. and Herz, J., *Polymer*, **22**, 1504 (1981).

19. Hild, G., Okasha, R., Macret, M. and Gnanou, Y., *Makromol. Chem.*, **187**, 2271 (1986).
20. Richards, R. W. and Davidson, N. S., *Macromolecules*, **19**, 1381 (1986).
21. Zrinyi, M.,and Horkay, F., *Macromolecules*, **17**, 2805 (1987).
22. Brochard, F., *J. Phys. (Paris)*, **40**, 1049 (1979).
23. Munch, J. P., Candau, S., Herz, J. and Hild, G., *J. Phys. (Paris)*, **38**, 971 (1977).
24. Shibayama, M., Takahashi, H. and Nomura, S., *Macromolecules*, **28**, 6860 (1995).
25. Falcão, A. N., Pedersen, J. S., Mortensen, K. and Boué, F., *Macromolecules*, **29**, 809 (1996).
26. Rempp, P., Herz, J., Hild, G. and Picot, C., *Pure Appl. Chem.*, **43**, 77 (1975).
27. Vasiliev, V. G., Rogovina, L. Z. and Slonimsky, G. L., *Polymer*, **26**, 1667 (1985).
28. Orrah, D. J., Semlyen, J. A. and Ross-Murphy, S. B., *Polymer*, **29**, 1452 (1988).
29. Flory, P. J. and Rehner, J., *J. Chem. Phys.*, **11**, 521 (1943)
30. Ferry, J. D., "*Viscoelastic Properties of Polymers, 3rd ed.*" Wiley, NY, 1980.
31. Graessley, W. W., *Adv. Polym. Sci.* **16**, 1 (1974); **47**, 67 (1982).
32. Colby, R. H. and Rubinstein, M., *Macromolecules*, **23**, 2753 (1990).
33. Lin, Y.-H, *Macromolecules*, **20**, 885, 3080 (1987).
34. Iwata, K. and S. F. Edwards, *J. Chem. Phys.*, **90**, 4567 (1989).
35. Nemoto, N., Odani, H. and Kurata, M., *Macromolecules*, **4**, 458 (1971).
36. Masuda, T., Toda, N., Aoto, Y. and Onogi, S., *Polym. J.* **3**, 315 (1972).

37. Plazek, D. J., Riande, E., Markovitz, H. and Raghupathi, N., *J. Polym. Sci., Polym. Phys. Ed.*, **17**, 2189 (1979).
38. Takahashi, Y., Noda, I. and Nagasawa, M., *Macromolecules*, **18**, 2220 (1985).
39. Adam M. and Delsanti, M., *J. Phys. (Paris)* **44**, 1185 (1983); **45**, 1513 (1984).
40. Haug, V. A. and Meyerhoff, G., *Macromol. Chem.*, **53**, 91 (1962).
41. Speier, J. L., *Adv. Organomet. Chem.*, **17**, 407 (1979).
42. Kohjiya, S., Ono, A. and Yamashita, S., *Polym.-Plast. Technol. Eng.*, **30**, 351 (1991).
43. Macosko , C. W. and Saam, J. C., *Polym. Bull.*, **18**, 463 (1987).
44. He, X., A. Lapp, A., and Herz, J., *Makromol. Chem.*, **189**, 1061 (1988).
45. Kohjiya, S., Takada, Y., Urayama, K., Tezuka, Y. and Kidera, A., *Bull. Chem. Soc. Jpn.*, **69**, 565 (1996).
46. Andrady, A. L., Llorente, M., Sharaf, M. A., Rahalkar, R. R., Mark, J. E., Sullivan, J. L., Yu, C. U. and Falender, J. R., *J. Appl. Polym. Sci.*, **26**, 1829 (1981).
47. Daoud, M. and Jannink, G., *J. Phys. (Paris)*, **37**, 973 (1976).
48. Kuwahara, N. and Kaneko, M., *Makromol. Chem.*, **82**, 205 (1965).
49. Adachi, K., Imanishi, Y., Shinkado, T. and Kotaka, T., *Macromolecules*, **22**, 2391 (1989).
50. Stockmayer, W. H., *Pure Appl. Chem.*, **15**, 539 (1967).
51. Graessley, W. W., *Polymer*, **21**, 258 (1980).
52. Schaefer, D. W., *Polymer*, **25**, 387 (1984).

Chapter 6
Effects of Polymer Concentration at Crosslinking on Swelling and Elastic Properties of End-Linked Oligo(dimethylsiloxane) Networks

6.1 Introduction

In the previous chapter, the swelling and elastic properties of the networks crosslinked in solution using polydimethylsiloxane (PDMS) as a prepolymer were described. The PDMS had high molecular weight enough to be entangled in uncrosslinked state. The dependence of elastic modulus of PDMS networks in preparation state (E_i) on polymer concentration at crosslinking was in accord with the concentration dependence of plateau modulus of polymer solutions, which strongly suggests that trapped entanglements dominantly contribute to elasticity of crosslinked networks. In this chapter, the networks considered are prepared by end-linking oligodimethylsiloxanes (ODMS) which is not entangled in uncrosslinked state due to the low molecular weight. It is very interesting to investigate that trapped entanglements are formed or not in this system, and if any, how is the magnitude of their contribution to elastic modulus of polymer networks.

In the previous chapter, polymer volume fraction and initial Young's modulus in equlibrium swollen state (ϕ_e and E_s, respectively) were measured as a function of polymer volume fraction in preparation state (ϕ_o) in respect to the networks prepared by end-linking PDMS. The experimental results were compared with predictions by the two theories (*i.e.*, the affine model and the c^* theorem) describing equilibrium swelling of polymer networks. The ϕ_o dependence of ϕ_e and E_s obtained experimentally showed the crossover at $\phi_o \approx \phi^{**}$ as predicted by the affine model, where ϕ^{**} is the value

of ϕ_o at which the excluded volume effect for polymer chains is completely screened. The crossover in ϕ_o dependence of ϕ_e and E_s is a evidence of the validity of the affine model, but the exponents for ϕ_o dependence of ϕ_e and E_s (in the region $\phi_o<\phi^{**}$) predicted by the affine model and the c^* theorem were accidentally close to each other, which made the discussion about the difference between the two theories somewhat ambiguous. However, in respect to the networks prepared using ODMS as a prepolymer, there expected to be a significant difference between the exponents for ϕ_o dependence of ϕ_e and E_s predicted by the two theories. As described in Chapter 5, the theoretical exponents for ϕ_o dependence of of ϕ_e and E_s are dependent on the exponent (x) for ϕ_o dependence of the length of elastically effective chain (N_{el}). (See, Eqs. (5.6), (5.7), (5.11) and (5.12).) The value of x is changed by the degree of contribution of trapped entanglements to elastic modulus which is greatly influenced by the molecular weight of prepolymer used. Actually, the employment of ODMS as a prepolymer has enabled us to discuss the difference between the two theories more clearly, as will be demonstrated later.

In this chapter, the ϕ_o dependence of E_i, ϕ_e and E_s is investigated for the networks prepared by end-linking ODMS in solution. The contribution of trapped entanglements to elastic modulus is discussed on the basis of ϕ_o dependence of E_i. The ϕ_o dependence of ϕ_e and E_s obtained experimentally is compared with the predictions by the affine model and the c^* theorem. The theoretical predictions by the two theories were given previously in Chapter 5. (See, Eqs. (5.6), (5.7), (5.11) and (5.12).).

6.2 Experimental

The samples were prepared by hydrosilylation in toluene between methacryloyl(CH_2=C(CH_3)COO)-terminated oligodimethylsiloxane (ODMS) (Shinetsu Chemical, Co.) and tetrakisdimethylsiloxysilane (Chisso Co.). The number average molecular weight (M_n) of ODMS is M_n=4.4×10^3, which was determined from the intrinsic viscosity on the basis of the relation $[\eta]$(ml/g) =7.55×10^{-2}•$M_n^{0.50}$ for ODMS (2×10^3 ≤ M_n ≤ 1×10^4) in toluene at 25°C.[1] The value of M_n of ODMS is lower than the critical molecular weight (=1.66×10^4) for the formation of entanglements for PDMS.[2] The value of M_w/M_n measured by gel permeation chromatography was 1.7 where M_w is the weight average molecular weight.

The network samples were prepared in the same mannar as described in Chapter 5. The solutions with the eight kinds of polymer volume fraction (ϕ_o') (0.331 ≤ ϕ_o' ≤ 1) were prepared, and the ratio of silane hydrogens to methacryloyl groups (r) was varied at each ϕ_o'. The reaction was made at 100°C for 24h. The details of evaluation for ϕ_e, ϕ_o and weight fraction of soluble species (w_{sol}) are described in Chapter 5.

The reaction condition (100°C and 24h) employed was determined from the following preliminaly experiment. We compared the values of w_{sol} for the samples with ϕ_o' =0.411 prepared under various reaction temperature and reaction time. We adopted the reaction condition at which the sample with the least w_{sol} was obtained as a regular one.

The r dependence of ϕ_e at each ϕ_o' was investigated to obtain network samples with the least amount of structural defect. The samples with r=r_{opt} at which the r dependence of ϕ_e at each ϕ_o' showed the maximum were used for the measurements of ϕ_e, E_i and E_s. The details of r dependence of ϕ_e at each

ϕ_o' are described later. The value of w_{sol} for all the samples prepared at $r=r_{opt}$ were less than ten weight percent.

The dynamic Young's moduli of network samples in preparation and equilibrium swollen state (designated as E_i' and E_s', respectively) were measured by means of DVE-V4 Rheospectra (Rheology Engineering, Co., Japan). The measurements were made at room temperature under compression mode, and the strain amplitude was 0.01. The frequency (ω) was varied from $1s^{-1}$ to 100 s^{-1}. Both E_i' and E_s' for all the samples were almost constant over the examined range of ω. We adopted the average values of E_i' and E_s' over $1s^{-1} \leq \omega \leq 100\ s^{-1}$.

The values of ϕ_o, r_{opt}, ϕ_e , E_i' and E_s' at each ϕ_o' are summarized in Table 6-1.

6.3 Results and Discussion

6.3.1 r Dependence of ϕ_e at Each ϕ_o'

Figure 6-1 indicates r dependence of ϕ_e at ϕ_o'=0.331, 0.411, 0.531, 0.620. As can be seen, the r dependence of ϕ_e at each ϕ_o' shows the clear maximum which locates at $r>1$. The samples prepared at $\phi_o' \geq 0.656$ showed the similar behavior in r dependence of ϕ_e, and the data are not shown here. The results in Fig. 6-1 are qualitatively in accord with those obtained for the networks prepared by PDMS (See, Fig. 5-1). As there is the larger amount of structural defect such as dangling chains and loop in network, a network shows the smaller value of ϕ_e, *i.e.*, swells larger.[3] The value of r having the maximum of ϕ_e was regarded as the optimal condition ($r=r_{opt}$) that network samples with the least amount of structural defect are obtained. The major origin of $r_{opt}>1$ is mainly attributed to unequal reactivity of reactive sites in crosslinker due to steric hindrance, the details of which are described in

Table 6-1. Polymer volume fraction of the solution for preparation (ϕ_o'), polymer volume fraction and dynamic Young's modulus of the network in preparation state (ϕ_o and E_i', respectively) and in equilibrium swollen state (ϕ_e and E_s', respectively) and, the optimal ratio of silane hydrogen to methacryloyl group (r_{opt}).

ϕ_o'	ϕ_o	r_{opt}	E_i' $\times 10^{-5}$(Pa)	E_s' $\times 10^{-5}$(Pa)	ϕ_e
1.00	1.00	1.76	20.4	7.52	0.275
0.801	0.777	1.70	12.7	4.46	0.216
0.701	0.654	1.76	9.90	4.11	0.208
0.656	0.601	1.60	8.92	3.57	0.194
0.620	0.585	1.90	9.04	3.40	0.195
0.531	0.504	1.61	7.24	2.99	0.180
0.411	0.381	1.76	4.49	1.59	0.140
0.311[a]	0.298	2.00	1.83	0.872	0.109

[a]This sample has many structural defects. The data were omitted for the determination of the exponents for the ϕ_o dependence of E_i', ϕ_e and E_s'.

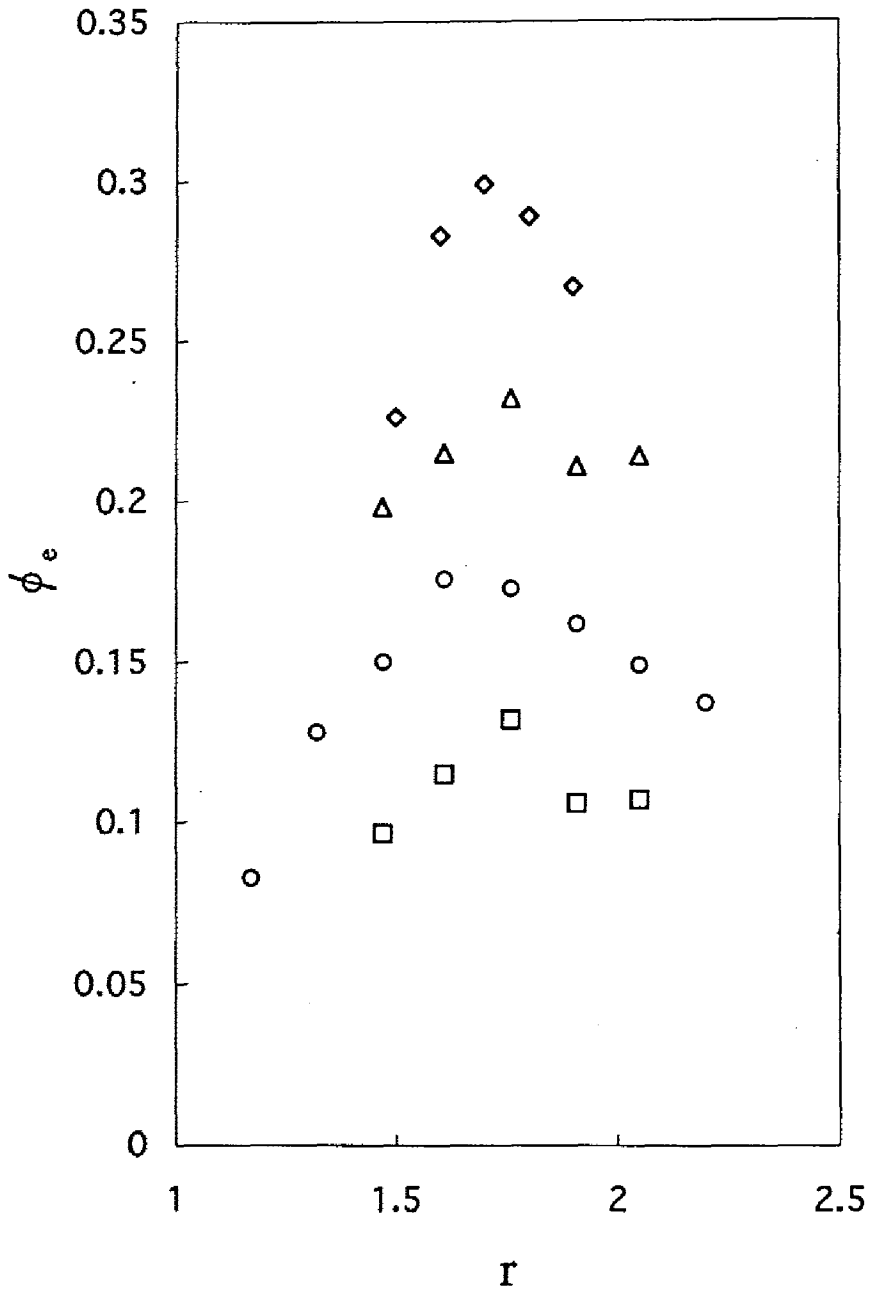

Figure 6-1. The ratio of silane hydrogens to vinyl groups (r) dependence of the polymer volume fraction of equilibrium swollen network (ϕ_e) for the samples prepared at ϕ_o' =0.331 (□); 0.411 (○); 0.531 (△); 0.620 (◇). ϕ_o' is the polymer volume fraction in solution for sample preparation.

Chapter 5. The data for the samples prepared at $r=r_{opt}$ for the analysis of ϕ_o dependence of E_i', ϕ_e and E_s' are employed.

6.3.2 ϕ_o Dependence of E_i'

Figure 6-2 shows the double logarithmic plots of E_i' *vs.* ϕ_o. It is found that ϕ_o dependence of E_i' in the region $\phi_o \geq 0.381$ is expressed by $E_i' \propto \phi_o^{1.52}$, and the value of E_i' at $\phi_o=0.298$ deviates downward from this relation. The exponent was determined from the least square method. As is well-known, the non-negligible degree of loop formation occurs at the crosslinking in solution with low concentration.[4] Actually, $\phi_o'=0.331$ at which the sample with $\phi_o=0.298$ was prepared is close to $\phi^* \approx 0.34$ evaluated from $[\eta]$ of the prepolymer. Here, ϕ^* is the threshold value of polymer volume fraction at which overlapping of prepolymer chains occur. The elastic modulus of a network having many loops is lower than that expected for network with no loops, because loop structure does not contribute to elastic modulus. The low value of E_i' at ϕ_o =0.298 should be due to the considerable number of loops in the network structure. The value of w_{sol} for the sample prepared at $\phi_o'=0.331$ was comparable to those at $\phi_o' \geq 0.411$. This suggests that the reaction at $\phi_o'=0.331$ proceeded to the same degree as that at $\phi_o' \geq 0.411$, but the considerable part of reaction was consumed for loop formation. The preparation of polymer network with small number of defects may be difficult in the region $\phi_o \approx \phi^*$ due to inevitable loop formation. The abrupt decrease of elastic modulus at $\phi_o'=0.331$ suggests that the number of loop defects is considerable at $\phi_o' \leq 0.331$, while it is small enough not to prevent the quantitative discussion about elasticity of networks prepared at $\phi_o' \geq 0.411$. The data of the sample prepared at $\phi_o'=0.331$ in the determination of

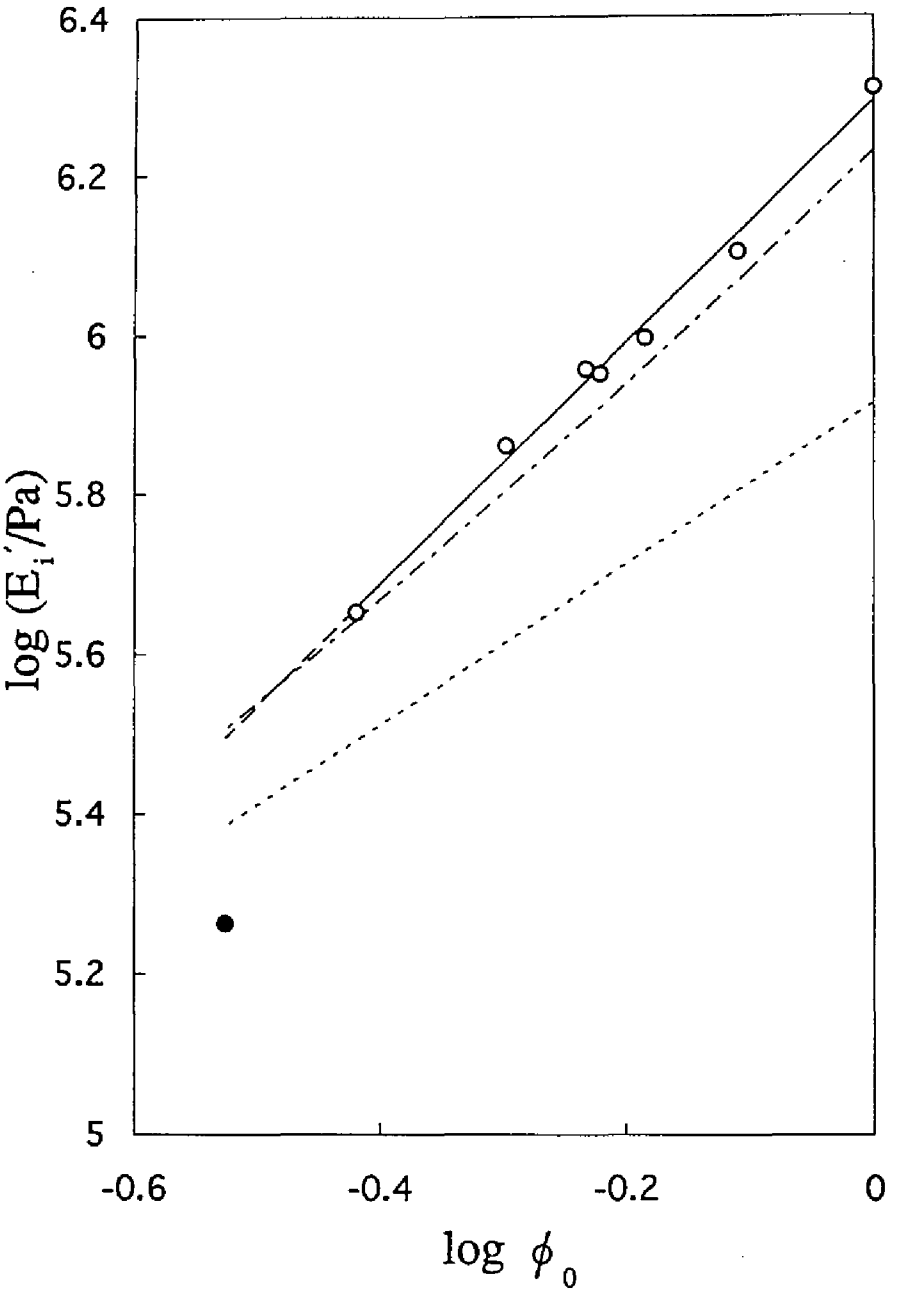

Figure 6-2. The ϕ_o dependence of E_i'. ϕ_o and E_i' is the polymer volume fraction and the dynamic Young's modulus of the network at preparation state, respectively. The sample with ϕ_o =0.298 (•) has many structural defects. The slope of the solid line is 1.52. The dash-dot line represents Eq. (6.2) with M_{ch}=8.8×10^3, M_{eo}=8.1×10^3 and ρ=0.975g/cm^3. The dashed line stands for the ϕ_o dependence of the affine limit of the constrained junction theory (Eq. (6.4)).

exponents for ϕ_o dependence of E_i' , ϕ_c and E_s' were omitted, because it has many structural defects.

The exponent α=1.52 for ϕ_o dependence of E_i' ($E_i' \propto \phi_o^{\alpha}$) in Fig. 6-2 is fairly lower than α=2 expected for networks in which trapped entanglements dominantly contribute to elastic modulus. We explain the experimental exponent quantitatively on the basis of the following simple evaluation forϕ_o dependence of E_i. We express the number density of total elastic chains contributing to elastic modulus (ν_{ef}) as a sum of the number density of a chain between neighboring chemical crosslinks (ν_{ch}) and that between neighboring trapped entanglements (ν_e) as follows.

$$\nu_{ef}(\phi_o) = \nu_{ch}(\phi_o) + \nu_e(\phi_o) = \frac{\rho\phi_o}{M_{ch}} + \frac{\rho\phi_o}{M_e(\phi_o)} \qquad (6.1)$$

where ρ is the density of prepolymer, M_{ch} is the molecular weight between neighboring chemical crosslinks, and M_e is the molecular weight between neighboring trapped entanglements. Using the value of M_e for network prepared in bulk state (M_{eo}), we express $\nu_{ef}(\phi_o)$ as

$$\nu_{ef}(\phi_o) = \frac{E_i(\phi_o)}{3RT} = \frac{\rho\phi_o}{M_{ch}} + \frac{\rho\phi_o^2}{M_{eo}} \qquad (6.2)$$

where the relation[5] $M_e(\phi_o) = M_{eo}\,\phi_o^{-1}$ is used. Equation (6.2) corresponds to the modification of the Langley[6] and Graessley's[7] expression of elastic modulus under the condition that thermal fluctuation of crosslinks is fully suppressed and trapping factor is equal to unity, *i.e.*,

$$\frac{E_i(1)}{3RT} = \nu_{ch}(1) + \frac{G_N^o}{RT} \qquad (6.3)$$

where G_N^o is the plateau modulus of polymer melt in uncrosslinked state. Patel *et al.*[3] showed that shear moduli of model networks by end-linking in bulk state the PDMS with a series of molecular weights is well described by Eq. (6.3). From Eq. (6.2), if the number of chemical crosslinks is much larger than that of trapped entanglements (namely, $\nu_{ch}(\phi_o) \gg \nu_e(\phi_o)$), the

relation $E_i \propto \phi_o^1$ is obtained. (As described later, this situation is very difficult to realize.) On the other hand, when the total number of junctions is dominantly occupied by the number of trapped entanglements (namely, $\nu_e(\phi_o) \gg \nu_{ch}(\phi_o)$), we get the relation $E_i \propto \phi_o^2$. The latter relation was experimentally confirmed for PDMS networks using the prepolymer with $M_p > M_c$, which was described in Chapter 5. The value of M_{ch} for end-linking type of network can be regarded as M_p under the complete progress of end-linking reaction and r=1. However, this condition is difficult to realize,[3,8,9] as is seen in Fig. 6-1 and the non-zero value of w_{sol}. In this case, $M_{ch}=M_p$ is a poor approximation. The correct value of M_{ch} has often been calculated on the basis of the Macosko and Miller model[10] of nonlinear polymerization.[3,8,9] According to this model, M_{ch} is calculated from the values of M_p, w_{sol} and r for the preparation in bulk state. The details of this model are described in Ref. 10. Using r=1.76 and $w_{sol}=7.41\times10^{-2}$ for ϕ_o=1, we obtain $M_{ch}=8.8\times10^3$ for the system in this study. The value of M_{ch} larger than molecular weight of prepolymer ($M_p=4.4\times10^3$) is due to r_{opt} larger than unity, and the non-zero value of w_{sol}.[3,8-10] Assuming that M_{eo} is the same as the molecular weight between entanglements ($=8.1\times10^3$) determined from G_N^o of PDMS melt in uncrosslinked state,[5] we can calculate the ϕ_o dependence of E_i using Eq. (6.2) with $M_{ch}=8.8\times10^3$, $M_{eo}=8.1\times10^3$ and ρ=0.975g/cm^3. The results are represented by the dash-dot curve in Fig. 6-2. It is found that the dash-dot curve fairly well explains ϕ_o dependence of E_i obtained experimentally, and the curve is approximated by a straight line, although its slope is slightly lower than the experimental value of α. For the network system in this study, the two terms in Eq. (6.2) concerning chemical crosslinks and trapped entanglements are of the same order, resulting in α intermediate between unity and two.

By eliminating the second term originating from trapped entanglements in Eq. (6.2), we get ϕ_o dependence of E_i corresponding to the affine limit of the constrained junction theory[11] as follows.

$$\frac{E_i(\phi_o)}{3RT} = \frac{\rho\phi_o}{M_{ch}} \tag{6.4}$$

The constrained junction theory[11] considers that trapped entanglements act as the suppression of thermal fluctuation of crosslinks, but do not contribute to elastic modulus. When the thermal fluctuation of crosslinks is fully suppressed (*i.e.*, affine limit), elastic modulus in the constrained junction theory has the maximum. Equation (6.4) corresponds to ϕ_o dependence of the maximum of E_i predicted by the constrained junction theory. The prediction by Eq. (6.4) is represented by the dashed line in Fig. 6-2. The dashed line is located under all the data points at $\phi_o \geq 0.381$, which clearly indicates that the constrained junction theory, which neglects the contribution of trapped entanglements to elastic modulus, under-estimates elastic modulus. The value of E_i' at $\phi_o=0.298$ is lower than the prediction by Eq. (6.4), which results from many defects in the network structure.

The under-estimation of Eq. (6.4) for ϕ_o dependence of E_i means that trapped entanglements significantly contribute to elastic modulus, even if there are no entanglements in uncrosslinked state. The reason why trapped entanglements are formed without entanglements in uncrosslinked state is qualitatively explained as follows: Even if the length of prepolymer is too short to form entanglement couplings, some degree of overlapping of prepolymer chains exists in uncrosslinked state when ϕ_o is larger than ϕ^*. Most of the overlapping points of polymer chains are trapped by the introduction of chemical crosslinks, leading to trapped entanglements. In order to obtain polymer networks with no or negligible amount of trapped entanglement, the network must be prepared at $\phi_o \approx \phi^*$. However, as

mentioned before, the preparation of polymer networks at $\phi_o \approx \phi^*$ with negligible amount of structural defect is very difficult due to loop formation inevitably accompanying the reaction at low concentration.

6.3.3 ϕ_o *Dependence of* ϕ_e and E_s'

The value of x ($N_{el} \propto \phi_o^x$) is experimentally determined to be -0.52 ($=1-\alpha$) from ϕ_o dependence of E_i'. As mentioned in Sec. 5.2, the theoretical exponents for ϕ_o dependence of ϕ_e and E_s depends on x. Here, using $x=-0.52$ obtained experimentally, we calculate the exponents predicted by the affine model and the c^* theorem, respectively. From Eqs. (5.6) and (5.11), the ϕ_o dependence of ϕ_e predicted by each theory is obtained as

$$\phi_e \propto \phi_o^{0.53} \qquad (\phi_o < \phi^{**}) \qquad (6.5a)$$

$$\propto \phi_o^{0.63} \qquad (\phi_o > \phi^{**}) \qquad \text{(affine model)}, \qquad (6.5b)$$

and

$$\phi_e \propto \phi_o^{0.37} \qquad (c^* \text{ theorem}). \qquad (6.6)$$

Here, $\nu=0.57$, which was the value reported for PDMS in toluene,[12] was used. The ϕ_o dependence of E_s derived from each theory is obtained from Eqs. (5.7) and (5.12) with $x=-0.52$ and $\nu=0.57$ as follows.

$$E_s \propto \phi_o^{1.3} \qquad (\phi_o < \phi^{**}) \qquad (6.7a)$$

$$\propto \phi_o^{1.5} \qquad (\phi_o > \phi^{**}) \qquad \text{(affine model)}, \qquad (6.7b)$$

and

$$E_s \propto \phi_o^{0.89} \qquad (c^* \text{ theorem}). \qquad (6.8)$$

As can be seen in Eqs. (6.5)-(6.8), there is a significant difference in the theoretical exponents between the two theories, in contrast to the case in PDMS networks treated in Chapter 5. (See, Table 5-1.)

We show ϕ_o dependence of ϕ_e in Fig. 6-3. The relation between ϕ_o and ϕ_e in the region $\phi_o \geq 0.381$ is found to be expressed by $\phi_o \propto \phi_e^{0.652}$. The data

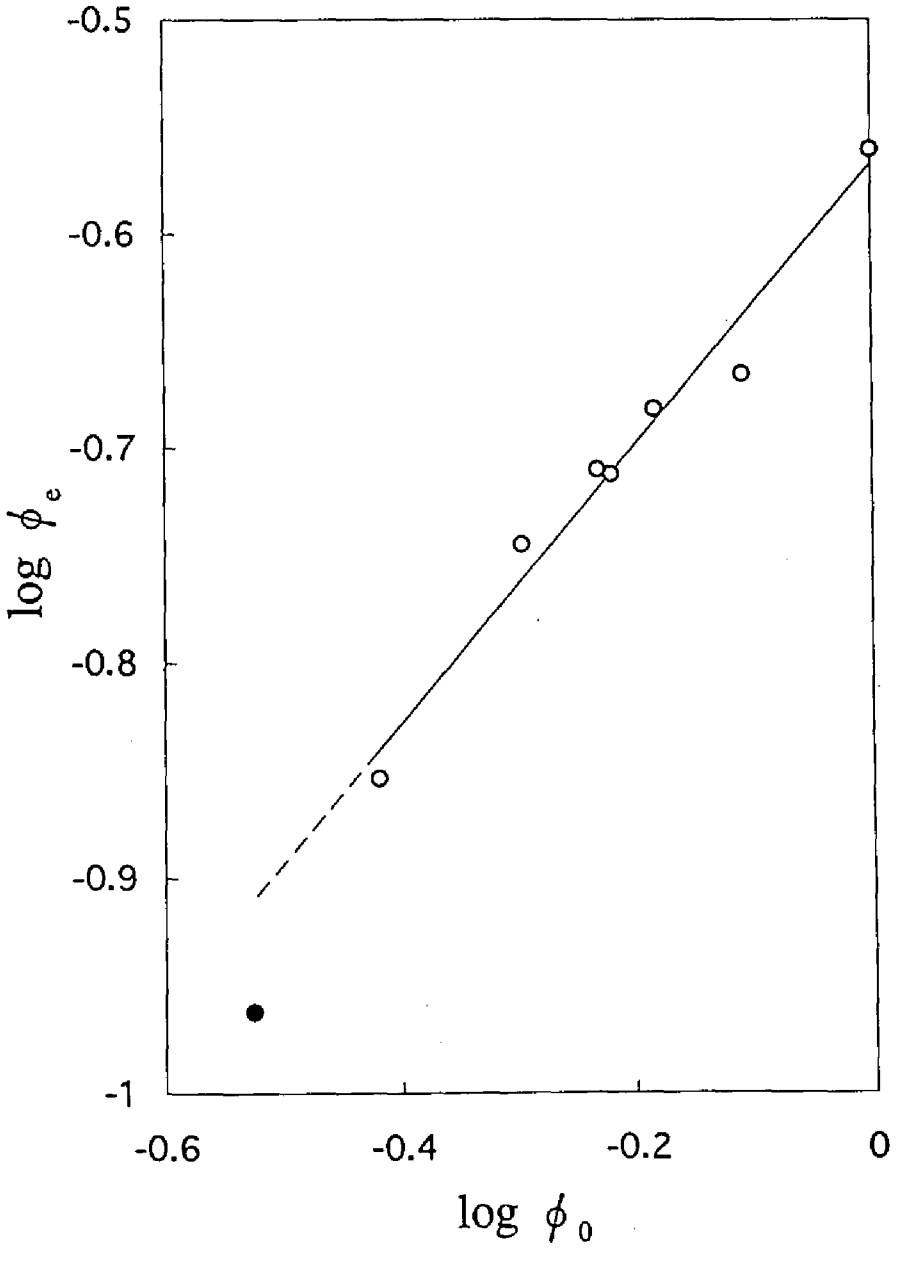

Figure 6-3. The ϕ_o dependence of ϕ_e. ϕ_o and ϕ_e is the polymer volume fraction of the network at the preparation state and the fully swollen state, respectively. The sample with ϕ_o =0.298 (●) has many structural defects. The slope of the solid line is 0.652.

for the sample with ϕ_o=0.298, which has many structural defects, is much lower than the value expected from the above relation. A network with many structural defects swells larger (shows the smaller ϕ_e) due to low elasticity than that having negligible amount of defect does. Although the affine model predicts the crossover in ϕ_o dependence of ϕ_e at $\phi_o \approx \phi^{**} \approx 0.60$[13], the crossover is not experimentally observed. However, the experimental exponent is in good agreement with the theoretical prediction in the region $\phi_o > \phi^{**}$. On the other hand, the exponent predicted by the c^* theorem is much lower than the experimental value.

Figure 6-4 shows ϕ_o dependence of E_s'. The ϕ_o dependence of E_s' in the region $\phi_o \geq 0.381$ obeys the relation $E_s' \propto \phi_o^{1.49}$. The data of the sample with ϕ_o=0.298 is located under the extrapolation by the above relation, which results from many structural defects not contributing to elastic modulus. The exponent obtained experimentally agrees very well with the prediction in the region $\phi_o > \phi^{**}$ by the affine model, although the crossover in ϕ_o dependence predicted by the theory is not seen in the experiment. On the other hand, the experimental exponent is much higher than the theoretical value of the c^* theorem.

As mentioned above, both the ϕ_o dependence of ϕ_e and E_s' obtained experimentally agree well with the predictions in the region $\phi_o > \phi_o^{**}$ by the affine model. The reason why the crossover in ϕ_o dependence of ϕ_e and E_s' was not experimentally observed is not clear at present, but it may be attributed to low molecular weight of ODMS used. When molecular weight of a polymer is sufficiently low, the excluded volume effect is negligible.[14,15] Actually, the experimental relation between $[\eta]$ and M_n in respect to ODMS in toluene[1] ($[\eta] \propto M_n^{0.50}$) gives ν=0.50. This means that end-to-end distance of ODMS chain in uncrosslinked state is equal to the unperturbed dimension

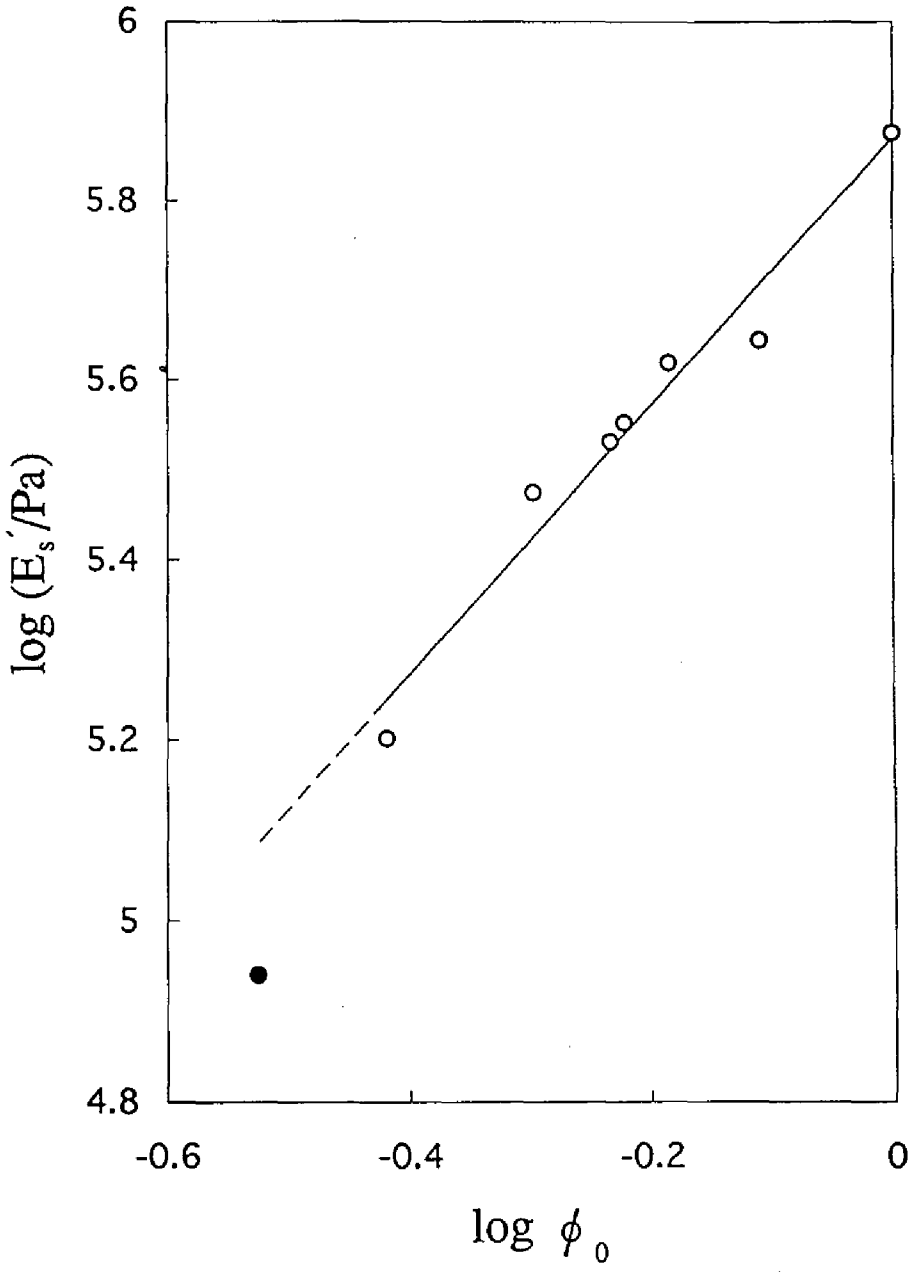

Figure 6-4. The ϕ_0 dependence of E_s. ϕ_0 is the polymer volume fraction of the network at preparation state, and E_s is the dynamic Young's modulus of the fully swollen network. The sample with ϕ_0 =0.298 (●) has many structural defects. The slope of the solid line is 1.49.

over the entire range of ϕ_o. The concept of concentration blob in scaling theory postulates that a prepolymer as a constituent of network behaves as an excluded volume chain, since a network itself is affected by excluded volume effect. Nevertheless, the negligible excluded volume effect of prepolymer itself may diminish ϕ_o dependence of R_o, which identifies the region $\phi_o<\phi^{**}$ with $\phi_o>\phi^{**}$. In addition to the above supposition, it should be mentioned that the difference in the predicted exponents in $\phi_o>\phi^{**}$ and $\phi_o<\phi^{**}$ is small, which makes the experimental confirmation of crossover behavior difficult.

On the other hand, the considerable discrepancies are observed between the experimental results for ϕ_o dependence of ϕ_e and E_s' and the predictions by the c^* theorem. In Chapter 5, we indicated that the c^* theorem did not succeed in the description of ϕ_o dependence of ϕ_e and E_s' for the network system where high degree of overlapping of polymer chains exists in preparation state. Including the present results for the system where overlapping degree of polymer chains is relatively low, we conclude that the complete disinterpenetration of the network chains in equilibrium swollen state, which is a strong postulate of the c^* theorem, does not occur, irrespective of overlapping degree of polymer chains in preparation state. The success of the affine model in the description of experimental results in previous and present studies means that the displacement of crosslinks moves affinely on swelling independently of overlapping degree of polymer chains in preparation state, and it is necessary to regard ϕ_o as a reference state in order to describe theoretically tequilibrium swelling of polymer networks crosslinked in solution.

Candau *et al.*[17] reported $\phi_o \propto \phi_o^{0.71}$ and $E_s \propto \phi_o^{1.8}$ for PDMS networks in toluene, and argued that the experimental results were well explained using Eqs. (5.11) and (5.12) with $x=-1$ by the c^* theorem. Their results and

conclusion are different from those in this study, which is due to the following reasons: Their results are likely to be influenced by the considerable amount of structural defects in the samples, because their samples were prepared at r=1, not at r=r_{opt}; and they a priori assumed x=−1 without the experimental evidence such as the data of ϕ_o dependence of E_i. The condition x=−1 is expected for networks in which trapped entanglements dominantly contributes to elastic modulus, *i.e.*, networks prepared by long prepolymer chains which are well entangled in uncrosslinked state. Since the molecular weight of PDMS prepolymer in their study (M_p=9.7×10^3) is much lower than M_e(=1.66×10^4), the employment of x=−1 should be not suitable for their experimental condition.

6.3.5 ϕ_e Dependence of E_s'

Figure 6-5 indicates the double logarithmic plots of E_s' *vs.* ϕ_e. All the data fall on the straight line with the slope of 2.30. This result is in accord with the theoretical prediction $E_s' \propto \phi_e^{2.4}$ by Eq. (5.8) with ν=0.57. It should be noted that the data for the sample with ϕ_o=0.298, which has many structural defects, is located on the line, meaning that Eq. (5.8) does not depend on the details of the network structure. This result is naturally expected by the fact that Eq. (5.8) simply embodies the Flory-Rehner's assumption. Equation (5.8) is valid regardless of the details of network structure, if the network concerned is in equilibrium swollen state. The absolute values of E_s and ϕ_e are influenced by structural defects, respectively, but the influence is cancelled in the relation between E_s and ϕ_e. Equation (5.8) and the related scaling relations, *i.e.*, the ϕ_e dependence of physical quantities of equilibrium swollen networks are the universal laws independent of the details of network structure. However, we cannot discuss the

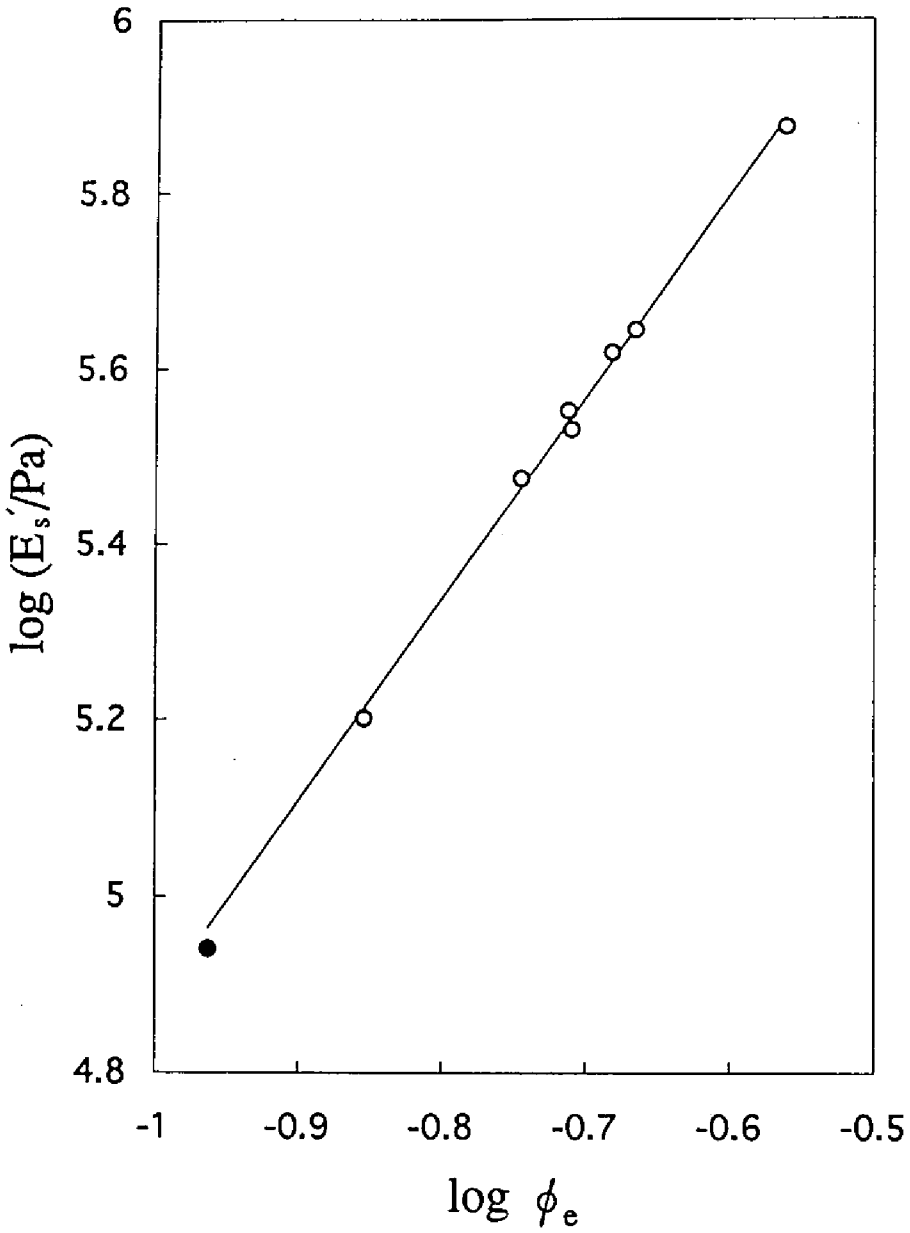

Figure 6-5. The ϕ_e dependence of E_s. ϕ_e and E_s is the polymer volume fraction and the dynamic Young's modulus of the equilibrium swollen network, respectively. The sample with ϕ_o =0.298 (●) has many structural defects. The slope of the solid line is 2.30.

interspersion state of network chains on the basis of the ϕ_c dependence. As can be seen in Figs. 6-3 - 6-5, the examination of ϕ_o dependence of physical properties of equilibrium swollen networks is necessary in order to obtain the definite description of equilibrium swelling.

6.4 Conclusions

The swelling and elastic properties of the networks prepared by end-linking short polymer chains in solution were investigated as a function of polymer concentration at crosslinking. The preparation concentration dependence of elastic modulus in preparation state suggests that trapped entanglements are formed by the introduction of crosslinks, and those contribute to elastic modulus considerably, even if the prepolymers are non-entangled in uncrosslinked state. The experimental exponents for preparation concentration dependence of the degree of equilibrium swelling and the elastic modulus in equilibrium swollen state were well explained by the affine model considering preparation concentration as a reference state, although the subtle crossover in concentration dependence predicted by the model was not observed. On the other hand, the exponents predicted by the c^* theorem were much lower than the experimental ones. These results strongly suggest that network chains do not disinterpenetrate each other in equilibrium swelling state, and the displacement of crosslinks affinely moves on swelling. It was also shown that the dependence of physical quantities of equilibrium swollen networks on equilibrium concentration, which has been experimentally investigated by many researchers, is insufficient to test the theories for equilibrium swelling of polymer networks crosslinked in solution.

References

1. Bianchi, U., Dalpiaz, M. and Patrone, E., *Makromol. Chem.*, **80**, 112 (1964).
2. Orrah, D. J., Semlyen, J. A. and Ross-Murphy, S. B., *Polymer*, **29**, 1452 (1988).
3. Patel, S. K., Malone, S., Cohen, C., Gillmor, J. R. and Colby, R. H., *Macromolecules*, **25**, 5241 (1992).
4. Vasiliev, V. G., Rogovina, L. Z. and Slonimsky, G. L., *Polymer*, **26**, 1667 (1985).
5. Ferry, J. D., "*Viscoelastic Properties of Polymers, 3rd ed.*" Wiley, NY, 1980.
6. Langley, N. R. and Polmanteer, K. E., *J. Polym. Sci.; Polym. Phys. Ed.*, **12**, 1023 (1974).
7. Dossin, L. M. and Graessley, W. W., *Macromolecules*, **12**, 123 (1979).
8. Gottlieb, M., Macosko, C. W., Benjamin, G. S.,Meyers, K. O. and Merril, E. W., *Macromolecules*, **14**, 1039 (1981).
9. Valles, E. M., Rost, E. J. and Macosko, C. W., *Rubber Chem. Technol.*, **57**, 55 (1984)
10. Macosko, C. W. and Miller, D. R., *Macromolecules*, **9**, 199, 206 (1976).
11. Flory, P. J. and Erman, B., *Macromolecules*, **15**, 800 (1982).
12. Haug, V. A. and Meyerhoff, G., *Macromol. Chem.*, **53**, 91 (1962).
13. Adachi, K., Imanishi, Y., Shinkado, T. and Kotaka, T., *Macromolecules*, **22**, 2391 (1989).
14. Yamakawa, H. and Stockmayer, W. H., *J. Chem. Phys.*, **57**, 2843 (1972)
15. Kitagawa, T., Sadanobu, J. and Norisuye, T., *Macromolecules*, **23**, 602 (1990).

16. de Gennes, P. G., "*Scaling Concepts in Polymer Physics*", Cornell University Press, Ithaca, NY, 1979.
17. Candau, S., Peters, A. and Herz, J., *Polymer*, **22**, 1504 (1981).
18. Munch, J. P., Candau, S., Herz, J. and Hild, G., *J. Phys. (Paris)*, **38**, 971 (1977).
19. Hild, G., Okasha, R., Macret, M. and Gnanou, Y., *Makromol. Chem.*, **187**, 2271 (1986).
20. Richards, R. W. and Davidson, N. S., *Macromolecules*, **19**, 1381 (1986).
21. Zrinyi, M.,and Horkay, F., *Macromolecules*, **17**, 2805 (1987).
22. Shibayama, M., Takahashi, H. and Nomura, S., *Macromolecules*, **28**, 6860 (1995).
23. Falcão, A. N., Pedersen, J. S., Mortensen, K. and Boué, F., *Macromolecules*, **29**, 809 (1996).

Chapter 7
Mechanical Properties of Deswollen Polydimethylsiloxane Networks with Supercoiled Structure

7.1 Introduction

In Chapters 5 and 6, the elasticity of swollen polymer networks was investigated. In this chapter, the elasticic properties of *deswollen* polymer networks which are prepared by removing solvent completely from the networks crosslinked in solution are examined. The deswelling process is accompanied by the collapse of network chains due to the volume decrease of material, which complicates the quantitative understanding of elasticity of deswollen networks. The contraction of polymeric network chains on deswelling has often been called *supercoiling*.[1-4] The supercoiled chains is expected to have a more contracted conformation compared with Gaussian chains. Actually, recent neutron scattering experiments showed[5,6] that the radius of gyration of a network chain in fully deswollen state is smaller than the unperturbed dimension. Vasiliev *et al.*[4] argued the existence of supercoiling on the basis of their experimental result that the density of deswollen network prepared at low concentration is higher than that of network crosslinked in the bulk state. However, the details of the conformation of supercoiled chains and the effects of supercoiling on mechanical properties of polymer networks are not elucidated.

Recently, the topological structure of collapsed polymer systems, which is represented by deswollen networks, has attracted attention.[7-9] Several authors[7-9] have discussed the applicability of "polymer chain in an array of obstacles" (PCAO) model[7-12] to collapsed polymer systems. The PCAO is modeled by a random walk on the lattice with the obstacles corresponding to

topological constraints. The fractal dimension (D) of PCAO model for a closed random walk (a ring chain) is reported[7-12] to be D=3 or 4 depending on whether with or without the excluded volume effect, respectively. The PCAO model has strongly collapsed conformation compared with Gaussian chain (D=2). Obukhov *et al.*[7] have applied the PCAO model to supercoiled structure, and predicted that deswollen networks with supercoiled structure have the rather different stress-elongation relation from a network composed of Gaussian chains. They have also pointed out[7] the possibility of high extensibility for the deswollen networks prepared at low concentration, which originates from the reduction of end-to-end distance of network chains on deswelling and the decrease of trapped entanglements by lowering preparation concentration.

The experiments on the elasticity of deswollen networks have been reported by several researchers.[3,13-15] Vasiliev *et al.*[4] indicated that the concentration dependence of elastic modulus of deswollen networks prepared at low concentrations is quite different from the prediction by the classical theory of rubber elasticity. According to their results, the considerable degree of supercoiling occurs for networks prepared at low concentration, and with the network chains having relatively large polymerization index (N). In the other studies,[13-15] the effect of supercoiling on elasticity was not clearly observed, which is due to their experimental conditions where the magnitude of supercoiling was small; The preparation concentrations were not so low, and/or N of the network chain was small.

The complicated concentration dependence of elastic modulus of deswollen networks, which implies the formation of supercoiled structure, have been reported,[3] but the stress-elongation relation of deswollen networks with supercoiled structure, which includes the important information about

the topological structure of networks, has never been experimentally investigated. In this study, we have prepared the networks by end-linking procedure with the prepolymer having relatively large N over the wide range of concentration. The concentration dependence of elastic modulus and stress-elongation relation of deswollen networks is investigated. The effects of supercoiling on elastic modulus and stress-elongation behavior are demonstrated by comparing the mechanical properties of networks between in preparation and deswollen state. (We call later a network in preparation state the *original network.*) The stress-elongation behavior of deswollen networks with supercoiled structure is analyzed on the basis of the treatment of large deformation for a flexible polymer chain by Pincus.[16] The fractal dimension of supercoiled structure is evaluated from the dependence of stress on elongation ratio in large deformation region. We also show that the deswollen network prepared at low concentration exhibits a remarkable extensibility.

7.2 Experimental

The original network samples (before deswelling) were common to Chapter 5 and this chapter. The details of the preparation of original networks are described in Chapter 5. The original networks were prepared in toluene by end-linking the bifunctional polydimethylsiloxane whose weight average molecular weight is 4.7×10^4. Polymer volume fraction at preparation (ϕ_o') was varied from $0.0985\leq\phi_o'\leq1$. The sample with $\phi_o'=0.0985$ was newly prepared for this study. The crosslinking reaction at $\phi_o'\geq0.191$ was made at 100°C for 24h, but the sample with $\phi_o'=0.0985$ was cured for 3 days since the cure for 24h was insufficient for complete reaction. After the reaction, original network samples were divided into the

two parts. One was used for the mechanical measurements as original network sample. The other was kept in air to obtain fully deswollen network for mechanical measurements. The complete drying required about several days. The effect of drying rate on the structure of deswollen networks will be described later. Polymer volume fraction of a network in preparation state (ϕ_o) was re-calculated by subtracting the unreacted prepolymer from ϕ_o'. The fraction of unreacted prepolymer was less than 8wt% for samples with $\phi_o' \geq 0.191$. For the sample with $\phi_o'=0.0985$, the sol fraction was 12.1wt%, which was somewhat larger than those for other samples. This would be due to the difficulties involved in the crosslinking reaction at very low concentration.

The drying rate of samples possibly influences the structure of dry networks. In order to check the effect of deswelling methods on the structure of dry network, we prepared the dry network with $\phi_o'=0.191$ by removing solvent as slowly as possible: The composition of solvent for deswelling was changed gradually, *i.e*, the ratio of methanol to toluene was gradually stepped up from 0% to 100% with the step of 20%. The achievement of equilibrium swelling at each stage was checked through the weighing of samples. The size of deswollen sample in 100% methanol was comparable to that of dry sample. Finally, methanol was vaporized in air to obtain the dry network. The dry network sample prepared by the slow deswelling process showed the same stress-elongation behavior and elastic modulus as that prepared by drying the original network sample in air. This result suggests that the two deswelling methods are regarded as quasi-static process. We did not employ the slow deswelling process described above as the standard deswelling method in this study, because the process requires a longer period, *i.e.*, several months.

Stress-elongation relation and initial Young's modulus of samples in preparation and dry state (E_i and E_d, respectively) were measured by the uniaxial elongation at room temperature. The initial length of samples was *ca.* 20mm, and the elongation was carried out at the constant crosshead speed (v) of 10mm/min. This condition satisfied the quasi-equilibrium condition, which was confirmed by the fact that the stress-elongation relation of each sample was independent of v in the region of $v \leq 20$mm/min. The effect of unreacted species in samples on the elastic behavior was eliminated, because unreacted species do not contribute the elastic behavior of networks under equilibrium condition. The elongational experiment for the original network with ϕ_o=0.0877 could not be made due to the softness of material. The values of ϕ_o, r_{opt}, E_i and E_d at each ϕ_o' are tabulated in Table 7-1.

7.3 Results and Discussion

7.3.1 Effect of Supercoiling on Elastic Modulus

In Chapter 5 and 6, it was shown that ϕ_o dependence of elastic modulus of original and fully swolllen networks is interpreted in terms of the model proposed by Panyukhov[17] together with our consideration about the effect of trapped entanglements and the concentration regime in preparation state on elasticity. The model is based on the assumption of the affine displacement of crosslinking points relative to global network. Here, we attempt to interpret ϕ_o dependence of elastic modulus of fully deswollen networks by means of this model. The expression of the elastic modulus (E) of network with polymer volume fraction ϕ, which is prepared at ϕ_o, is given by Eq. (5.3) as follows.

$$E(\phi_o, \phi) \propto \frac{\phi}{N_{cf}(\phi_o)} \lambda_s^2 \alpha_T^2 \qquad (7.1)$$

Table 7-1. Polymer volume fraction of the solution in preparation (ϕ_o'), polymer volume fraction and initial Young's modulus of the network in preparation state (ϕ_o and E_i, respectively) and initial Young's modulus of the fully deswollen network (E_d) and, the optimal ratio of silane hydrogen to vinyl group (r_{opt}).

ϕ_o'	ϕ_o	r_{opt}	$10^{-4}E_i$ (Pa)	$10^{-4}E_d$ (Pa)
1.00	1.00	1.15	34	34
0.861	0.852	1.20	28	30
0.725	0.709	1.14	19	22
0.564	0.544	1.07	8.9	16
0.430	0.411	1.24	5.8	14
0.298	0.281	1.18	2.6	10
0.191	0.179	1.20	0.89	6.9
0.0985	0.0877	1.10	----	3.3

[a]The values of E_i for the samples with $\phi_o \geq 0.179$ have been reproduced from Table 2-2 in Chapter 2.

where $N_e(\phi_o)$ is the length in polymerization index between neighboring junctions at ϕ_o regardless of whether these are trapped entanglements or chemical crosslinks, λ_s is the swelling coefficient defined as $\lambda_s = (\phi/\phi_o)^{-1/3}$, and α_T is the expansion coefficient defined as $\alpha_T = R_o/R$. Here, R_o is the root of mean square end-to-end distance of the connected prepolymer at ϕ_o, and R is the end-to-end distance of the prepolymer chain in unconnected state in the solution at ϕ. According to scaling theory,[2] R scales as $R \propto \phi^{(2\nu-1)/(2-6\nu)}$ in semidilute regime where ν is the excluded volume exponent, while R in concentrated regime is equal to the unperturbed dimension corresponding to $\nu=1/2$. Equation (7.1) with $\phi=\phi_o$ gives the description of E_i ($=E(\phi_o,\phi_o)$) as $E_i \propto \phi_o N_e(\phi_o)^{-1}$. The expression of E_d ($=E(\phi_o,1)$) is obtained from Eq. (7.1) with $\phi=1$ as $E_d \propto \phi_o^{1/(9\nu-3)} N_e(\phi_o)^{-1}$ in which $\nu=0.57$ in the region $\phi_o<\phi_o^{**}$ and $\nu=1/2$ in $\phi_o>\phi_o^{**}$ is employed, respectively. Here, ϕ_o^{**} is the value of ϕ_o at the boundary in respect to R_o between the semidilute and concentrated regimes, and $\nu=0.57$ is the value reported for PDMS in toluene.[18] The relation between E_i and E_d is obtained as follows.

$$E_d \approx \phi_o^{(-9\nu+4)/(9\nu-3)} E_i \qquad (7.2)$$

Figure 7-1 shows the plots of $E_d \phi_o^{(9\nu-4)/(9\nu-3)}/E_i$ against ϕ_o. Here, we used $\nu=0.57$ for the samples prepared at the region $\phi_o<0.6$, and $\nu=1/2$ for those at $\phi_o>0.6$. The value of ϕ_o^{**} was regarded as $\phi_o^{**}=0.60$, which was reported by Adachi *et al.*.[19] The validity of this treatment for ϕ_o^{**} was discussed in Chapter 5. It is seen in Fig. 7-1 that the quantity, $E_d \phi_o^{(9\nu-4)/(9\nu-3)}/E_i$, is almost equal to unity in $\phi_o>0.7$, while it is larger than from unity in the region $\phi_o<0.7$ and the deviation from unity becomes larger as ϕ_o decreases. The model (Eq. (7.1)) considers the changes of the two physical quantities accompanying deswelling for the evaluation of elastic modulus: the number density of elastic effective chains and the end-to-end distance of network

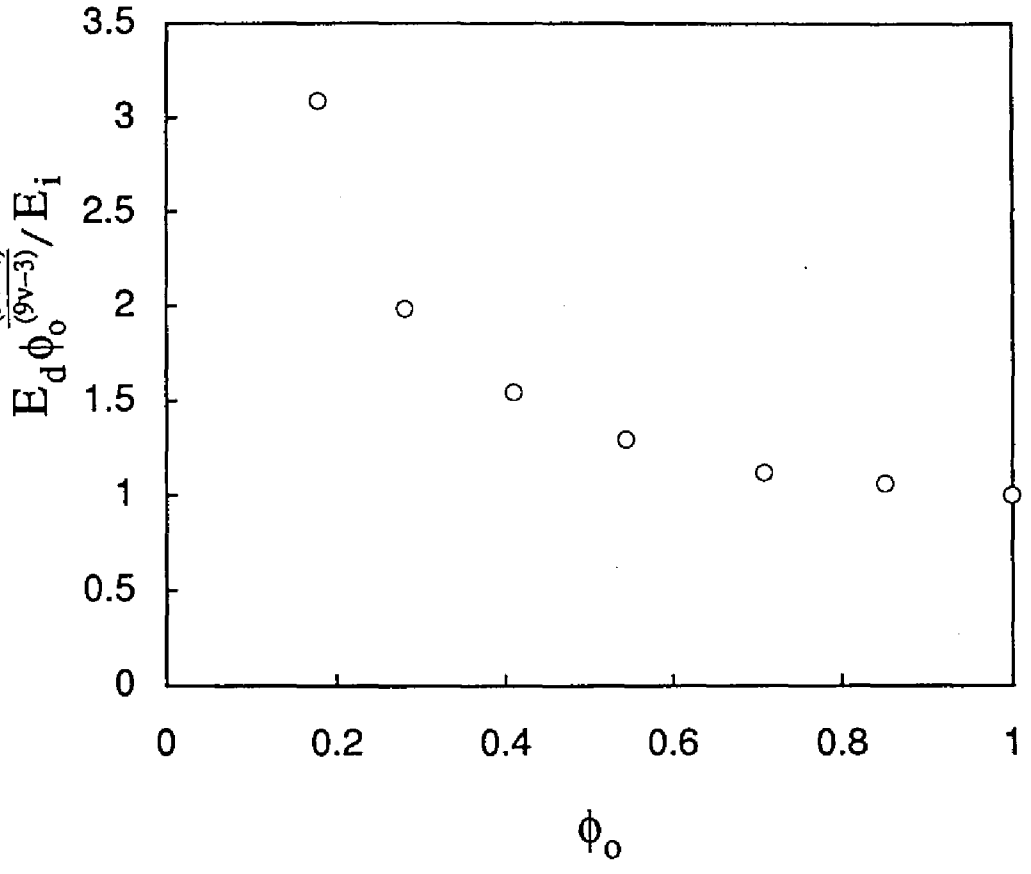

Figure 7-1. Plots of $E_d\phi_o^{(9\nu-4)/(9\nu-3)}/E_i$ against ϕ_o. ν=0.57 and ν=1/2 are used for the samples prepared at ϕ_o<0.6 and ϕ_o>0.6, respectively.

chains. The change of end-to-end distance of network chains is estimated on the basis of the consideration for the Gaussian or excluded volume chain. The end-to-end distance of network chains in deswollen state should be smaller as the volume decrease on deswelling is larger. In low ϕ_o region where the volume decrease of network accompanying deswelling is large ($\lambda_s<1$), the conformation of network chains in dry state deviates largely from Gaussian conformation. The phase space around network chains is expected to decrease due to the contracted conformation of supercoiled chains, which leads to the higher elastic modulus than that predicted by the theory for the Gaussian or excluded volume chain. This effect of supercoiling on elastic modulus is recognized by the experimental values higher than unity in low ϕ_o region in Fig. 7-1.

On the other hand, it is seen in Fig. 7-1 that Eq. (7.1) succeeds in the description of experimental results in high ϕ_o region. In high ϕ_o region, the magnitude of supercoiling of network chains is small, because the volume change accompanying deswelling is small, namely, $\lambda_s \approx 1$.

7.3.2 Effect of Supercoiling on Stress-Elongation Behavior

Figure 7-2 shows the double logarithmic plots of reduced stress against elongation ratio for original networks. The stress (σ_e) is the engineering stress defined by the force divided by the cross-sectional area in undeformed state. The elongation ratio (λ) is defined by $\lambda=l/l_o$ where l_o and l is the length of sample in undeformed and deformed state, respectively. The stress in Fig. 7-2 is renormalized by E_i of each sample. The dashed curve corresponds to the stress-elongation relation for Gaussian network[20] expressed as $\sigma_e/E_i = (\lambda - \lambda^{-2})/3$. It is seen that the experimental curves are described by the dashed curve in small λ region, while those deviate downwards from the dashed

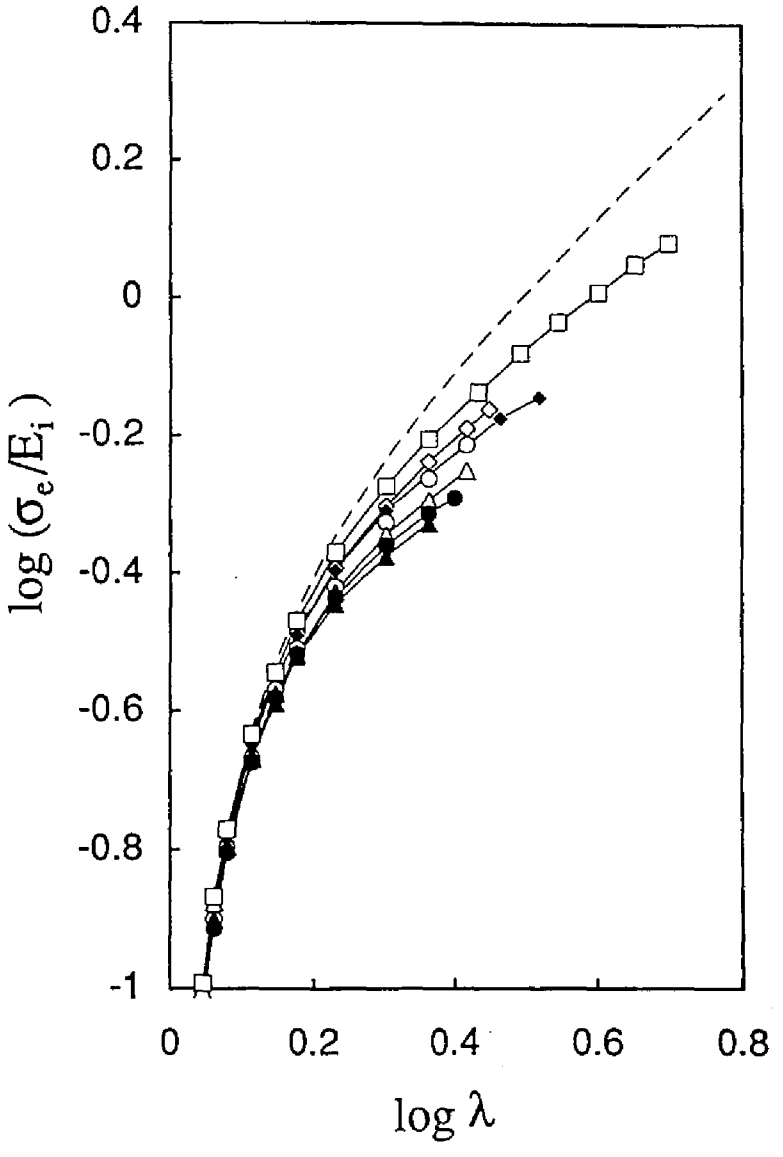

Figure 7-2. Double-logarithmic plots of σ_e/E_i against λ for the original networks. Symbols: (▲) 1; (●) 0.852; (△) 0.709; (○) 0.544; (◆) 0.411; (◇) 0.281; (□) 0.179 where each value corresponds to ϕ_o. The dashed curve represents the stress-elongation relation for the Gaussian network.

curve as λ increases. This is the well-known result for the stress-elongation behavior of usual elastomers.[1,4,22] Qualitatively, the downward deviation is interpreted similarly as the C_2 term in the Mooney-Rivlin equation.[1,4,22] The major factor for the downward deviation has often been attributed to the effect of entanglements.[1,4,22] The number of trapped entanglements decreases as ϕ_o is lowered. It can be seen in Fig. 7-2 that as the network is prepared at lower concentration, the degree of deviation from the dashed curve is smaller, which supports the above consideration qualitatively. The decrease of ϕ_o, *i.e.*; the decrease of the number of trapped entanglements also leads to the increase of extensibility as seen in Fig. 7-2.

Figure 7-3 indicates the stress-elongation relations for deswollen networks. The stress is renormalized by E_d of each sample. It is found that the stress-elongation relations of deswollen networks are classified into two groups: the networks prepared at $\phi_o \leq 0.281$, and those at $\phi_o \geq 0.411$. The overlapping of the curves suggests that the deswollen networks in each group have the common topological features. The major difference of curves in each group is only in the extensibility. The dependence of σ_e on λ for the deswollen networks with $\phi_o \leq 0.281$ is found to obey $\sigma_e \propto \lambda^{0.65}$ in the region $2.1 \leq \lambda \leq 5.5$. It is also seen that the deswollen network prepared at $\phi_o = 0.0877$ shows the high extensibility reaching $\lambda \simeq 18$. The detailed analysis of the dependence of σ_e on λ and the extensibility will be discussed later.

Figure 7-4 shows the comparison of the stress-elongation relation in the deswollen and preparation state for $\phi_o = 0.411$ and $\phi_o = 0.179$. Stress for the deswollen and original network is reduced by E_d and E_i, respectively. The dry network prepared at $\phi_o = 0.411$ is found to show almost the same stress-elongation relation as the original network. For all other samples prepared at $\phi_o \geq 0.411$, the curves for dry and preparation state almost overlap each other,

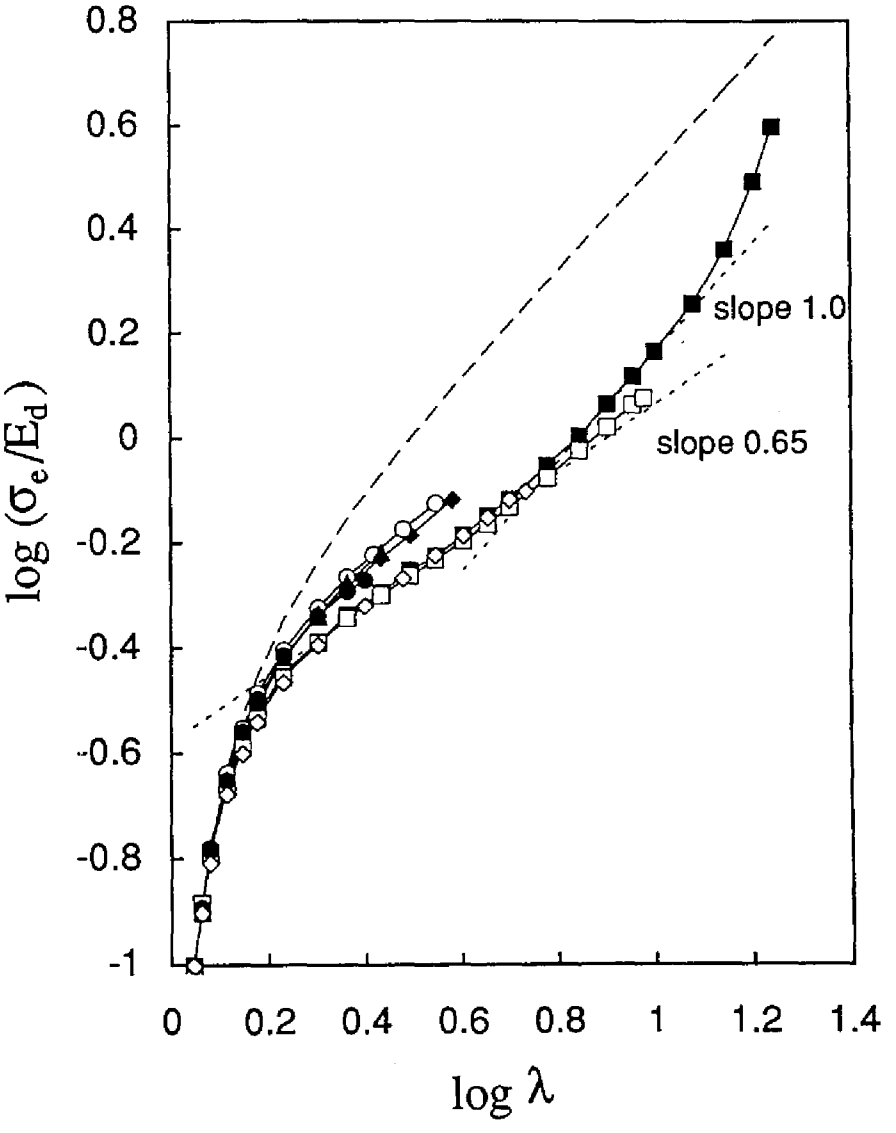

Figure 7-3. Double-logarithmic plots of σ_e/E_d against λ for the fully deswollen networks. The symbol (■) is the data for ϕ_o=0.0877. The other symbols are the same as in Fig. 7-2. The dashed curve represents the stress-elongation relation for the Gaussian network.

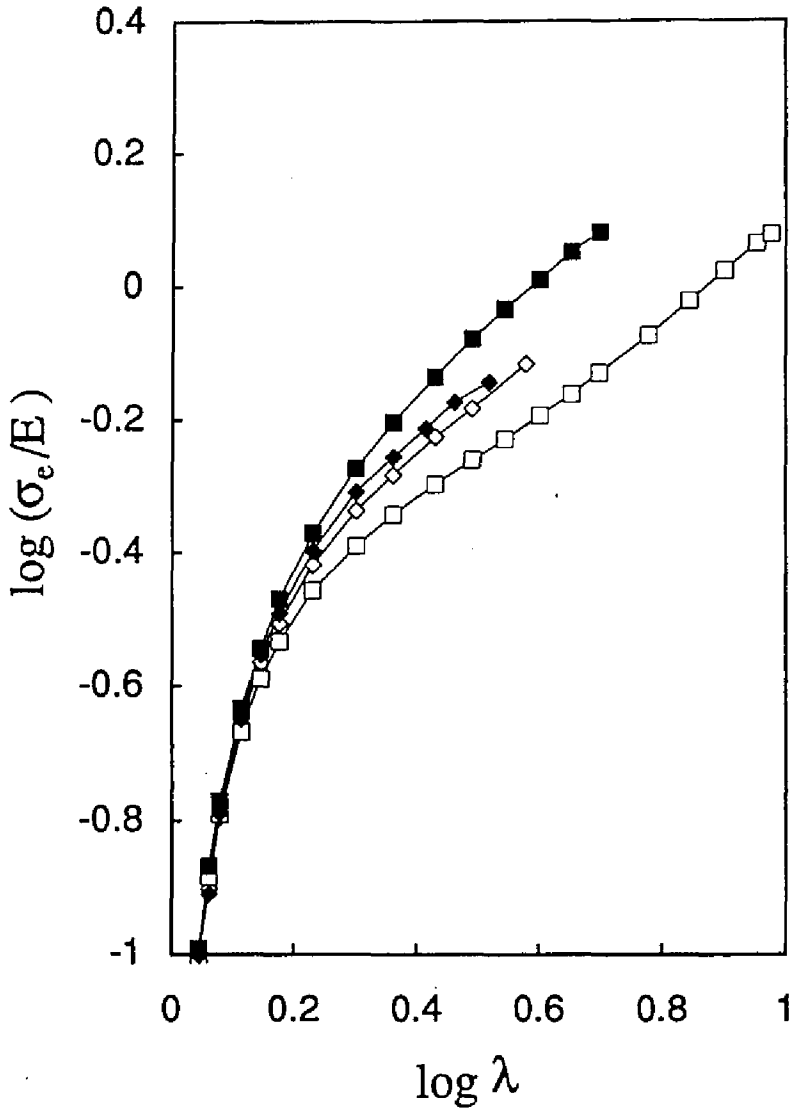

Figure 7-4. Comparison of the reduced stress-elongation relations of the original and the dry networks. The stress for the original and the dry network is reduced by E_i and E_d, respectively. Symbols: (□) dry network with ϕ_o=0.179; (■) original network with ϕ_o=0.179; (◇) dry network with ϕ_o=0.411; (◆) original network with ϕ_o=0.411.

(and the data are not shown in the figure), suggesting that the deswelling does not has the great influence on the stress-elongation behavior for the networks prepared at $\phi_o \geq 0.411$, and the topological structure of networks does not change greatly on deswelling. The effect of supercoiling on E_d is also relatively small in the region $\phi_o \geq 0.411$ as seen in Fig. 7-1.

On the other hand, the stress-elongation behavior of dry network prepared at $\phi_o = 0.179$ deviates much from that of Gaussian network as indicated in Fig. 7-3, and is rather different from that of the original network as shown in Fig. 7-4. The similar result is obtained for the sample with $\phi_o = 0.281$. The large difference of stress-elongation behavior between the dry and original network in the region $\phi_o \leq 0.281$ should be due to the supercoiled structure formed on deswelling, the details of which will be described later. The stress-elongation relations of deswollen networks with supercoiled structure have the weaker dependence of σ_e on λ in the region $\lambda \leq 5.5$ compared with those of original networks. The stress-elongation relation in $\lambda \leq 5.5$ is independent of ϕ_o, and the relation $\sigma_e \propto \lambda^{0.65}$ in $2.1 \leq \lambda \leq 5.5$ is common to the stress-elongation behavior for the dry networks with supercoiled structure. In the region $\phi_o \leq 0.281$, the effect of supercoiling on Young's modulus is also large as seen in Fig. 7-1.

The clear classification of stress-elongation relations into two groups appears to suggest that the supercoiling of network chains occurs abruptly at a critical value of ϕ_o, which is located at $0.281 \leq \phi_o \leq 0.411$. On the other hand, the effect of supercoiling on elastic modulus appears in the region $\phi_o \leq 0.54$, and increases gradually as ϕ_o decreases as seen in Fig. 7-1. Elastic modulus may be more sensitive to the supercoiling of network chains than stress-elongation relationship. However, the overlapping of stress-elongation curves in low ϕ_o region strongly suggests that the supercoiled structure settles into

the steady one specific to the system in this study as ϕ_o decreases. We estimate the fractal dimension (D) of the (steady) supercoiled structure from the dependence of σ_e on λ under the disentanglement process of supercoiled structure as shown below.

7.3.3 Analysis of disentanglement process of supercoiled structure

We analyze here the stress-elongation behavior of deswollen networks on the basis of the treatment of large deformation for a flexible polymer chain by Pincus.[16] According to their treatment,[16] a strongly stretched polymer chain is regarded as the nearly linear sequence of the smaller units (Pincus blobs) with the size of ξ_p. Features of Pincus blob are summarized as follows:[2,7,16,21] Inside a Pincus blob (the distance $r < \xi_p$), an applied force (f) is a weak perturbation, while f is a strong perturbation at the scale $r > \xi_p$. This condition postulates the relation $f\xi_p \approx k_B T$; and the correlation inside a Pincus blob ($r < \xi_p$) is the same as for the global chain. This means that the structure of global chain is preserved inside a Pincus blob during elongation process as long as the network structure concerned is not completely disentangled by elongation, and the blob size is given by $\xi_p \approx a' g_p^{1/D}$ where a' is the unit length, and g_p is the number of monomers in Pincus blob, and D is the fractal dimension of the polymer chain. Assuming the affine deformation in the scale larger than the size of the polymer chain, we obtain the following relation between λ and f.[2]

$$\lambda \approx \frac{(N/g_p)\,\xi_p}{R^o} \approx \frac{N a'}{R^o}\left(\frac{a' f}{k_B T}\right)^{D-1} \tag{7.3}$$

where R^o is the end-to-end distance of the polymer chain in undeformed state. The global stress for the network composed of the above polymer chains, σ_e, is related to f through $\sigma_e \approx \mu R^o f$ where μ is the number density of effective elastic chains. We get the following relation between σ_e and λ.

$$\sigma_e \propto \lambda^{1/(D-1)} \tag{7.4}$$

It can be seen in Fig. 7-3 that the dependence of σ_e on λ for the deswollen networks with supercoiled structure obeys $\sigma_e \propto \lambda^{0.65}$ in the region $2.1 \leq \lambda \leq 5.5$. Considering the region $2.1 \leq \lambda \leq 5.5$ as the disentanglement process of supercoiled structure, we evaluate the fractal dimension for supercoiled structure to be D=2.5 from Eq. (7.4). This fractal dimension (D=2.5) is larger than D=2 for Gaussian chain, while it is smaller than D=3 or 4 for PCAO model. The exponent of the dependence of σ_e on λ ($\sigma_e \propto \lambda^p$) is p=1 for Gaussian network, and p=1/2 and 1/3 for PCAO model with D=3 and 4, respectively. Obukhov *et al.*[7] predicted $\sigma_e \propto \lambda^{1/3}$ by applying the PCAO model with D=4 to supercoiled structure. Our experimental result suggests that the present supercoiled chain is more contracted than Gaussian one, while it is not collapsed as strongly as PCAO models. The reason for the smaller D in this study than those of PCAO model might be that PCAO model requires the very long network chain: N/N_{ef} in PCAO model is so large that the distance between neighboring obstacles is regarded[7,12] as $bN_{ef}^{1/2}$. The value of $N/N_{ef}(1)$ in this study is estimated to be *ca.* 6 using $M_e \approx 8100$ for PDMS[22] where M_e is the molecular weight between neighboring entangled points in melt in uncrosslinked state. Furthermore, the value of N/N_{ef} for the networks prepared at low ϕ_o becomes much smaller, because N_{ef} increases as ϕ_o decreases. From the viewpoint of N/N_e, the experimental condition in this study may not match sufficiently with the situation where PCAO model is applicable.

7.3.4 Analysis of the whole elongation process of supercoiled structure

We clarify here the changes in the topological structure of supercoiled chains during the whole elongation process by comparing the stress-

elongation behavior in the deswollen and preparation state. Here, we assume that crosslinking points moves affinely relative to the global network on deswelling and elongation. We define the reduced elongation ratio for deswollen network (λ_p) by regarding the undeformed state of original network as the reference state for elongation as follows.

$$\lambda_p = \phi_o^{1/3} \lambda \tag{7.5}$$

Figure 7-5 indicates the stress-elongation relation for the deswollen network with ϕ_o=0.179 where λ_p is employed as elongation ratio ($\lambda_p \approx 0.56\lambda$). The stress-elongation relation for the original network with ϕ_o=0.179 is also shown in the figure ($\lambda_p=\lambda$). The stress in the figure for the deswollen and original network is reduced by E_d and E_i, respectively. It is seen that the disentanglement process of supercoiled structure begins at $\lambda_p \approx 1.2$, meaning that the disentanglement of supercoiled chains starts when the end-to-end distance of network chains reaches the distance slightly larger than R_o. The disentanglement process of supercoiled structure continues up to $\lambda_p \approx 3.1$, and then the dependence of σ_e on λ becomes stronger in $\lambda_p > 3.1$. The following two significant points should be noted for the comparison of stress-elongation curves of the deswollen and original network in Fig. 7-5: Both curves coincide just at $\lambda_p \approx 3.1$ where the supercoiled structure has been completely disentangled; Both curves almost overlap each other in the region $\lambda_p \geq 3.1$, *i.e.*, after the complete disentanglement of supercoiled structure. These results suggest that the topological structure of network chains of deswollen gel just at the end of the disentanglement process of supercoiled structure is similar to that of the original network elongated to λ=3.1. Figure 7-6 shows the schematic representation for the whole elongation process of deswollen network with supercoiled structure and the corresponding states of the original network.

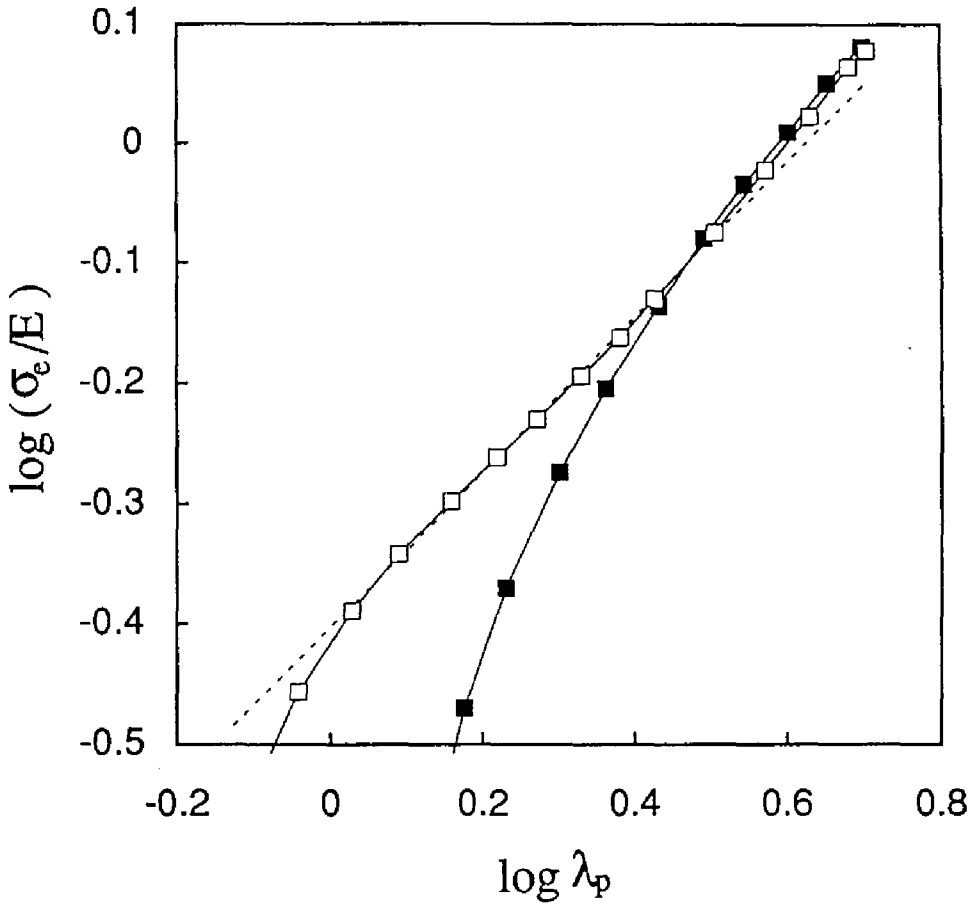

Figure 7-5. Comparison of the reduced stress-elongation relations of the network with ϕ_o=0.179 at the preparation and the dry state. λ_p is the reduced elongation ratio defined by Eq. (7.5). Symbols: (□) dry state; (■) preparation state. The dashed straight line has a slope of 0.65.

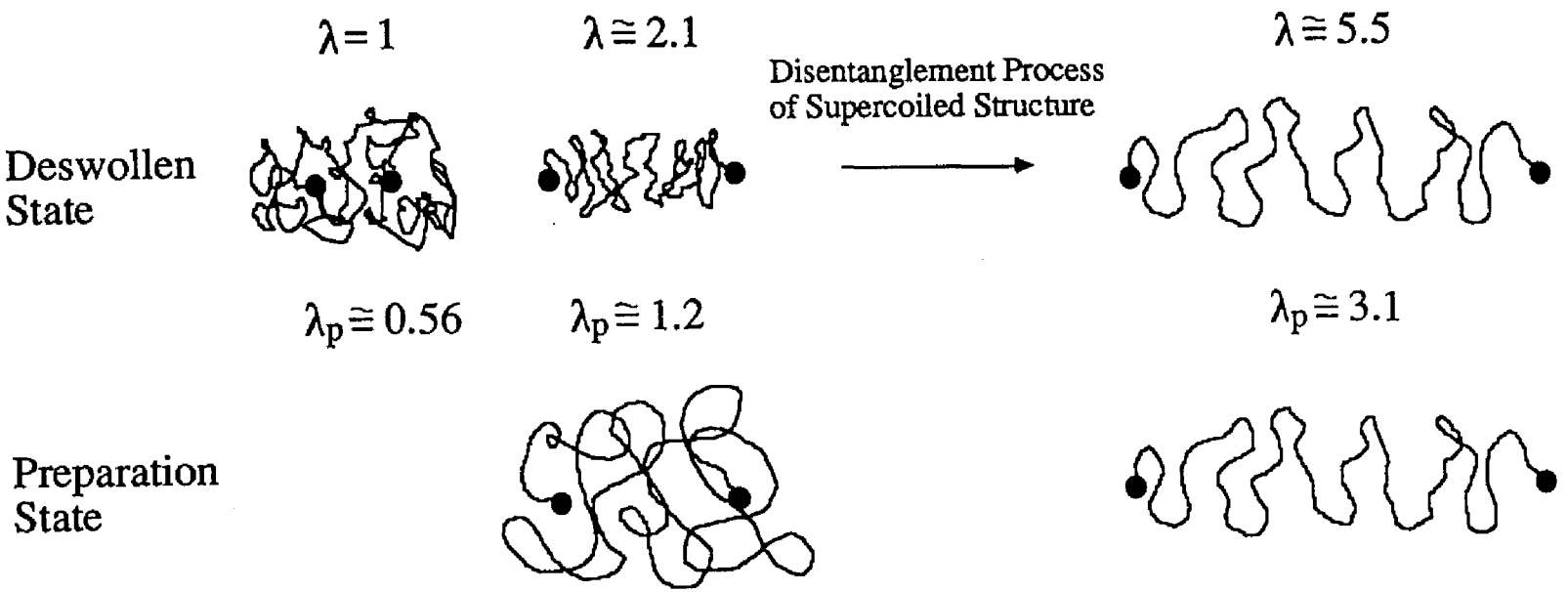

Figure 7-6. Schematic representation for the whole elongation process of deswollen networks with supercoiled structure. The corresponding state of the original network is also shown.

It should be noted that the stress-elongation behavior of dry network prepared at ϕ_o=0.0877 has the interesting features. It can be seen in Fig. 7-3 that the dependence of σ_e on λ obeys $\sigma_e \sim \lambda^{0.65}$ in the region $2.1 \leq \lambda \leq 5.5$ as similarly as for ϕ_o=0.179, while in the region $7 \leq \lambda \leq 12$ where the supercoiled structure is completely disentangled, the relation is expressed as $\sigma_e \sim \lambda^{1.0}$ corresponding to that for a Gaussian network in the large deformation region. The region $5.5 \leq \lambda \leq 7$ is the marginal regime where the dependence of σ_e on λ changes from $\lambda^{0.65}$ to $\lambda^{1.0}$. The linear relation between σ_e and λ in the region $7 \leq \lambda \leq 12$ suggests that the topological structure of the network chains where the supercoiled structure is completely disentangled is similar to that of the Gaussian chain. In Fig. 7-2 we showed that the stress-elongation behavior in preparation state is closer to Gaussian one as ϕ_o decreases. The stress-elongation behavior of the original network with ϕ_o=0.0877 is expected to be closer to Gaussian one than that with ϕ_o=0.179, though it was not measured due to the softness of the material. If the stress-elongation behavior of the original network with ϕ_o=0.0877 is assumed to be Gaussian, the whole elongation process of dry network with ϕ_o=0.0877 is interpreted in the same manner as indicated in Fig. 7-6.

The crossover in the dependence of σ_e on λ from the specific behavior of the structure concerned to Gaussian behavior has been theoretically predicted by several authors.[7,23] However, the crossover was not reported experimentally at all, which is due to the fact that usual polymer networks do not possess the high extensibility enough to bear the large elongation reaching the crossover region. The perfect crossover to Gaussian behavior may occur for the networks with high extensibility and few trapped entanglements, because the dependence of σ_e on λ in high λ region for ϕ_o=0.179 obeys $\sigma_e \sim \lambda^{0.77}$, while the perfect crossover to Gaussian behavior is observed for

ϕ_o=0.0877. The exponent smaller than unity for ϕ_o=0.179 might result from the effect of trapped entanglements. Actually, the stress-elongation behavior of the original network with ϕ_o=0.179 does not agree perfectly with Gaussian one due to the effect of trapped entanglements as seen in Fig. 6-2. The perfect crossover to Gaussian behavior for ϕ_o=0.0877 would be due to no or negligible amount of trapped entanglements in the network. The estimation of the amount of trapped entanglements for the network with ϕ_o=0.0877 will be shown later.

In Fig. 7-3 the stress-elongation curve of the dry network with ϕ_o=0.0877 is found to indicate the upturn in the region λ>12. The strong dependence of σ_e on λ in the region λ>12 is due to the deviation of the network structure from Gaussian one by the large elongation. The large elongation leads to the approach to the full extension of network chains. It is well-known[22] for the stress-elongation behavior of crosslinked rubbers that the approach to the full extension of network chains results in the strong dependence of σ_e on λ.

7.3.5 High extensibility of the deswollen network prepared at low concentration

The deswollen network prepared at ϕ_o=0.0877 exhibits the remarkable extensibility reaching $\lambda\approx$18 as seen in Fig. 7-3. (Here, we mention that the perfect size recovery has been observed for the deswollen network with ϕ_o =0.0877 elongated up to $\lambda\approx$15.) The possibility of high extensibility for deswollen networks prepared at low ϕ_o has been theoretically pointed out by Obukhov *et al.*.[7] The high extensibility results from the two main factors: the reduction of the distance between neighboring junctions on deswelling; the decrease in the number of trapped entanglements, which is an origin of

failure, due to the low ϕ_o. It is qualitatively confirmed in Fig. 7-3 that the extensibility of deswollen networks increases as ϕ_o decreases. According to their simple evaluation for extensibility of polymer network,[7] the theoretical limit of extensibility (λ_{max}) for the deswollen network prepared at ϕ_o is estimated as follows.

$$\lambda_{max} \approx \frac{a N_{ef}(\phi_0)}{a N_{ef}^{1/2}(\phi_0)\, \phi_o^{1/3}} = \frac{N_{ef}^{1/2}(\phi_0)}{\phi_o^{1/3}} \qquad (7.6)$$

The quantity, $N_{ef}(\phi_o)$, for the system in this study was obtained as $N_{ef}(\phi_o) \approx N_{ef}(1)\phi_o^{-1.1}$ from ϕ_o dependence of E_i in the region $\phi_o \geq 0.179$ in Chapter 5. The value of $N_{ef}(1)$ is estimated to be *ca.* 13 Kuhn segments from M_e=8100[22] and the number of real bond per freely joint link for PDMS ($\approx$17).[23] If $N_{ef}(\phi_o) \approx N_{ef}(1)\phi_o^{-1.1}$ is employed for the estimation of N_e at ϕ_o=0.0877, the calculated value of N_{ef} is found to be much larger than N of the prepolymer. Here, N of the prepolymer with M=4.7×10^4 is estimated to be *ca.* 75 Kuhn segments. This means that the number of trapped entanglements is negligible compared with that of chemical crosslinks for the network at ϕ_o =0.0877. Accordingly, we should use N of the prepolymer instead of N_{ef} in Eq. (7.6) for the network with ϕ_o=0.0877. We get $\lambda_{max} \approx 20$ from Eq. (7.6) with N =75. It is well known[24] that the failure phenomena is primarily governed by the defects of the sample, which complicates the quantitative comparison of experimental results with the theory. However, the experimental failure point for the dry network with ϕ_o =0.0877 ($\lambda \approx 18$) is close to the theoretical value. Here, we should mention that $\lambda \approx 18$ is the highest extensibility that we have observed for the samples with ϕ_o =0.0877, and that is not an average one.

7.4 Conclusions

The formation of supercoiled structure on deswelling of PDMS networks crosslinked in solution was demonstrated by investigating the preparation concentration dependence of the elastic modulus and the stress-elongation behavior of deswollen networks. The pronounced effects of supercoiling on mechanical properties of deswollen networks appeared for the networks prepared at low concentration at which the volume decrease is large on deswelling. The deswollen networks with supercoiled structure had the higher elastic modulus than that expected by the theory for Gaussian or excluded volume chain, and show the stress-elongation relation with the region where the dependence of stress on elongation is much weaker compared with that for the original network. On the other hand, the deswollen networks prepared at high concentration, whose volume does not change largely on deswelling, showed the elastic modulus explained by the theory, and the similar stress-elongation behavior to the original networks.

The fractal dimension of supercoiled structure was estimated from the dependence of stress on elongation ratio in terms of the concept of Pincus blob. The dependence of stress on elongation ratio under the disentanglement process of supercoiled structure is independent of preparation concentration, and common to the deswollen networks with supercoiled structure. The obtained fractal dimension was larger than that of Gaussian chain, and smaller than those of PCAO model. The supercoiled chain is expected to be contracted in comparison with the Gaussian one, but not collapsed so strongly as the PCAO models.

The reduced stress-elongation behavior of deswollen network, where the elongation ratio is reduced by the undeformed state of the original network, was similar to the stress-elongation relation of the original network

after the supercoiled structure is completely disentangled. This suggests that after the complete disentanglement of supercoiled structure, the topological structure of network chains of deswollen networks is identical with that of the elongated original network.

The deswollen networks with supercoiled structure prepared at low concentration showed the remarkable extensibility originating from the reduction of the distance between network junctions and the decrease in the number of trapped entanglements. Especially, the extensibility of the deswollen network prepared at *ca.* 9% has reached *ca.* 1700%, which was found to be close to the theoretical limit of extensibility for the sample.

References

1. Graessley, W. W., *Adv. Polym. Sci.*, **16**, 1 (1974).
2. de Gennes, P.-G., "*Scaling Concepts in Polymer Physics*", Cornell University Press, Ithaca, NY, 1979.
3. Vasiliev, V. G., Rogovina, L. Z. and Slonimsky, G. L., *Polymer*, **26**, 1667 (1985).
4. Heinrich, G., Straube, E., and Helmis, G., *Adv. Polym. Sci.*, **85**, 33 (1988).
5. Bastide, J., in "*Physics of Finely Divided Matter*", Proceedings of Physics, Vol. 5, Springer-Verlag, Berlin, 1985.
6. Picot, C., *Prog. Coll. & Polym. Sci.*, **75**, 83 (1987).
7. Obukhov, S. P., Rubinstein, M. and Colby, R. H., *Macromolecules*, **27**, 3191 (1994).
8. Khokhlov, A. R. and Nechaev, S. K., *Phys. Lett.*, **112A**, 156 (1985).
9. Grosberg, A. Y. and Nechaev, S. K., *Macromolecules*, **24**, 2789 (1991); *Adv. Polym. Sci.*, **106**, 1 (1993); *Macromolecules*, **26**, 3200 (1993).
10. Helfand, E. and Pearson, D. S., *J. Chem. Phys.*, **79**, 2054 (1983).
11. Rubinstein, M., *Phys. Rev. Lett.*, **57**, 3023 (1986).
12. Nechaev, S. K. and Khokhlov, A. R., *Phys. Lett. A*, **126**, 431 (1988).
13. Price, C., Allen, G., de Candia, F., Kirkham, M. C. and Subramaniam, A., *Polymer*, **11**, 486 (1970).
14. Johnson, R. M. and Mark, J. E., *Macromolecules*, **5**, 41 (1972).
15. Ong. C. S. M. and Stein, R. S., *J. Polym. Sci., Polym. Phys. Ed.*, **12**, 1599 (1974).
16. Pincus, P., *Macromolecules*, **9**, 386 (1976).
17. Panyukhov, S. V., *Sov. Phys. JETP*, **71**, 372 (1990).
18. Haug, V. A. and Meyerhoff, G., *Macromol. Chem.*, **53**, 91 (1962).

19. Adachi, K., Imanishi, Y., Shinkado, T. and Kotaka, T., *Macromolecules*, **22**, 2391 (1989).
20. Treloar, L. R. G., "*The Physics of Rubber Elasticity*", 3rd Ed., Clarendon Press, Oxford, 1975.
21. Daoudi, S. *J., Phys. (Paris)*, **38**, 1301 (1977).
22. Ferry, J. D., "*Viscoelastic Properties of Polymers*", 3rd Ed., Wiley, NY, 1980.
23. "*Polymer Handbook*", 2nd Ed., Brandup, J., Immergut, E. H., Eds., Wiley, NY, 1975.
24. Nielsen, L. E., "*Mechanical Properties of Polymers and Composites*", Marcel Dekker, Inc., NY, 1975.

Summary

In Chapter 1, the motives of this thesis were described along with the historical background of the research field in respect to the swelling and elastic properties of polymer network systems. The current problems remaining unsolved in this research field, which are treated in this thesis, were briefly reviewed.

In Chapter 2, initial Poisson's ratio (μ_o) of gels obtained under the condition that the swelling induced by applied strain is negligible, was discussed. A method to measure μ_o of gels during uniaxial elongation was established. The value of μ_o was obtained from measurements of the size of gels in the directions parallel and perpendicular to stretching direction. The measurements were made under the condition that elongation rate is so fast that the strain-induced swelling is negligible. The values of μ_o for the three kinds of Poly(vinyl alcohol) (PVA) gels were measured. The value of μ_o of the PVA gels swollen in good solvent (a mixture of dimethylsulfoxide and water) was close to 1/2 meaning that the gel can be regarded as an incompressible material. The value of μ_o close to 1/2 reflects the high flexibility of PVA chains in the network. The annealed PVA gels with the higher degree of crystallinity in good solvent (water) showed the slightly smaller value of μ_o in comparison to the unannealed PVA gels. The annealing developed the size of microcrystalline domains acting as crosslinking points, which should lower the flexibility of PVA chains, resulting in the lower μ_o. The value of μ_o of the PVA gels in poor solvent (ethanol) was *ca.* 0.3, which is comparable to μ_o of glassy polymers. The PVA gels in ethanol were opaque, indicating the two-phase structure composing of the PVA-rich phase and the solvent-rich one. Since the glass transition temperature of PVA is

much higher than the room temperature, most of the PVA chains in the gel are in the glassy state, leading to the same order of μ_0 as glassy polymers.

In Chapter 3, the effects of strain-induced swelling on μ_0 and mechanical relaxation (stress relaxation and creep) of swollen gels were theoretically investigated. Two types of the limiting values of Poisson's ratio according to the short and long time scale were defined as μ_0 and μ_∞. Equilibrium Poisson's ratio μ_∞ is obtained under the condition that the time scale for elongation is so long that the strain-induced swelling is equilibrated. Time dependence of μ of a gel during and after uniaxial elongation was calculated on the basis of the kinetics of a constrained gel. The numerical results demonstrated the intermediate value of μ between μ_0 and μ_∞ in the time scale between the two extreme cases. From the thermodynamical consideration based on the Flory-type free energy for a constrained gel, the degree of the strain-induced swelling and the resultant mechanical relaxation was found to strongly depend on the deformation modes. The degree of volume increase and the magnitude of stress reduction and creep for an equi-biaxially stretched gel were much larger than those for a uniaxially one. Time dependence of the strain-induced swelling was calculated from the kinetics of a constrained gel. Process of mechanical relaxation caused by the strain-induced swelling was calculated in respect to a thin disk-shaped gel for biaxial elongation, and a long rod-shaped gel for uniaxial elongation. In respect to a gel under constant stress, if the anisotropy in diffusional dimensionality originating from the anisotropy in gel geometry is taken into account, it is expected that the overshoot of the size in load-free direction occurs: As the time increases, the size in load-free direction exceeds the equilibrium value, and then, it decreases to the equilibrium one. The reason for the overshoot behavior of size in load-free direction is that the time

dependence is governed by the two kinds of diffusion modes different in the character and characteristic time, *i.e.*, the longitudinal diffusion mode controling the volume change of gels, and the transverse one governing the shape change without volume change.

In Chapter 4, the stress-strain relations of polymer networks in the bulk state under pure shear deformation were investigated from the viewpoint of strain energy density function (W). Especially, the behavior of the partial derivatives of W in respect to the invariants of deformation tensor ($\partial W/\partial I_i$; i=1,2,3) was investigated in small deformation region. The assumption of incompressibility (μ_o=1/2) which has conventionally been employed for elastomers, was eliminated, and the experimental values of μ_o were used for the analysis of stress-strain relations. The values of $\partial W/\partial I_i$ (i=1,2,3) at zero strain limit were theoretically derived on the basis of the infinitesimal elasticity theory for compressible materials. The theoretical limiting values of $\partial W/\partial I_i$ (i=1,2,3) at small strain were obtained as $\partial W/\partial I_1 = 5G/8$, $\partial W/\partial I_2 = -G/8$ and $\partial W/\partial I_3 = -3G/8$ where G is the shear modulus. Three kinds of the segmented polyurethaneureas (SPUs) different in the molecular weight of soft segment block were employed as the samples. The stress-strain relations of the SPUs under pure shear deformation were measured, and the values of μ_o for the SPUs were evaluated from the two kinds of experiments: the dimensional changes during uniaxial elongation; and the stress ratio under pure shear deformation. The values of μ_o obtained were smaller than 1/2, which shows that the SPUs should be treated as a compressible material. As the molecular weight of soft segment block increases, the value of μ_o became larger. The asymptotic behavior of $\partial W/\partial I_i$ (i=1,2,3) in the experiments was satisfactorily explained by the theoretical predictions. The experimental data for pure shear deformation of isoprene rubber reported by Kawabata *et al.*,

styrene-butadiene rubber, nitrile-butadiene rubber and butadiene rubber reported by Fukahori *et al.* were re-analyzed using the experimental values of μ_0. The behavior of $\partial W/\partial I_i$ (i=1,2,3) at small deformations for the four types of rubber vulcanizates was similar to that for SPUs, and their asymptotic behavior was also well explained by the theory. It was also shown for the SPUs and four types of rubber vulcanizates that the classical theory of rubber elasticity succeeds to a degree in large deformation region, but it can not describe the asymptotic behavior of $\partial W/\partial I_i$ (i=1,2,3) at small deformation region. The success of the theory in this study in many rubber systems suggests that W for real elastomers must have the asymptotic form as described by the infinitesimal elasticity theory for compressible materials, although the difinite functional form of W at large deformations remains still unknown.

In Chapters 5 and 6, the degree of equilibrium swelling and the elastic modulus of the networks crosslinked in solution were investigated as a function of the polymer concentration at crosslinking in order to elucidate the thermodynamics of swelling and the relationships between the elasticity and the topological network structure. For examining the effect of entangled state of prepolymer before crosslinking on the elasticity of resultant crosslinked network, two types of networks were prepared in toluene by end-linking polydimethylsiloxane (PDMS) and oligodimethylsiloxane (ODMS), respectively. The PDMS has the molecular weight high enough to be entangled in uncrosslinked state, while the molecular weight of ODMS is so low that any entanglements are not formed in uncrosslinked state. Model networks having as small amount of structural defect as possible were prepared by varying the reaction conditions such as reaction temperature, reaction time, and molar ratio of crosslinker to prepolymer. The model

networks prepared by PDMS and ODMS were used as samples in Chapters 5 and 6, respectively.

In Chapter 5, the dependence of the initial Young's modulus in preparation state (E_i) on polymer volume fraction at preparation (ϕ_o) scaled as $E_i \sim \phi_o^{2.1}$ which is analogous to the concentration dependence of plateau modulus of polymer solutions. This similarity indicates that trapped entanglements act similarly as chemical crosslinks, and those dominantly contribute to elastic modulus. The ϕ_o dependence of both the polymer volume fraction and the initial Young's modulus of equilibrium swollen networks (ϕ_e and E_s, respectively) showed the crossover at $\phi_o \approx \phi^{**}$ where ϕ^{**} is the polymer volume fraction at which the excluded volume effect of polymer chains is fully screened. The crossover in ϕ_o dependence ϕ_e and E_s was not explained by the c^* theorem which considers ϕ^* (the value of ϕ at which the overlapping of network chains begins) as a reference state irrespective of ϕ_o. The ϕ_o dependence of ϕ_e and E_s and the crossover behavior were quantitatively described by the affine model which takes ϕ_o as a reference state and assumes the affine displacement of crosslinks on swelling.

In Chapter 6, ϕ_o dependence of E_i, ϕ_e and E_s was investigated for the networks prepared by end-linking ODMS. The ϕ_o dependence of E_i and the absolute values of E_i suggested that trapped entanglements are formed and considerably contribute to elastic modulus, even if the prepolymers are not entangled in uncrosslinked state. The magnitude of the contribution of trapped entanglements to elastic modulus is smaller than that in the networks prepared by PDMS, which led to the more significant difference in the theoretical exponents for ϕ_o dependence of ϕ_e and E_s between the c^* theorem and the affine model, compared with the networks prepared by PDMS. This

enabled us to discuss the differences between the two theories more clearly. The experimental results for ϕ_o dependence of ϕ_e and E_s were well explained by the affine model, while the theoretical exponents by the c^* theorem were much lower than the experimental ones. The following conclusions were obtained from the results in Chapters 5 and 6: Trapped entanglements are inevitably involved in networks (at least, in networks prepared by end-linking method) irrespective of the length of prepolymer, and trapped entanglements contribute to elastic modulus similarly as chemical crosslinks, although the maginitude of its contribution is influenced by the length of prepolymer used; and the displacement of crosslinks moves affinely on swelling, and the complete disinterpenetration of network chains as the c^* theorem predicts does not occur in equilibrium state. It was also shown that ϕ_e dependence of physical properties of equilibrium swollen networks, which has been experimentally investigated by many researchers, is insufficient to test the molecular theories for equilibrium swelling of polymer networks.

In Chapter 7, the details of supercoiled structure which is formed by removing solvent (deswelling) from networks crosslinked in solution was investigated through the mechanical properties of deswollen PDMS networks. The effects of supercoiling on the mechanical properties of networks were clearly observed in respect to the deswollen networks prepared at low concentrations at which the volume decrease of material on deswelling is large. Deswollen networks with supercoiled structure showed the higher elastic modulus than that predicted by the theory for Gaussian chain, and the much weaker dependence of stress (σ_c) on elongation (λ) in the region $\lambda<6$ in comparison with the networks in preparation state. The fractal dimension (D) of supercoiled structure was evaluated to be 2.5 from λ dependence of σ_c common to the samples prepared at low concentration on the basis of the

scaling treatment of large deformation of a flexible polymer. The value of D obtained experimentally suggests the conformation of supercoiled chains is contracted in comparison to that of Gaussian chain (D=2), while it is not strongly collapsed relative to that of "polymer chain in an array of obstacles" models (D=3 or 4) which are often theoretically applied to collapsed polymer systems. The remarkable extensibility (λ_{max}≈18) of the deswollen network prepared at low concentration (ϕ_o≈0.09) was experimentally and theoretically demonstrated. This high extensibility was attributed to the two factors: the decrease in the number of trapped entanglements which is a origin to limit extensibility due to the low concentration at crosslinking; and the reduction in the end-to-end distance of network chains in undeformed state on deswelling. The theoretical value of λ_{max} based on the above consideration was in good agreement with the experimenal one.

LIST OF PUBLICATIONS

Originals

1. "Poisson's Ratio of Poly(vinyl alcohol) Gels"
   Urayama, K., Takigawa, T. and Masuda, T., *Macromolecules*, **26**, 3092 (1993). (Chapter 2)

2. "Time Dependent Poisson's Ratio of Polymer Gels in Solvent"
   Takigawa, T., Urayama, K. and Masuda T., *Polym. J.*, **26**, 225 (1994). (Chapter 3)

3. "Stress Relaxation and Creep of Polymer Gels in Solvent under Uniaxial and Biaxial Deformations"
   Urayama K., Takigawa T. and Masuda T., *Rheologica Acta*, **33**, 89 (1994). (Chapter 3)

4. "Ultra-high Extensibility of Deswollen Polysiloxane Networks"
   Urayama, K., Ikeda, Y. and Kohjiya, S., *J. Soc. Rubber Ind., Jpn.*, **68**, 814 (1995). (in Japanese) (Chapter 7)

5. "Crossover of the Concentration Dependence of Swelling and Elastic Properties for Polysiloxane Networks Crosslinked in Solution"
   Urayama, K. and Kohjiya, S., *J. Chem. Phys.*, **104**, 3352 (1996). (Chapter 5)

6. "Stress-Strain Behavior of Segmented Polyurethaneureas under Pure Shear Deformation"
   Takigawa, T., Yamasaki, S., Urayama, K. and Masuda, T., *Rheologica Acta*, **35**(June), OOO (1996). (Chapter 4)

7. "Elastic Properties of Real Elastomers at Small Deformations"
   Takigawa, T., Urayama, K., Yamasaki, S. and Masuda, T., *Angew. Makromol. Chem.*, OOO(June), OOO (1996). (Chapter 4)

8. "Uniaxial Elongation of Deswollen Polydimethylsiloxane Networks with Supercoiled Structure"
   Urayama, K. and Kohjiya, S., *Polymer* in press. (Chapter 7)

9. "Elastic Modulus and Equilibrium Swelling of Networks Crosslinked by End-linking Oligodimethylsiloxane at Solution State"
   Urayama, K., Kawamura T. and Kohjiya, S., submitted to *J. Chem. Phys.*. (Chapter 6)

Reviews

1. "Poisson's Ratio of Polymer Gels"
   Urayama, K., *Kaigai-Kobunshi-Kenkyu*, **41**, 12 (1995). (in Japanese)

2. "Swelling and Mechanical Properties of Polymer Gels from Viewpoint of Poisson's Ratio"
   Urayama, K., Kohjiya, S., Takigawa, T. and Masuda, T., *J. Soc. Rubber Ind. Jpn*, **68**, 444 (1995). (in Japanese)

Other Publications

Originals

1. "Critical Behavior of Modulus of Poly(vinyl alcohol) Gels near the Gelation Point"
   Takigawa, T. Kashihara, H., Urayama, K. and Masuda, T., *J. Phys. Soc. Jpn.*, **59**, 2598 (1990).

2. "Critical Behavior of the Intrinsic Viscosity of poly(vinyl alcohol) Solutions near the Gelation Point"
   Takigawa, T., Urayama, K. and Masuda, T., *J. Chem. Phys.*, **93**, 7310 (1990).

3. "Critical Behavior of the Specific Viscosity of Poly(vinyl alcohol) Solutions near the Gelation Threshold"
   Takigawa, T., Urayama, K. and Masuda, T., *Chem. Phys. Lett.*, **174**, 259 (1990).

4. "Structure and Mechanical Properties of Poly(vinyl alcohol) Gels Swollen by Various Solvents"
   Takigawa, T., Kashihara, H., Urayama, K. and Masuda, T., *Polymer*, **33**, 2334 (1992).

5. "Comparison of Model Prediction with Experiment for Concentration-Dependent Modulus of Poly(vinyl alcohol) Gels near the Gelation Point"
   Takigawa, T., Takahashi, M., Urayama, K. and Masuda, T., *Chem. Phys. Lett.*, **195**, 509 (1992).

6. "Simultaneous Swelling and Stress Relaxation Behavior of Uniaxially Stretched Polymer Gels"
   Takigawa, T., Urayama, K., Morino, Y. and Masuda, T., *Polym. J.*, **25**, 929 (1993).

7. "Theoretical Studies on the Stress Relaxation of Polymer Gels under Uniaxial Elongation"
Takigawa, T., Urayama, K. and Masuda, T., *Polym. Gels & Networks*, **2**, 59 (1994).

8. "GPC Analysis of Polymer Network Formation : 1. Bifunctional Siloxane Monomer / Crosslinker System"
Kohjiya, S., Takada, Y., Urayama, K., Tezuka, Y. and Kidera A., *Bull. Chem. Soc. Jpn.*, **69**, 565 (1996).

9. "Structure and Viscoelastic Properties of Segmented Polyurethane Blends"
Takigawa, T., Oodate, M., Urayama, K. and Masuda, T., *J. Appl. Polym. Sci.*, **59**, 1563 (1996).

10. "Poisson's Ratio of Polyacrylamide (PAAm) Gels"
Takigawa, T., Morino, Y., Urayama, K. and Masuda, T., *Polym. Gels & Networks*, **4**, 1 (1996).

Reviews

1. "Divergence and Crossover in Concentration Dependent Compliance of Polymer Network Systems"
Masuda, T., Takigawa, T., Takahashi, M. and Urayama, K., in "*Theoretical and Applied Rheology I*", Moldenaers, P. and Keunig, R., Eds., Elsevier, Amsterdam, 1992.

Acknowledgements

The present thesis has been written based on research carried out at the Research Center for Biomedical Engineering, Kyoto University, from 1989 to 1993 under the direction of Professor Toshiro Masuda, and at the Institute for Chemical Research, Kyoto University, from 1994 to 1995 under the guidance of Professor Shinzo Kohjiya. The author wishes to express his sincere gratitude to Professors Toshiro Masuda and Shinzo Kohjiya for their continuous guidance, encouragement and valuable comments.

The author is sincerely grateful to Dr. Toshikazu Takigawa for his instructive discussion, helpful advice, and collaborations throughout this study.

The author would also thank Professor Keisuke Kaji for his careful reading and corrections to this dissertation.

Thanks are also due to all of the members, past and current, of the laboratory including Messrs. Satoshi Yamasaki and Takanobu Kawamura for their kind help during this study.

Kenji Urayama

Kyoto, Japan
June, 1996